Ultrafast Excited State Dynamics in DNA and other Nanomaterials

Author: Stoichko Dimitrov Dimitrov

Boston College

The Graduate School of Arts and Sciences

Department of Chemistry

ULTRAFAST EXCITED STATE DYNAMICS IN DNA AND OTHER NANOMATERIALS

a dissertation

by

STOICHKO DIMITROV DIMITROV

Advisor: Prof. Torsten Fiebig

submitted in partial fulfillment of the requirements

for the degree of

Doctor of Philosophy

December, 2010

ULTRAFAST EXCITED STATE DYNAMICS IN DNA AND OTHER NANOMATERIALS

Stoichko Dimitrov Dimitrov

Advisor: Prof. Torsten Fiebig

ABSTRACT

Understanding the electronic nature of DNA is profound and has been attempted for decades. Photoexcitation of DNA with UV light deposits electronic energy in the base stack and prepares highly reactive excited states. These states are precursors for photoinduced damage reactions which can lead to mutations and ultimately to cell death. While many DNA photo products have been isolated and characterized, the primary events immediately after photon absorption are not yet understood. Recent studies with ultrafast lasers have revealed that the majority of excess energy gained by DNA with light absorbance is dissipated on the femtosecond and picosecond time scales. In this study double-stranded oligonucleotides with different base sequences, content and lengths were systematically examined using femtosecond pump-probe spectroscopy. The results indicate that excitations in DNA are delocalized over more than two bases and the extent of the delocalization depends strongly on the structure of the investigated systems. Exciton delocalization domains in the longer duplexes are larger than in the shorter ones. Also, single-stranded oligonucleotides show smaller extent of exciton delocalization than duplexes with the same length. In addition to the fundamental studies on DNA

photophysics, the properties and the structure of new molecular beacons based on thiazole orange dimers were studied. A full account of the optical and structural properties of the dimers in different base environments and orientations is presented here.

Currently, the development of efficient ways to utilizing solar energy is at the forefront of the scientific community due to the ever rising demand for energy. Both, colloidal semiconductor nanocrystals and single-walled carbon nanotubes are potential alternatives to conventional inorganic and organic materials in photovoltaic devices Thorough understanding of the charge transfer and related photophysical phenomena in these systems will answer the question whether these nanomaterials can be applied in future generations of solar cells. The photoinduced electron transfer in donor-acceptor CdSe/CdTe heterostructured nanorods, in which CdTe is grown on top of CdSe in a single rod structure, was studied. The electron transfer between the two nanocrystals occurs on the subpicosecond time scale, competing with the ultrafast relaxation mechanisms in the quantum confined nanocrystals. Furthermore, investigations on how quantum confinement influences the phonon wavepackets in semiconductor nanocrystals were carried out. Quantum beats corresponding to longitudinal optical phonon modes were observed in the femtosecond pump-probe spectra of colloidal CdTe nanocrystals. Size-dependent experiments revealed that the optical phonon frequencies and the exciton-phonon coupling strength do not depend on the crystal's size. Only the wavepacket dephasing time was influenced by the diameter of the particles which was correlated with the hole relaxation to the exciton band edge.

Electron donor-acceptor constructs, based on single-walled carbon nanotubes (SWNT), can be attained by noncovalent functionalization of the nanotubes with pyrene derivatives. However, charge transfer does not take place in the simplest pyrene-SWNT constructs. For the first time the pure SWNT-pyrene construct was isolated and investigated. Our results revealed that the optical properties of pyrene are drastically altered due to strong electronic interactions with the SWNT surface. In other words, aromatic molecules lose their electronic (and chemical) signature when non-covalently attached to carbon nanotubes.

ACKNOWLEDGEMENTS

Like all good journeys, the completion of this dissertation would not be possible without the support and guidance of many people.

First, I would like to thank my advisor, Professor Torsten Fiebig, for giving me the opportunity to work in his group and carry research that otherwise I would not have been able to perform. I am especially grateful for his patience, advice and discussions. The years I worked with him have been fulfilled with learning and inspirational experience for me.

I am very thankful to my committee members: Professor Mary Roberts for reviewing the dissertation and giving me very helpful suggestions; Professor Udayan Mohanty, for his continuous support and advice during these five years; I owe special thanks to Professor Dunwei Wang for the numerous very useful conversations we have had. I am also grateful to the Wang group for sharing their thoughts and experimental equipment with me.

I would like to thank the members of Professor Fiebig's group who all have contributed to this work with experiments and discussions: Qiang Wang, Dimitar Popminchev, Tianhong Chen, Professor Buchvarov and Anton Trifonov; to Milen Raytchev for mentoring me during my initial steps in the group and being my friend.

Also, I am grateful to Chad Dooley for being my friend. His ideas were critical for one of the projects in this dissertation.

In the last five years, my family has been behind me in every moment of despair or enthusiasm. Thank you Vese, Kaline, Maiko and Tatko.

DEDICATION

I would like to dedicate this dissertation to my father. Nothing was more important for him than my education and success.

TABLE OF CONTENTS

LIST OF FIGURES

LIST OF TABLES

LIST OF ABBREVIATIONS

2D	two-dimensional
3D	three-dimensional
A	adenine
AMP	adenosine monophosphate
BBO	ß-barium borate
CCD	charge-coupled device
CD	circular dichroism
CI	conical intersection
CMP	cytidine monophosphate
CT	charge transfer
dA	deoxyadenosine
dC	deoxycytidine
dCMP	deoxycytidine monophosphate
DFT	density functional theory
dG	deoxyadenosine

DOC	sodium deoxycholate
ds	double-stranded
dT	thymidine
ESA	excited state absorption
ESI	electrospray ionization
ET	electron transfer
FRET	Förster resonance energy transfer
fs	femtosecond
FWHM	full-width at half maximum
G	guanine
GSB	ground state bleaching
GVD	group velocity dispersion
HiPCO	high pressure carbon oxide disproportionation
hNR	heteromaterial nanorod
IC	internal conversion
IR	infrared

LO	longitudinal optical
MPA	3-mercaptopropionic acid
NaHTe	sodium hydrogen telluride
$NaBH_4$	sodium borohydride
NCs	nanocrystals
NHE	normal hydrogen electrode
NIR	near-infrared
NMR	nuclear magnetic resonance
NOPA	non-collinear optical parametric amplifier
NP	nanoparticle
NR	nanorod
ns	nanosecond
OD	optical density
PDI	perylene bisimides
p.p	pump-probe spectroscopy
ps	picosecond

PCET	proton-coupled electron transfer
Pyr	Pyrenebutyric acid
r	radius
$R_{\pm}$	rotary strength
S	Huang-Rhys parameter
SE	stimulated emission
ss	single-stranded
SVD	singular value decomposition
SWNT	Single-Walled Carbon Nanotubes
SWNT-Pyr	Single-Walled Carbon Nanotubes and pyrenebutyric acid complex
SWNT-DOC	Single-Walled Carbon Nanotubes suspensions with sodium deoxycholate
T	thymine
TCSPC	time-correlated single photon counting
TEM	transmission electron microscopy
T_m	melting temperature
TO	thiazole orange

UV	ultraviolet
V_{ij}	the electronic interaction energy
XPM	cross-phase modulation
μ	transition dipole moment

1 Introduction

This dissertation summarizes my research on the nature of the excited states and their relaxation dynamics in complex multichromophore systems and inorganic nanocrystals. In the past five years, I focused my efforts on studying the photophysical properties of DNA and pyrene-functionalized single-walled carbon nanotubes (SWNT), the electron transfer and exciton-phonon interactions in CdTe and CdSe nanocrystals, and the optical properties of new types of molecular beacons. A central element in all of my investigations is pump-probe spectroscopy, a laser technique that is applied to follow excited state dynamics on the femtosecond, picosecond and nanosecond time scale. These time scales are decisive for the photophysical processes that determine the properties of the various systems studied here.

Because of the thematic diversity of my projects, the dissertation chapters consist of an introduction to each specific topic followed by results, discussion and conclusion sections. In the following paragraphs I present a short outline of the experiments and the main findings presented in each chapter.

The femtosecond broadband pump-probe spectroscopy setup is described in **Chapter 2**. A typical procedure for data analysis is included. Additionally, information about the steady-state spectroscopy techniques and common conditions for the experiments are listed.

The beginning of **Chapter 3** presents an introduction to the field of DNA photophysics. Then, the results from our investigations on the length dependent photophysical properties of short double-stranded oligonucleotides are discussed. DNA duplexes with different lengths, base sequences and base content were synthesized by our collaborators from Northwestern University, the group of Prof. Fred Lewis. Because of the inherent differences in the spectroscopic properties of the oligonucleotides, the studies on adenine and thymine hairpins were separated from the studies on guanine and cytosine hairpins. The conclusions from the femtosecond experiments can be summarized as follows. The ultrafast relaxation of the electronically excited states in the duplexes are length and base-sequence dependent. The difference between rigid duplexes and more flexible single-stranded oligonucleotides is discussed. Our investigations provide strong evidence for the importance of excitons and exciton delocalization in DNA photophysics. The work presented here is another step in our ongoing efforts to reveal the mechanisms of energy dissipation in DNA.

Chapter 4: Nucleic acid recognition probes, particularly molecular beacons have been widely used for genetic screening and biosensors. New and promising alternatives to the common FRET readout systems are molecular beacons that shift their emission wavelengths upon hybridization with target DNA sequence.[1] Wagenknecht et al. designed such beacons using dimers of thiazole orange (TO).[2] However, the optical spectroscopic properties of the dimeric TO surrogates were poorly understood; specifically, the appearance of blue-shifted absorbance and red-shifted fluorescence, accompanied by increased fluorescence quantum yields. The analysis of the femtosecond

pump-probe and fluorescence excitation spectra revealed that a multitude of structural ensembles, stacked and unstacked TO dimers, coexist in the base surrogated oligonucleotides. The main ensemble is a TO interstrand ground state dimer (so-called "H-aggregate") which contributes to the blue-shifted absorption spectrum. On the other hand, the increased and red-shifted fluorescence band was explained with TO excimer formation.

Chapter 5 presents my work with inorganic semiconductor nanocrystals and is divided into two parts. **Chapter 5.1:** The spectral properties of semiconductor nanocrystals depend strongly on their size. Due to quantum confinement their conduction and valence bands have new discrete structures. In this regime the role of phonons and exciton-phonon interactions in the dissipation of energy is not clear. We used femtosecond laser pulses to excite phonon wavepackets in CdTe semiconductor nanocrystals in order to study their properties. The excited wavepackets modulated the pump-probe signal and oscillations were observed. Their frequencies correspond to the longitudinal optical phonons in bulk CdTe (162 cm^{-1}). The phonons are coupled to the $1S\text{-}2S_{3/2}$ exciton state.

To study how quantum confinement affects the exciton-phonon interactions, we synthesized crystals with different sizes. The results from the pump-probe experiments showed that the energy of the phonons and the exciton-phonon coupling strength are independent of the particles' size (absence of quantum confinement). However, the phonon wavepacket dephasing times are size-dependent: particles with smaller diameters

have shorter dephasing times, while particles with larger diameters have longer dephasing times. The loss of coherence in the phonon wavepacket happens by an alternative deactivation pathway, most likely a nonadiabatic surface crossing to the nanocrystals' surface states, and not by multiphonon processes. **Chapter 5.2:** Many inorganic photovoltaic devices suffer from poor conversion efficiencies.[3] Heteromaterial semiconductor nanocrystals, in which p-n type junctions are attained through growing two different materials on top of each other in a single rod structure (CdTe over CdSe seed), were recently synthesized and suggested to possess properties suitable for photovoltaics.[4] We studied the charge transfer dynamics in type-II CdSe/CdTe donor-acceptor nanorods using broadband femtosecond pump-probe spectroscopy. Our results revealed that photoinduced electron transfer occurs in 500 fs. Thus, electron transfer on this timescale is comparable to electron transfer in dye-sensitized solar cells and can compete with the ultrafast relaxation processes in quantum confined nanocrystals.[5]

Chapter 6: Pyrene derivatives attached to the sidewalls of SWNT are used for the construction of photovoltaic devices, but there are rather few studies on the optical and electronic properties of the basic SWNT-pyrene complex (SWNT-Pyr). In initial efforts toward finding suitable pyrene derivatives for efficient charge separation processes, we investigated the properties of SWNT-Pyr. For this purpose, SWNT were dispersed in aqueous solutions of pyrenebutyric acid. Using multiple extraction steps, we successfully isolated SWNT-Pyr. The optical spectroscopic properties of the complex suggest that there are strong electronic interactions between pyrene and SWNT that change the properties of the pyrenebutyric acid.

Finally, **Chapter 7** provides a brief discussion of my views for future research directions/experiments that could contribute to the advancement of the scientific fields touched in this dissertation.

2 Experimental methodologies

2.1 Femtosecond UV-Vis pump-broadband probe spectroscopy

2.1.1 Introduction

Femtosecond broadband pump-probe spectroscopy is the central experimental technique used for all investigations presented in this dissertation. It measures the change in the absorptivity of a system excited by a laser pulse with respect to the absorptivity of the same but unexcited system. The absorption change is recorded at different delay times. The pump-probe spectra give direct information about the temporal evolution of the excited states of molecules or inorganic crystals. Understanding the photoinduced processes in novel materials is critical for the successful construction of photonic devices. For example, electron transfer after a photon absorption event is an important process in the work of photovoltaics. Thus, understanding the electron transfer dynamics and the competing nonradiative and radiative relaxation processes is of major importance in the development of efficient devices. Femtosecond pump-probe spectroscopy can be successfully applied to study such processes in various materials and phases (solid, liquid and gas).

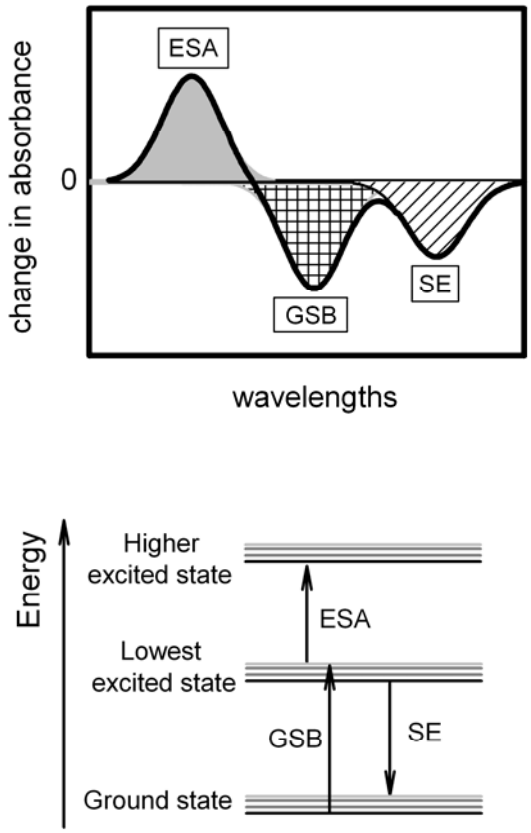

Figure 2.1 Signal contributions to the pump-probe spectrum (upper graph) and energy level diagram depicting the transitions contributing to the spectrum (bottom graph). The solid line represents the pump-probe spectrum. ESA, GSB and SE are abbreviations for excited state absorption, ground state bleaching and stimulated emission, respectively. GSB and SE bands correspond to the absorption and emission spectra.

.

An advantage over the common pump-probe spectroscopy technique is the use of broadband probe pulses to recording a pump-probe spectrum that provides detailed information about the spectral shapes, bandwidths, shifts and their change with the time. A typical spectrum can consist of three signals that arise from different transitions in the investigated system: (i) excited state absorption (ESA) is a positive signal arising from the light absorption of the already excited with the pump pulse states; it gives direct information about the properties of the excited states (ii) ground state bleaching (GSB) is a negative signal; it follows the initial depopulation and the consecutive repopulation of the ground state (iii) stimulated emission (SE) is a negative signal corresponding to the fluorescence spectrum of the system. Figure 2.1 illustrates a principle pump-probe spectrum and the corresponding transitions in an energy level diagram.

2.1.2 Femtosecond UV-Vis pump-broadband probe spectroscopy setup

A schematic representation of the UV-Vis pump-broadband probe setup is included in Figure 2.2. The light source used to generate both, pump and probe pulses, is a commercially available fiber oscillator with Ti:Sapphire chirped pulse amplifier (CPA-2010 Clark-MXR) producing a 1 KHz, 150 fs FWHM, 775 nm, 1 mJ (1W total power) pulse train.

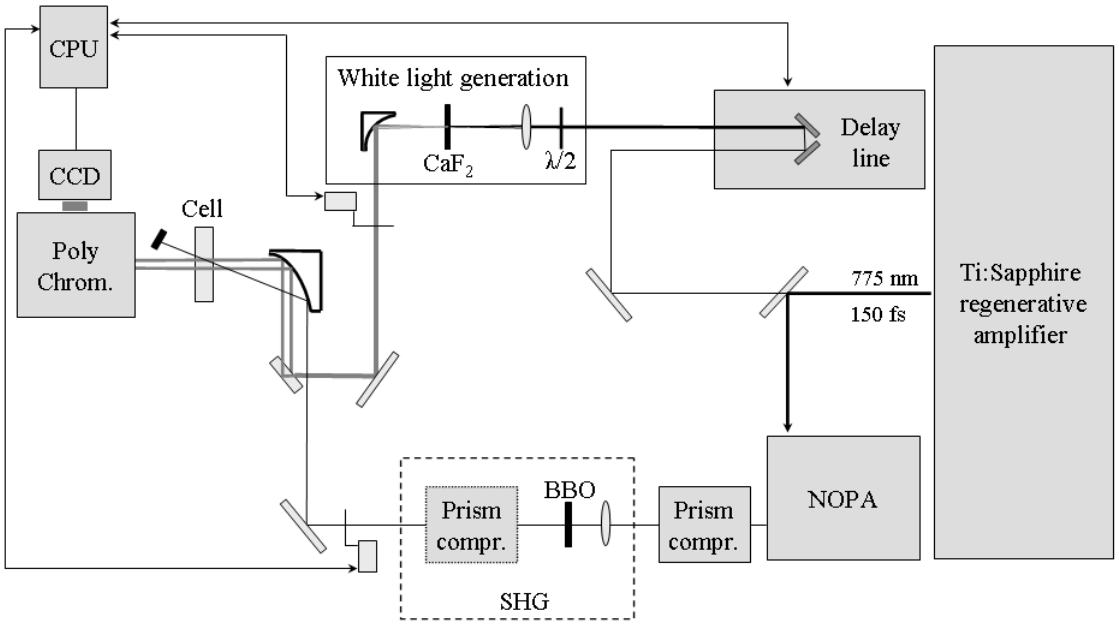

Figure 2.2 Schematic representation of the femtosecond broadband pump-probe experimental setup. The output of the laser is divided into two beams by a beam splitter. One beam is used to power the NOPA where the tunable pump pulse (450-720 nm, 30-40 fs) is generated. When UV pump pulses are desired the NOPA output is doubled with a BBO crystal and compressed to achieve ~70 fs pulses. The second beam is passed through a mechanical delay line and then focused in a CaF_2 plate to generate the white-light continuum used for probing.[6-9]

Approximately, one third of the laser output is split into two beams with uneven energies. The high energy beam (<320 μJ) is sent to a home-built non-collinear optical parametric amplifier (NOPA) for the generation of pump pulses and the second low energy beam (~2 μJ) is used for the generation of the broadband probe pulses.

The dual stage NOPA produces chirped pulses that are tunable between 450-720 nm and have energies of about 1-10 μJ.[10] The output pulses are compressed with two prism compressor to yield pump-pulse with 30-40 fs duration assuming a Gaussian shape.[11] For the investigations of the excited state dynamics of DNA hairpins UV pulses were received by second harmonic generation. The compressed output of the NOPA was focused in a β-barium borate (BBO) crystal (100 μm thickness) for frequency doubling, thus, achieving 240-350 nm pulses. Consecutively, the UV pulses were sent to a second prism compressor to compensate for the newly arisen chirp. Because the phase matching bandwidth of BBO is limited to 7 nm, the pulse was broadened to ~70 fs. In addition to the UV and VIS excitation wavelengths, the dual-stage NOPA enables the generation of NIR pulses by utilizing the Idler pulses that are generated during the amplification process. After a desired wavelength and pulse-width have been achieved, the pump beam is focused into the sample and spatially overlapped with the probe beam.

The broadband probing pulses are generated by tightly focusing the second part of the output of the laser (~2 μJ, 775 nm) in a rotating 3 mm thick CaF_2 crystal.[6-9] Rotation is necessary in order to avoid damage of the crystal. The resulting broadband probe beam is collimated by 30° off-axis parabolic mirror with off-axis focus length – 77 mm and then passed through two filters with high reflectivity at 775 nm to cut-off the fundamental 775 nm wavelength. Typically, the white-light received from this procedure has a spectrum from 310-750 nm. However, when other input excitation wavelengths are used, broadband light in the UV or NIR can be produced. Figure 2.3 shows the range of probe

wavelengths that can be covered using CaF_2 by pumping the crystal with three different seed wavelengths.

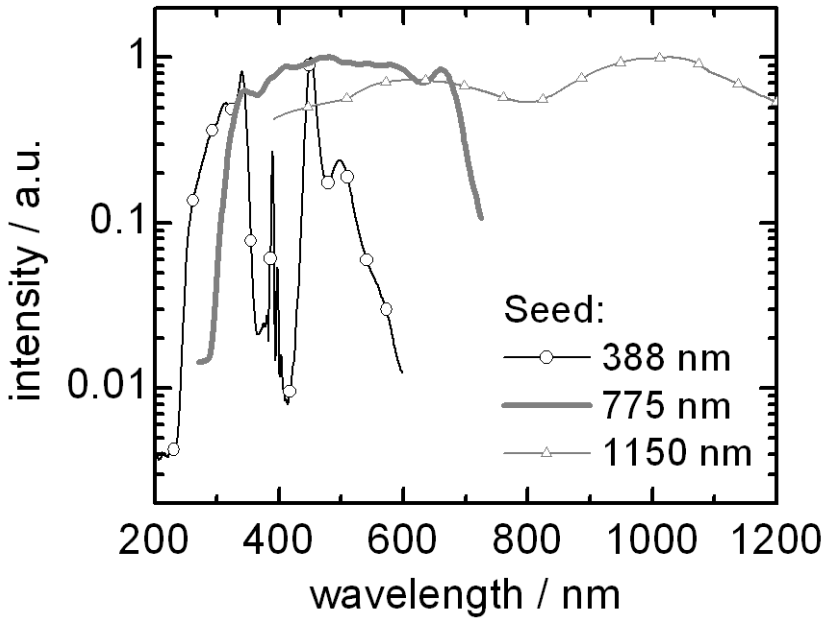

Figure 2.3 Normalized broadband spectra generated by pumping a CaF_2 crystal with a 150 fs laser pulse at 388 nm, 775 nm and 1150 nm.

2.1.3 Measurement principle

A measurement of the pump-probe spectrum requires two probe pulses; one is to be a reference and the second to be a probe. Hence, the broadband beam is spatially split in two beams using a wedged beamsplitter. The reflection from the front surface of the beamsplitter (4%) produces the probe beam, and the reflection from the second surface is

the reference. Subsequently, the two beams are directed to a parabolic mirror that focuses them into the sample. The probe and the pump are overlapped completely in the sample (spot size ~200-600 μm), while the reference passes through a different sample volume, far enough to avoid any overlap with the pump beam. Although the pump and the probe beam overlap, they are set to have an angle of ~5°. This is done to spatially separate their course and prevent the pump from entering into the spectrometer. Only the probe and reference beams are detected by a CCD array independently and simultaneously. The sample cells used in all experiments have 1 mm light path and 1.25 mm fused silica windows.

An imaging polychromator disperses the two beams before they are detected by the CCD array that is cooled down to -10°C. During the completion of this dissertation two different spectrographs were used: Oriel spectrograph Model 77400 and TRIAX 180, Jobin Yvon. For better sensitivity of the experiment the signals were recorded in four step cycles. One shutter is put on the path of the pump beam and another on the probe/reference beams.[12] The signals are collected for all possible combinations of opened and closed shutters and because probe and reference are measured separately the total number of data collections in the software sums to eight. The following signals are recorded for a full cycle:

$I^{pr+p}_{(probe)}, I^{pr+p}_{(ref)}$ – all shutters are open;

$I^{pr}_{(probe)}, I^{pr}_{(ref)}$ – the pump shutter is closed but the probe shutter is open. The CCD camera records the spectrum of the probe and reference beam superimposed to noise;

$I^{p}_{(probe)}, I^{p}_{(ref)}$ – the probe shutter is closed but the pump shutter is open. Emission, scattering and noise are recorded;

$I_{(probe)}, I_{(ref)}$ – all shutters are closed. Background noise is recorded.

Transient pump-probe signals are received by the formula:[12]

$$OD = -\lg\left[\left(\frac{I^{pr+p}_{(probe)} - I^{p}_{(probe)}}{I^{pr+p}_{(ref)} - I^{p}_{(ref)}}\right) \Big/ \left(\frac{I^{pr}_{(probe)} - I_{(probe)}}{I^{pr}_{(ref)} - I_{(ref)}}\right)\right]$$

For a better signal-to-noise ratio the cycles are repeated and thus few hundred pulses are recorded and integrated for obtaining a single spectrum.

A computer controlled translational stage (PI-M5.11) with 0.2 μm step resolution was used for delaying the probe pulse with respect to the pump pulse. The time window for all measurements is 2 ns. In a solution, molecules have different orientations and thus their transition dipole moments will be randomly aligned with respect to the laser pulses. Therefore, after excitation the diffusion of the molecules alters their relative orientations and produces unwanted signals in the transient spectra. To avoid contributions from these different orientation signals the polarization of the pump and the probe pulse were set to 54.7° (using λ/2 plate). The overall time resolution of the experiment is 100-120 fs. The spectral resolution of the setup for the 320-750 nm region is 7-10 nm.[10]

2.1.4 Chirp correction

The broadband probe pulses travel through multiple optical elements (filters, sample cell front, etc.) before they interact with the pump pulse in the excited sample volume. Because of group velocity dispersion (GVD), the white-light continuum (broadband probe pulse) is chirped. (Figure 2.4) GVD is the accumulation of different group delays of the different spectral components of the white-light continuum. Typically, for our instrument the spectrum is spread over 1-1.5 ps. Therefore, different spectral components of the white-light continuum are absorbed by the excited sample at different delay times. This difference is compensated by a procedure that consists of initial experimental determination of the delay times of the white-light components and subsequent recalculation of the chirp “free” pump-probe spectra in the software.

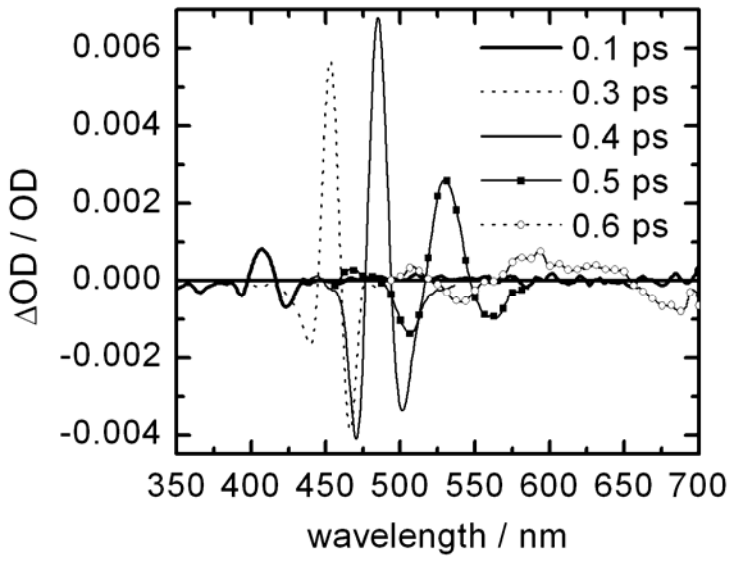

Figure 2.4 Cross phase modulation (XPM) artifact generated in dichloromethane.

A convenient way to experimentally determine the chirp involves a standard measurement of the broadband pump-probe spectra of a pure solvent placed in a typical sample cell. It is based on cross-phase modulation (XPM), a nonlinear process resulting from the interactions between probe and pump pulses in the solvent.[13-16] The XPM signals are difficult to describe using a Gaussian shape and moreover the chirp determination is complicated by the decrease in the accuracy of the measurement in the red part of the spectrum. However, this method of time-zero correction yields satisfactory results. The time delay of the maximum of the XPM signal at different wavelengths, which gives the relative time delay between all probe wavelengths, is fitted with a continuous function that is then used in the recalculation of the measured spectra. Simply,

the time vector from the data matrix is shifted for each detected wavelength. Due to the fact that the data matrix is discrete, but the function is continuous, the optical density between two data points is received by linear interpolation. In the herein presented work, analyses of single wavelength kinetics were performed with raw non-chirped data.

2.1.5 Data analysis

The typical data analysis procedure starts with plotting the pump-probe spectra (Figure 2.5) to first identify the spectral features described in the previous section – ESA, bleaching and stimulated emission. Subsequently, single wavelength kinetics are analyzed by numerical deconvolution of an instantly rising spectral component $F_\lambda(t)$ with an experimental response function assumed to be a Gaussian function g(t).[10,17]

$$g(t) = \frac{1}{\sqrt{\pi}\sigma} \exp\left[-\left(\frac{t - \tau_0}{\sigma} \right)^2 \right]$$

$F_\lambda(t)$ is set to be a sum of i-number exponents.

$$F_\lambda(t - \tau) = \sum_{i=1}^{n} c_i \exp\left[-\left(\frac{t - \tau}{\tau_i} \right) \right]$$

The temporal evolution of the single wavelength signal is given by the following equation:

$$S_\lambda(t) = \int_{-\infty}^{t} g(\tau) F_\lambda(t-\tau) d\tau$$

The analytical solution of the integral is:

$$S_\lambda(t) = \sum_{i=1}^{n} \frac{c_i}{2} \exp\left[-\frac{1}{\tau_i}\left(t - \tau_0 - \frac{\sigma^2}{4\tau_i} \right) \right] \left\{ 1 - erf\left[\frac{1}{\sigma}\left(t - \tau_0 - \frac{\sigma^2}{2\tau_i} \right) \right] \right\}$$

Here τ_i is the time constant and c_i is the amplitude of the component *i*; *erf* is the error function; the full width at half-maximum of the experimental response (t_{FWHM}) is related to $\sigma = t_{FWHM} / 2\sqrt{\ln 2}$; τ_0 is the time shift parameter that is used in the determination of the physical time-zero. Finally, fitting with this function against the experimental data yields all these parameters. Usually, they are compared to the results from a second complementary analysis carried out with a commercial software package, Surface Xplorer Pro (Ultrafast Systems, LLC), with which both single wavelength and global fitting can be performed.

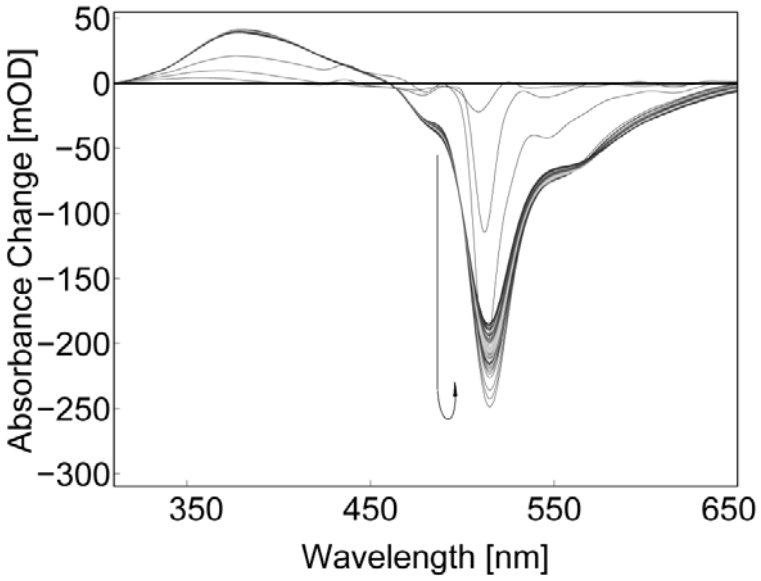

Figure 2.5 Typical temporal evolution of the pump-probe spectra of thiazole orange (surrogated in DNA) in the time range -0.1 ps to 10.0 ps. The excitation wavelength is 515 nm. The arrow shows the temporal evolution of the pump-probe spectrum.

2.2 Steady state spectroscopy

Fluorescence spectra were measured using Fluorolog-3, Jobin Yvon Inc. and 1 cm fused silica sample cells were used. The absorption of the samples at the excitation wavelengths was kept < 0.1. Also, for quantum yield determinations the sample and reference absorptions were kept the same. Steady-state absorption spectra were recorded with a Varian Cary 50 spectrometer. All experiments were carried out at room temperature.

3 Excited states and ultrafast relaxation in double-stranded oligonucleotides

3.1 Introduction to DNA photophysics

The absorption of UV light by DNA could lead to irreversible photochemical reactions that can cause genetic mutations and ultimately to the formation of cancerous cells.[18-20] However, only a small number of the excited DNA molecules in the cells undergo such reactions.[21] How does DNA dissipate the excess energy after absorption of photons so effectively that damage is not a frequent event? On the other hand, why are there any photochemical reactions induced by UV-light and what are the mechanisms of product formation? These questions have puzzled scientists for over 40 years and only after the development of femtosecond lasers and powerful computational techniques, the field of DNA photophysics achieved significant advancement.[21-23]

Most of the solar spectrum reaching the surface of the Earth is above 290 nm (light with higher energy is absorbed in the atmosphere) and from the DNA constituent molecules only the nucleobases absorb light above this wavelength.[24,25] During the early work in the field of DNA photophysics, in the 1960s, it was believed that the UV absorption spectrum of the natural DNA is simply a linear combination of the spectra of the nucleic acid constituents.[25, 26] Therefore, the photostability of DNA, which is of great importance for the existence of life on Earth, should depend exclusively on the properties of the nucleobases. However, extensive experimental and theoretical work have shown

that the excited states of single-stranded (ss) and double-stranded (ds) oligonucleotides are different from that of the monomeric bases. To date, the nature of these states and their extent of delocalization (the number of bases over which the excitation energy is distributed) have not been fully elucidated. It is known that most of the excitations are not localized on a single base, but instead predominantly delocalized. Also, they have lifetimes significantly longer than the lifetimes of the monomer bases. The investigations presented in this dissertation provide another step towards the full understanding of the excited state properties of DNA.

In this section of chapter 3, I introduce the reader to the research that has contributed to our present understanding of the excited state properties of single bases (3.1.1) and oligonucleotides (3.1.2).

3.1.1 Single bases

The nucleobases are remarkably photostable under illumination with UV light.[27] They have very low fluorescence quantum yields, on the order of 10^{-4}, due to very fast internal conversion to their electronic ground states.[24] In the case of adenine, less than 200 fs are required for the excited state population to decay to the ground state.[24,28-30] The mechanisms governing this ultrafast relaxation are relatively well understood. They involve very effective non-radiative channels during which excess energy in the form of heat is dumped into the surrounding bath.[21,27]

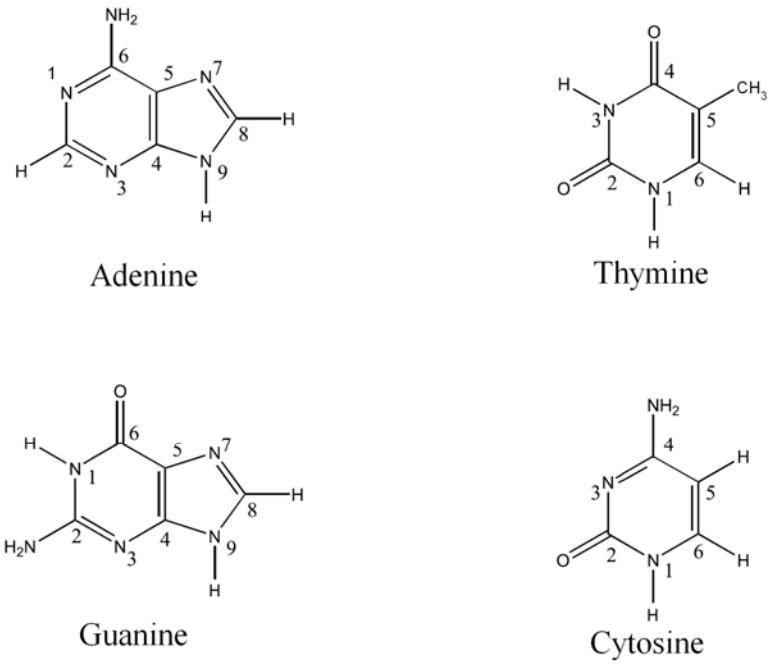

Figure 3.1 Structures of the four nucleobases: adenine (A), thymine (T), guanine (G) and cytosine (C).

The absorption spectrum of the bases is composed of transitions to bright $^1\pi\pi^*$ states. In addition, the bases have closely lying dark states ($^1n\pi^*$, $^3\pi\pi^*$ and $^3n\pi^*$) that do not significantly contribute to the spectrum; instead, they can be populated through internal conversion or intersystem crossing. After the absorption of UV photons, that is the initial population of the lowest energetically $^1\pi\pi^*$ states, vibrational relaxation along the excited state potential surface brings a wavepacket to a conical intersection (CI) with the ground state. For the pyrimidine bases, the CI is accessible by out-of-plane motions of the C_5 substituent which are induced by pyramidalization of the C_5 atom and lengthening of the double bond between C_5=C_6. (See Figure 3.1 for structures) For the purine bases, the out-

of-plane motions are induced by twisting of the C_2=N_3 bond. Due to these almost barrierless CIs, the passage of the wavepackets between the two potential surfaces is fast and efficient. However, during the surface crossing the bases are far from their equilibrium structures. In order to reach the bottom of the ground state potential surface they undergo large scale molecular motions and energy transfer to the environment. For example, in adenine, the internal conversion from the bright $^1\pi\pi^*$ state dissipates 4 eV of energy into the hot ground state, which then lives for approximately 2 ps.[21]

Although most of the excited states in pyrimidine bases relax by internal conversion, femtosecond pump-probe spectroscopy measurements revealed that pyrimidines have a second (minor) channel for energy relaxation. The states mediating this channel have been assigned to singlet $^1n\pi^*$ states.[31,32] Only the population of states with a dark character, such as $^1n\pi^*$, can explain the lack of a second time component in the emission decays recorded with a femtosecond fluorescence upconversion technique and furthermore the solvent dependent lifetimes of thymine, 1-cyclohexyluracil and 5-fluorouracil (derivatives of the natural bases).[27,31,32] Therefore, the absorption of photons from pyrimidine bases populates bright $^1\pi\pi^*$ states that have two competing pathways for relaxation. Most of the excited-state population decays to the ground state directly through internal conversion, whereas a small amount of the bases relaxes to the singlet $^1n\pi^*$ states.[33-37] It should be noted that the purine bases relax only by internal conversion directly to the ground state and monoexponential decays were recorded both from time-resolved absorption and fluorescence measurements.

In addition to the singlet relaxation channels, the pyrimidines have triplet states that are populated with very low quantum yields.[21,32,38-40] For example, for 1-cyclohexyluracil the quantum yield for triplet formation is <1%. The exact mechanism for the intersystem crossing is still a matter of debate. It is unclear whether the triplets are populated from the intermediate $^1n\pi^*$ or the bright $^1\pi\pi^*$ state.[21,32,38-40] However, the importance of the triplets for the photostability of DNA should not be underestimated. Regardless of their low quantum yields, they have very long lifetimes and could serve as precursors for the photochemical reactions damaging the nucleobases in DNA.

3.1.2 Oligonucleotides

The excited states of nucleobases and the mechanisms governing their relaxation to the ground state are an inseparable part of the discussion on the DNA properties. Nevertheless, due to the structure of the α-helix, the photophysical properties of the bases are altered and even their monomer character lost when they become part of DNA. Today, the main controversial points between scientists are whether the excitations in DNA are localized on a single base or delocalized over a number of bases in the stacks; and whether exciton or exciplex states are formed with (or after) light absorption.

There are several factors that are decisive for the fate of the excited states in DNA. They are hydrogen bonding between bases of opposing strands, electronic interactions between bases in the base stacks, the structural inhomogeneity and the structural

fluctuations of the macromolecule. The absorption spectrum of DNA bears similarity with the spectrum of the single bases; thus, suggesting that all of the listed factors do not significantly influence the excited states of the bases. Recent quantum chemical calculations on 4-aminopyrimidine included in a base-stack showed that steric hindrance and coulombic interactions do not restrain the ring puckering leading to the conical intersections (described in the previous section).[41] As a result, the excited state of this base was estimated to relax roughly with the same time constant as the free base in aqueous solutions. As a matter of fact, the sub-picosecond relaxation of the singlet excited states of the bases can explain the photostability of DNA, that is, the lack of frequent damage with the absorption of UV-light. Nevertheless, the hypochromism of the absorption at 260 nm and the strong circular dichroism effects observed for both single- and double-stranded oligonucleotides with different base sequences suggest that *there are* indeed interactions between bases without which the above properties would not be observed.[42]

In the 1960s Eisinger et al. showed that the excited states of DNA dimers have properties different to that of the monomers.[25,26] These authors measured the fluorescence spectrum of concentrated dimer and monomer nucleotides at 77 K and observed that the emission from the dimers is broader and red-shifted compared to the monomers. The changes in the fluorescence spectrum were attributed to an excimer and exciplex formation. By definition excimers and exciplexes are dynamically formed states, which are not directly excited by photons, but instead they are formed after nuclear rearrangements of the neighboring bases. Note that in this case, the Frank-Condon states

are localized on a single base, and consecutively energy and electronic charge is transferred to the neighboring bases. Excimers are "homo-dimers" and exciplexes are formed from two different bases "hetero-dimers". They have partial charge transfer character as the degree of charge separation is determined by the constituent bases and their difference in the redox potentials.[22,43] For clarity, the term exciplex is adopted in this discussion. In 2004 Crespo-Hernandez et al. reported that the excited states of synthetic single-stranded adenine polymers, measured by pump-probe spectroscopy, decay orders of magnitude more slowly than the excitations in the monomers.[44] Following this work, more groups have reported longer lifetimes for both single- and double-stranded oligonucleotides with various base sequences.[45-51] Based on these observations it can be concluded that excited state relaxation in DNA occurs at least ten times slower than in the corresponding single bases. [21,45]

One possible explanation of the elongated lifetimes is that electrostatic and steric effects, due to both base stacking and base pairing, slow down or inhibit the motions of the bases during internal conversion. This model is supported only by quantum chemical/molecular mechanics calculations on a single adenine incorporated in $(dA)_{10}(dT)_{10}$ duplex, but experiments do not show such evidence.[52] Instead experimental data discard this possibility: Femtosecond fluorescence anisotropies of poly(dA)poly(dT) and single bases behave differently;[53] Also, the isotope effects observed for alternating $(AT)_n$ and $(GC)_n$ duplexes do not exist for the corresponding mononucleotides.[45,54,55]

Ever since the pioneering work of Eisinger et al., excimers have been frequently invoked in discussions on the DNA photophysics.[26] Typically, the assignment of excimer formation in oligonucleotides is based on observations of broad red-shifted emission and elongated lifetimes.[45,46,50,56] Kohler et al. measured the transient absorption of single strand $(dA)_{18}$ and double strand $(dA)_{18}(dT)_{18}$ with femtosecond time resolution and found that both oligonucleotides decay with similar time constants. Based on their results, they concluded that intrastrand dAdA excimers are formed in single- and double-stranded structures.[45] Furthermore, Kwok et al. proposed that there could be two distinct excimer states with different lifetimes existing in the oligonucleotides.[46,56] However, no further explanation was provided for the difference between the two types of excimers. The most important conclusion from these studies is that for nonalternating DNA oligonucleotides vertical base stacking and *not* base pairing determines the mechanisms for singlet excited states relaxation.[45] Unlike the dA-rich sequences, dT oligonucleotides do not have states with a collective character as they decay in mononucleotide fashion.

In principle, fs time-resolved spectroscopy should be able to resolve the formation of the exciplexes, which would manifest itself as a rise (i.e. negative amplitude) in the transient signals. However, such a rise time component has never been observed, and there are two possible reasons for that. First, not all excited bases in the oligonucleotides participate in the formation of "collectively excited" states. Hence, overlap of the signals from single bases and exciplexes complicates the detection of the exciplex formation. Second, the excimer formation may be faster than the instrument response functions (<100 fs), which suggests that excimers are formed after very minor nuclear

rearrangements. The latter consideration, however, is counterintuitive because of the aforementioned strongly red-shifted emission bands, which imply large scale motions of the molecules and thus a slower excimer formation.

Markovitsi et al. argued that dAdA excimers are not responsible for the emission from $(dA)_n$ and $(dA)_n(dT)_n$ oligonucleotides, because the steady state fluorescence spectrum of poly(dA) and poly(dA)poly(dT) do not coincide as poly(dA)poly(dT) peaks at 327 nm and poly(dA) at 360 nm.[57,58] Femtosecond fluorescence upconversion (detects emission decays on the femtosecond time scale) and time-correlated single photon counting (records emission decays at longer ns time scales) experiments showed that the emission decays multiexponentially as most of the emission oscillator strength, i.e. the signal, is "lost very quickly" for a subpicosecond.[49,58,59] Hence, the steady-state emission spectrum of DNA originates predominantly from bright states with ps lifetimes.[60]

Very important for the assignment of the bright emitting states were fluorescence anisotropy measurements with 100 fs resolution performed by the Markovitsi group.[49,58,59] The anisotropy of the oligonucleotides at the earliest detectable times is lower from that of the mononucleotides. Also, in the course of the first ps (the time during which most of the emission has decayed) the anisotropy of the oligonucleotides decays, while the anisotropy of the mononucleotides stays constant. Based on these observations, it was suggested that a multitude of delocalized Frenkel excitons are excited in DNA upon photon absorption.[58,61-64] In the molecular exciton theory, applicable for molecular aggregates, such excitons are linear combinations of the excited

states of each of the monomeric chromophores.[65,66] In DNA, the exciton delocalization is induced by the dipolar interactions between bases in the base stack and is strongly dependent on the conformation of the molecule. Calculations by Markovitsi et al., which included conformational disorder by sampling molecular dynamics simulations, showed that the excitons can be delocalized over several bases. [61-64] In the case of a perfect double helix with 20 base pairs, the delocalization extends over the full length of the oligonucleotide.[63] On these grounds, it was proposed that: 1) the absorption of UV-light excites delocalized excitons, which then relax by internal conversion through the manifold of states until the bottom of the exciton band is reached and 2) the energy and the lifetime of the lowest energy excitons depend strongly on the conformation of the system.[49,58,59]

The Fiebig group first provided experimental estimate of the extent of exciton delocalization in homo-adenine DNA systems.[47] Broadband pump-probe spectra of ss $(dA)_n$ oligonucleotides with different lengths were compared. Excitons were found to span over 3 to 4 bases in the base-stacks. More detailed explanation of the procedure used in the determination of the exciton delocalization can be found in Chapter 3.2, where similar analysis is performed for dA-dT duplexes. Theoretical calculations agree well with our experimental results.[67,68] Specifically, Tonzani and Schatz calculated the exciton delocalization in $(dA)_n$ (n = 2, 4, 6, 9, 11) and found that excitons extend over 3 bases.[68] They used molecular dynamics simulations to model the structures of the oligonucleotides and derived the exciton delocalization by finding the bases with molecular orbitals participating in the first absorption band. The absorption spectra were

calculated at the level of DFT. Conwell et al. also estimated that excitons in ds $(dA)_n(dT)_n$ delocalize over several bases.[67] These authors focused on the properties of charge transfer excitons and proposed that in ds oligonucleotides the charge transfer excitons have energies close to the energies of the lowest transitions.

The role of base pairing in the photophysics of DNA is discussed in this paragraph. In 2005 Crespo-Hernandez et al. compared the decay dynamics of transient pump-probe signals from alternating and nonalternating dA-dT duplexes upon exchanging H_2O with D_2O.[45] They observed that the lifetimes of the alternating structures – but not the nonalternating – were influenced by the solvent substitution. Very similar results were obtained in subsequent experiments with alternating $(dGC)_9 \cdot (dGC)_9$.[55] The alternating duplexes have elongated lifetimes in D_2O. In addition, femtosecond fluorescence upconversion experiments showed that the emission from a single dG-dC base pair decays faster than the emission from the mononucleotides.[69,70] To achieve stable hydrogen bonding between dG and dC Schwalb et al. substituted the deoxyribose unit with non-polar tert-butyldimethylsilyl and used chloroform solvent instead of water. An explanation for the listed observations were sought from a previous theoretical calculations on dinucleotides.[71-73] They concluded that proton-coupled electron transfer (PCET) plays an important role in DNA energy dissipation. Both intra- and interstrand electron transfer could promote almost barrierless proton transfer between bases. [55,71-74] In that case, the lack of isotope effects for nonalternating oligonucleotides could be explained either by the extent of exciton delocalization or the degree of charge

separation. A large delocalization and a small degree of charge separation could result in a decrease of the driving force for proton transfer.

In the preceding paragraphs four general mechanisms for excited state relaxation in DNA were discussed. They are summarized as follows:

a) UV light excites single bases that consecutively rearrange to form excimers or exciplexes in the base-stacks;

b) UV light excites charge transfer states that serve as precursors for proton transfer between bases;

c) Exciton states are populated with the absorption of UV light. The degree of exciton delocalization depends on the base sequence, rigidity of the structures and dynamical fluctuations;

d) UV light excites single bases. They decay by an intrinsic monomer mechanism and do not form collective states. Because of steric hindrance and coulombic interactions, the lifetimes of the states increase.[75]

Although there is a controversy about the exact mechanism for excited state relaxation in DNA, it is possible and maybe even likely that all of these four models are to some extent valid and responsible for the photophysical properties of DNA.[74] Only recently one more general model has been proposed. Using pump-probe spectroscopy Takaya et al. estimated the excited state decay rates of series of dinucleotides.[43] Then, the rates were plotted against the driving force for charge recombination between the dimers. The

gas-phase ionization potentials of the donor base and the electron affinity of the acceptor base were used in the calculations of the driving force. The results from the plot were indicative for electron transfer in the inverted Marcus region. Following this study unified picture for the excited state relaxation of DNA was finally shaped.[22,74] UV-light excites collective, delocalized excitonic states, which then relax by intraband scattering through the exciton state manifold. When the bottom of the band is reached, the excitons "collapse" to form exciplexes that consecutively recombine to the electronic ground states. The degree of charge separation in the exciplexes depends on the redox potential difference $\left(E^{red}_{base1} - E^{ox}_{base2}\right)$ between base one and two. It can vary from highly polar contact ion pairs to non-polar excitonic resonance states.[22]

The investigations on the excited state properties of DNA have come a long way since the field of DNA photophysics emerged in the early 1960s.[26] However, it is evident that there are several schools of thought, which propose different mechanisms for exited state relaxation.[22,46,53,69,72,74,75] Most of them are strongly influenced by the experimental technique used in the investigations or the theoretical approach undertaken. Thus, the nature of the excited states and their relaxation mechanisms need further assessment and many questions are yet to be answered before we can claim to fully understand the photophysics of DNA. Some of these questions are: What is the nature of the Frank-Condon states in DNA? What is the extent of delocalization of the states, especially in more realistic double-stranded sequences? How do structure and its static and dynamic fluctuations influence the relaxation of the excited states? What is the role of base pairing and proton transfer in double-stranded sequences?[22,27,67,74]

The results presented in the next two sections of this chapter provide answers to some of the above questions. Particularly, I focused on investigating the length dependent optical properties of double-stranded dA-dT and dG-dC oligonucleotides. To date, the number of such experimental studies is scarce as most of them have focused on investigating longer structures.[43,47,49,76,77] For our purposes duplexes with different lengths, base sequences and base content were synthesized by the Lewis group at Northwestern University. The analysis of the results from femtosecond pump-probe spectroscopy measurements proved the importance of excitons in the relaxation dynamics of DNA. The extent of exciton delocalization and the existence of charge transfer excitons are discussed. Also, in a separate section, I discuss the inherent uncertainty of spectroscopic studies of biological systems with complex structures such as DNA. **Chapter 3.2** presents my studies on the length dependent properties of dA-dT duplexes and **Chapter 3.3** is devoted to dG-dC duplexes.

3.2 Excitons and exciton delocalization in double-stranded dA-dT oligonucleotides

3.2.1 dA-dT duplex structures

In order to study the size dependent properties of the excited states of double-stranded oligonucleotides, short nonalternating and alternating adenine and thymine hairpins with different length were synthesized. (Figure 3.2) The nonalternating structures have single uninterrupted deoxyadenosine strand that is connected by an alkane linker (12 carbons) to a second strand of deoxythymines. The shortest hairpins are four bases long while the longest have eight bases in the stacks. One alternating sequence **$(dAT)_3(dAT)_3$** was synthesized, too. Double-stranded oligonucleotides with a small number of bases are thermodynamically unstable in aqueous solutions and unfold to form ss structures. However, by linking two single strands with desired base sequence using an alkane chain, we are able to fabricate short duplexes that fold into stable B-DNA structures. The alkane linker has little if any influence on the excited states of the duplexes as evidenced by CD measurements and melting temperature curves. The chief advantage of the Fiebig/Lewis approach – which is described here – is the fact that they use structurally well-defined short duplexes. These model duplexes allow the systematic “aufbau” of double-stranded oligonucleotides and thus the probing of length-dependent spectroscopic properties. Note that such a degree of structural control is absent in all of the competitive studies.

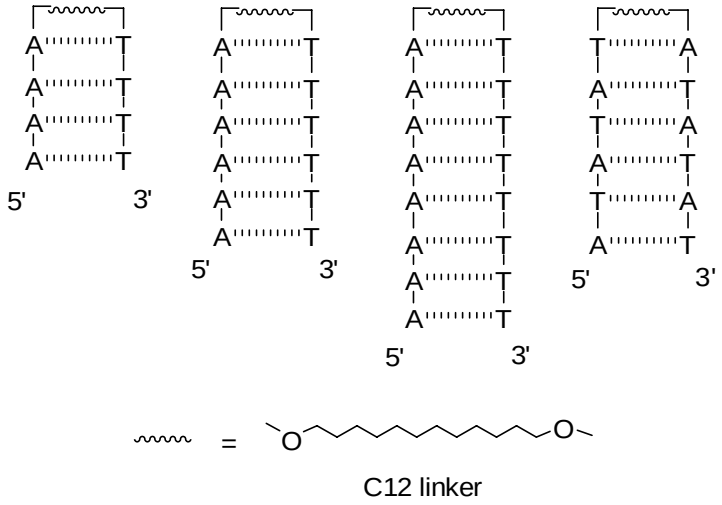

Figure 3.2 Structures of short DNA duplexes, from left to right: **$(dA)_4(dT)_4$**, **$(dA)_6(dT)_6$**, **$(dA)_8(dT)_8$**, and **$(dAT)_3(dAT)_3$**. Their melting temperatures are 35.0°, 54.1°, 59.7° and 49.6°C respectively.

3.2.2 Femtosecond broadband pump-probe spectroscopy results

One of the key advantages of fs broadband spectroscopy is the fact that one can simultaneously monitor the time-dependent population changes of multiple excited states.[45-47] The transient spectrum of ss and ds oligonucleotides is dominated by overlapping signals from localized on single base and delocalized over more than one base states.[46,47,56] In the present study we used white-light continuum extending from 310 to 700 nm to record the pump-probe spectra of the duplexes. For a control we measured ss adenine oligonucleotides (A-tracks) with 4, 6 and 8 bases in the stacks and a ds **$(dAT)_9(dAT)_9$** oligonucleotide. All experiments were carried out under the same experimental conditions (buffer, excitation wavelength, pump-pulse energy and

wavelength) which allowed us to make comparison between the excited state properties of the duplexes and the A-tracks. Samples were dissolved in 0.01 M sodium phosphate buffer (pH = 7.2) containing 0.1 M sodium chloride.

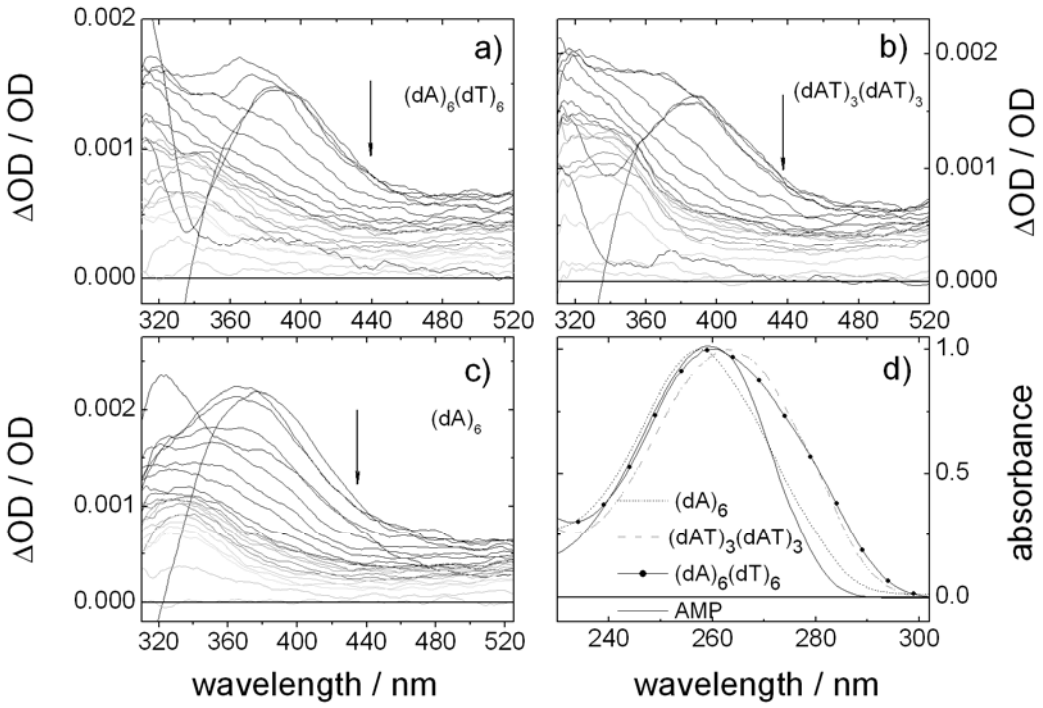

Figure 3.3 Temporal evolution of the pump-probe spectra of a) **$(dA)_6(dT)_6$,** b) **$(dAT)_3(dAT)_3$** and c) **$(dA)_6$** in the time range of 0.0 ps to 1.8 ns after excitation at 270 nm. Early spectra are shown in blue/green colors and late spectra in orange/red colors. Steady state absorption spectra normalized at the maximum of the ~260 nm band is shown in d).

Figure 3.3 exhibits the pump-probe spectra of **$(dA)_6$**, **$(dAT)_3(dAT)_3$**, **$(dA)_6(dT)_6$**. Right after excitation the spectra of the oligonucleotides consist of a band at ~370 nm that decays rapidly on a sub-1 ps time scale with the appearance of a new band with maximum around 335 nm. This band has a lifetime of a few hundred ps. There is a slight but noticeable red-shift of the maximum for the alternating structures (**$(dAT)_3(dAT)_3$** and **$(dAT)_9(dAT)_9$**) to that of the nonalternating sequences that could be attributed to different interactions between A-A and A-T bases in the stacks. As a matter of fact, the difference in the electronic coupling between neighboring bases in the ground state is clearly demonstrated by the steady state spectra (Figure 3.3d)), where **$(dAT)_3(dAT)_3$** shows a 5 nm red-shift at the lowest energy absorption band to that of the nonalternating structures.

3.2.3 Single wavelength fitting results

The analysis of the pump-probe spectra begins with single wavelength kinetics fitting of the ESA at 345 nm. Three exponents were needed for satisfactory fits for all investigated systems. From Table 1 we notice that the time constants of the nonalternating duplexes and the A-tracks remain unchanged for different lengths of the oligonucleotides. Moreover, the lifetimes of the A-tracks are very similar to those of the nonalternating duplexes. On average, the excited states of all nonalternating systems relax to the ground state with $\tau_1 \sim 0.5$ ps, $\tau_2 \sim 8$ ps and $\tau_3 \sim 200$ ps. These time constants are consistent with previously published data.[46,56] Crespo-Hernandez et al. first observed

that nonalternating ss dA and ds dA-dT oligonucleotides have similar decay dynamics and attributed this behavior to excimer formation.[45] According to these authors the excitation energy delocalizes only along the adenine base stack without the involvement of any interstrand states. Also, dT oligonucleotides decay to ground state by internal conversion for less than one ps.[45]

345 nm	c_1[%]	τ_1 [ps]	c_2[%]	τ_2 [ps]	c_3[%]	τ_3 [ps]
$(dA)_4(dT)_4$	64 ±2	0.50±0.03	17 ±1	9 ±1	20 ±1	200 ±20
$(dA)_6(dT)_6$	59 ±3	0.40±0.03	21 ±1	6 ±1	20 ±1	170 ±15
$(dA)_8(dT)_8$	58 ±2	0.55±0.04	23 ±2	8 ±1	19 ±1	190 ±25
$(dAT)_3(dAT)_3$	49 ±2	0.47±0.03	20 ±1	11 ±2	31 ±2	90 ±6
$(dAT)_9(dAT)_9$	32 ±3	0.39±0.05	30 ±3	17 ±2	38 ±3	120 ±10
$(dA)_4$	68 ±1	0.47±0.02	10 ±1	5 ±1	22 ±1	195 ±10
$(dA)_6$	65 ±1	0.55±0.02	10 ±1	12 ±2	25 ±1	210 ±15
$(dA)_8$	63 ±1	0.57±0.02	14 ±1	10 ±1	23 ±1	205 ±10
AMP	94 ±1	0.31±0.01	7 ±1	3.1±0.4		
TMP	98 ±175	0.01±0.03	2.0 ±0.2	1.3±0.2		

Table 1 Results from exponential fits of the temporal evolution of the ESA spectral components at 345 nm. The errors were estimated as described in **Chapter 2.1.5**.

Although the time constants obtained from our fits are independent of length and structures (ds vs. ss), the amplitudes of the components vary substantially with increasing length of the oligonucleotides. Specifically in the duplexes, the amplitude of the second component c_2 increases from 17% for **$(dA)_4(dT)_4$** to 23% for **$(dA)_8(dT)_8$**. This change

occurs in expense of the first time component which loses amplitude from shorter to longer duplexes; c_1 is 64% for **$(dA)_4(dT)_4$** and 58% for **$(dA)_8(dT)_8$**. Finally, the third longest component stays relatively unchanged for any duplex size. The A-tracks show length dependent behavior similar to that of the duplexes with one exception, that is, the changes in the amplitude with increasing length are not as pronounced as they are in the duplexes. Furthermore, although the A-tracks and duplexes exhibit similar length dependencies, the distribution of the three amplitudes are clearly different. In the A-tracks, c_3 is higher than c_2 and on the opposite, for the duplexes, c_2 is slightly higher than c_3.

3.2.4 Excitons in dA-dT duplexes

In previous experimental studies, the fast sub-ps time constant in the pump-probe spectra has been consistently assigned to relaxation of the bright $^1\pi\pi^*$ states of bases with mononucleotide character.[45,47] It is known that long oligonucleotides have improved base stacking.[47] Therefore, upon excitation of longer duplexes and A-tracks fewer bases will have mononucleotide character, i.e. fewer bases will decay with sub-ps lifetimes. Our results indicate toward similar behavior. The amplitude of τ_1 decreases with increasing length of the oligonucleotides. Accordingly, we assign τ_1 to the lifetime of excitations localized on a single base.

From Chapter 3.1 we know that excitons and excimers could – in principle – coexist in DNA.[22,43,74] The excitons serve as precursors for the formation of the longer living excimers.[21,22] Kohler suggested that exciton lifetimes are shorter than 100 fs.[74] On the other hand, Kwok et al. argued that instead of excitons there are two different types of excimers formed in ss A-tracks: shorter (~10 ps) and longer (~200 ps) living.[46,56] Nevertheless, these authors were unable to define the differences between these excimers. Using our length dependent data we are now able to confirm our previous prediction that excitons are formed in DNA and that they have lifetimes of >100 fs – approximately ten ps. However, first we elaborate on the proposal of Kwok et al. Due to the flexibility and the uncertainty of the structures of ss oligonucleotides it is reasonable to assume that they exist in different structural configurations. Therefore, τ_2 and τ_3 can in fact be the lifetimes of two different excimers. Another possibility is that excimers formed at the edges of the base stack can decay by different mechanisms than the excimers formed at the core of the base-stack. The former may involve stronger solvent contributions and larger nuclear reorganization in both formation and decay due to increased exposure to water, caused by fraying. We note that the lifetimes of the two different excimers estimated by means of femtosecond fluorescence upconversion and pump-probe spectroscopy are identical to the lifetimes of our second and third components. Thus, our size dependent data does not exclude the possibility for excimer formation. However, we are able to distinguish between the two states by comparing the kinetics of the duplexes with different lengths. We assign the short ps component to delocalized excitons and the long component to states with size-independent properties, most probably excimers. This conclusion is based

on our observation that the amplitude of the states, decaying with ~8 ps, increases with increasing length of duplexes and A-tracks. There are two factors that can influence the exciton delocalization. First, with increasing length of the oligonucleotides more bases become available to participate in the electronic excitation delocalization. Second, conformational disorder and stacking distance decrease with increasing length of the oligonucleotides which can lead to stronger electronic coupling between the bases; hence, longer exciton delocalization and higher oscillator strength of the transitions.[49, 78] Table 1 shows that for the A-tracks the amplitude of the excimer states (τ_3 ~ 200 ps) is higher than that of the excitons (τ_2 ~ 8 ps). Single-stranded oligonucleotides have less rigid structures with larger number of structural defects and unstacked bases (see amplitude of the first component). Moreover, dynamic fluctuations are more important in single-stranded structures than in the duplexes. Therefore, excimer formation and not exciton delocalization should be considered as a more favorable pathway for energy dissipation in the ss oligonucleotides compared to the double stranded duplexes. To conclude, three distinct states play a role in the relaxation dynamics of the investigated duplexes: 1) localized single base excitations that are $^1\pi\pi^*$ states; 2) longer living states that are weakly length dependent and could be assigned to dynamically formed excimers; and 3) delocalized exciton states that could directly decay to the ground state or populate the lower energetically excimers and live for tens of ps.

3.2.5 Extent of exciton delocalization in dA-dT duplexes

In the following part of the discussion we estimate the extent of exciton delocalization by performing an analysis similar to the one in our previous experimental work on ss adenine oligonucleotides.[47] At early times, the pump-probe spectra presented in Figure 3.3 consist of a band with maximum at ~370 nm that has been assigned to absorption from two different excited states. As we already showed, there are two types of bases in the investigated duplexes poorly-stacked and well-stacked. The absorption of UV-light from the former excites $^1\pi\pi^*$ states, while the absorption from the latter excites delocalized excitons. Because the steady-state absorption of the oligonucleotides and mononucleotides are almost the same, the similarity between early time spectra of the mononucleotides and oligonucleotides is anticipated. However, there are small but significant differences between their spectra. For example the steady-state absorption band of the ss adenine oligonucleotides is blue-shifted with ~3 nm and has larger full-width at the half maximum compared to AMP. Interestingly, the comparison between the pump-probe spectra of **$(dA)_6$** and AMP at three different times (0.08, 0.11, 0.14 and 0.17 ps) revealed the same differences. (Figure 3.4) Therefore, in addition to the localized, single base transitions (from unstacked bases) exciton states with various degrees of delocalization are being populated upon absorption of photons. In fact, only exciton states can explain the low fluorescence anisotropy on the femtosecond time scale measured for nonalternating and alternating dA-dT oligonucleotides.[49,59] In addition, several theoretical works used quantum chemical and exciton theory calculations to show that the Frank-

Condon states in oligonucleotides are delocalized excitons.[61,63,64,67,68,79] The decay of the monomer $^1\pi\pi^*$ states is observed in the pump-probe spectra by sub-ps disappearance of the band at 380 nm. At the same time, the excitons are expected to scatter through the multitude of exciton states until the bottom of the band is reached (~335 nm in the pump-probe spectrum).[22,49,58,59] This process takes only 100 fs, and consecutively, the "trapped" excitons relax for tens of ps to form the excimer states or directly relax to the ground state.

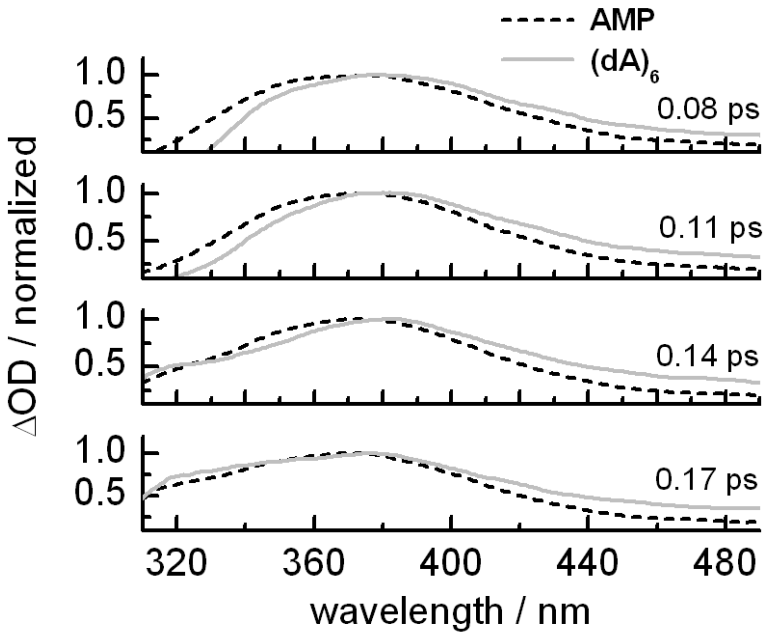

Figure 3.4 Comparison of the early time spectra of AMP to that of **$(dA)_6$** at four different time delays.

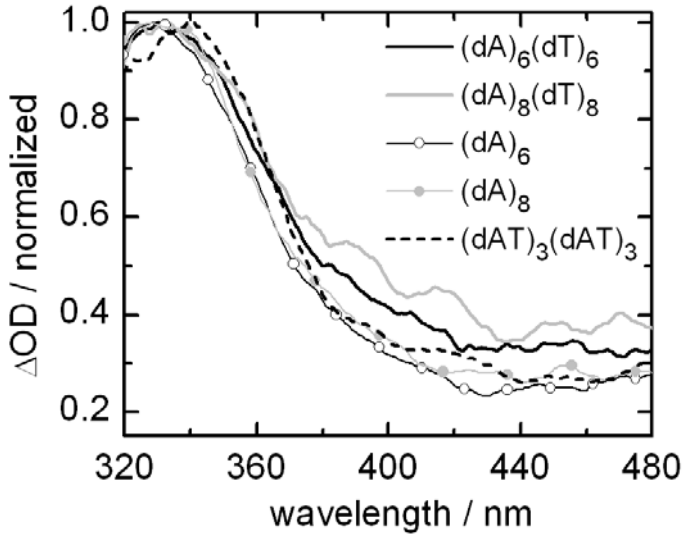

Figure 3.5 Averaged normalized spectra from 5 ps to 9 ps of **$(dA)_6$**, **$(dA)_8$**, **$(dA)_6(dT)_6$**, **$(dA)_8(dT)_8$** and **$(dAT)_3(dAT)_3$**.

From Figure 3.5, which compares the averaged normalized pump-probe spectra between 5 and 9 ps for **$(dA)_6$**, **$(dA)_8$**, **$(dA)_6(dT)_6$**, **$(dA)_8(dT)_8$** and **$(dAT)_3(dAT)_3$**, it is clear that the excited state absorption above 380 nm depends on the length and the structure of the DNA systems. Consistent with our previous interpretation, we believe that the observed spectral variations are a clear manifestation for exciton delocalization. The ESA spectrum above 380 nm results from interchromophoric interactions and reflects the electronic delocalization in the systems, while the band with maximum at 330 nm results from local transitions. In order to determine the extent of delocalization, we

followed the procedure used in ref. 47.[47,80] Shortly, the intensity ratio "ρ_{435}" between the long-wavelength 435 nm band (result of interchromophoric transitions) and the maximum at ~330 nm (result of local transitions) was calculated for all investigated systems. The following observations emerge from plotting ρ_{435} as a function of the number of bases in the stacks "n", see Figure 3.6. The ratio ρ_{435} for the nonalternating duplexes increases with their lengths; it is substantially higher than for their corresponding ss counterparts. Therefore, we can assume that in longer duplexes the excitons are delocalized over more bases. Also, the comparison between ss A-tracks and duplexes confirms the conclusion from the previous section (**Chapter 3.2.4**) that excitons tend to be more delocalized in the more rigid and better ordered duplex structures. In Figure 3.6, we have compared our results with the data points from Buchvarov et al. (light gray bars).[47] There is a good correspondence between past and present experiments which confirms the reproducibility and consistency of our results. However, from the available ρ_{435} values we can only vaguely conclude that the exciton delocalization in nonalternating dA-dT duplexes extends over ~4-6 bases.

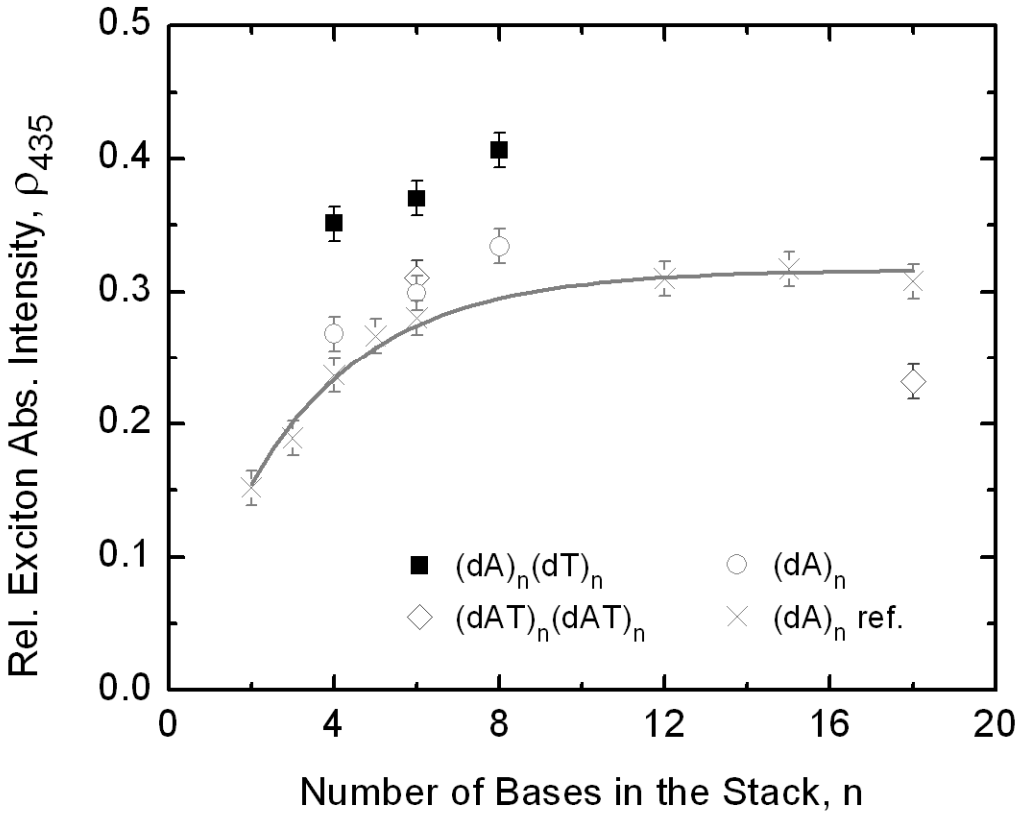

Figure 3.6 Exciton absorption intensity (3 ps after excitation) as a function of the stack length. Data from reference 47 was plotted with gray circles and the exponential fit with a gray line.

Finally, the alternating sequences show different behavior from that of the nonalternating ones. Clearly, disruption of the dA-dA stacks with dT leads to the reduction of the size of the delocalized exciton domains. Indication for the different

properties of the alternating sequences is already available from experiments reporting the existence of isotope effects only for alternating structures.[45,54,55,69] Charge transfer excitons and proton-coupled electron transfer might play a role in the subsequent of the excited base states in DNA relaxation.[45,54,55,67,69,72,73] However, this latter point remains speculative at the current time.

3.2.6 Conclusion

We used broadband femtosecond pump-probe spectroscopy to investigate the length dependent properties of the excited states of short synthetic dA-dT duplexes that form stable double-stranded structures at room temperature. The results from this work provide a more complete picture of the electronic energy delocalization in ds DNA oligonucleotides. We found that the extent of exciton delocalization in nonalternating duplexes increase with their length and is larger than that in ss oligonucleotides. Moreover, the difference between alternating and nonalternating structures was discussed. Our results indicate that the structure of the modeled DNA systems play a crucial role in the decay dynamics of the excited states and more rigid ds structures are prerequisite for larger degrees of exciton delocalization.

3.3 dG-dC oligonucleotides: ultrafast relaxation dynamics

3.3.1 Steady state spectroscopy results

In this section the spectroscopic properties of dG and dC duplexes with 2, 3 and 4 bases in a base stack are compared. The structures are shown in Figure 3.7 and the UV/Vis absorption spectra in Figure 3.8. The equimolar mixture of dGMP and dCMP (**dGdC**) was used for a reference system. Note that its absorption spectrum has two peaks at 255 and 270 nm. Thus, it is significantly different from the spectra of the duplexes.

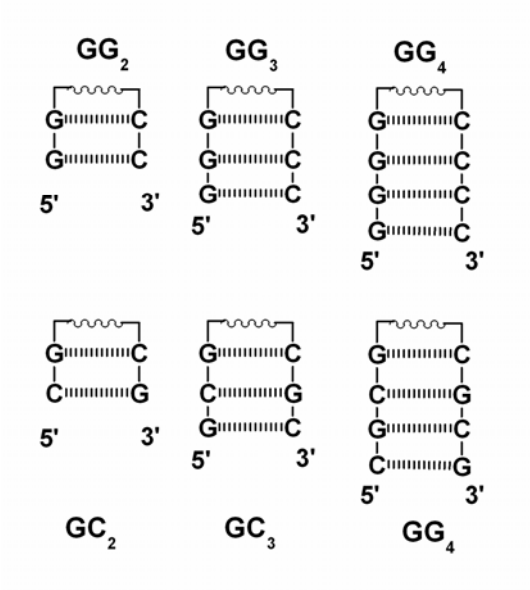

Figure 3.7 Structures of dG-dC duplexes

The absorption spectrum of the duplexes changes in the region of 270 nm where the oscillator strength of the band decreases with duplex length. In **GG$_4$** and **GC$_4$** the band at

270 nm is almost indistinguishable. Also, the intensity of the long-wavelength tail at ~300 nm of the hairpins increases with the number of GC base pairs in the duplex. Although alternating and nonalternating duplexes show similar length dependencies, there are noticeable differences between structures with the same length but different sequence. A representative plot comparing the absorption spectra of **GG_4** and **GC_4** is included in Figure 3.8c. The maximum of the absorption of **GG_4** is hypsochromically shifted to that of **GC_4** with 4 nm. Also, the spectrum of **GC_4** is less broadened than the one of **GG_4**. These two observations are valid for the shortest duplexes with the exception that the shift in the absorption maximum is smaller for duplexes with 3 bases and indistinguishable for the shortest duplexes.

The CD spectra of the duplexes, shown on Figure 3.9, evolve with an increasing number of bases (length). The CD spectrum of the intermediate **GG_3** shares the spectral fingerprints of **GG_2** and **GG_4**. Although the CD signals from **GG_4** can be easily mistaken with signals rising from G-quadruplexes,[69] we exclude the possibility for quadruplex formation in our samples based on studies on similar hairpins (in them a hexamethylene glycol linker was used instead of C_{12}) showing that the CD effects we observe indicate the formation of B-DNA structures.[81,82] The alternating sequences have also CD signals indicative for B-DNA conformations.

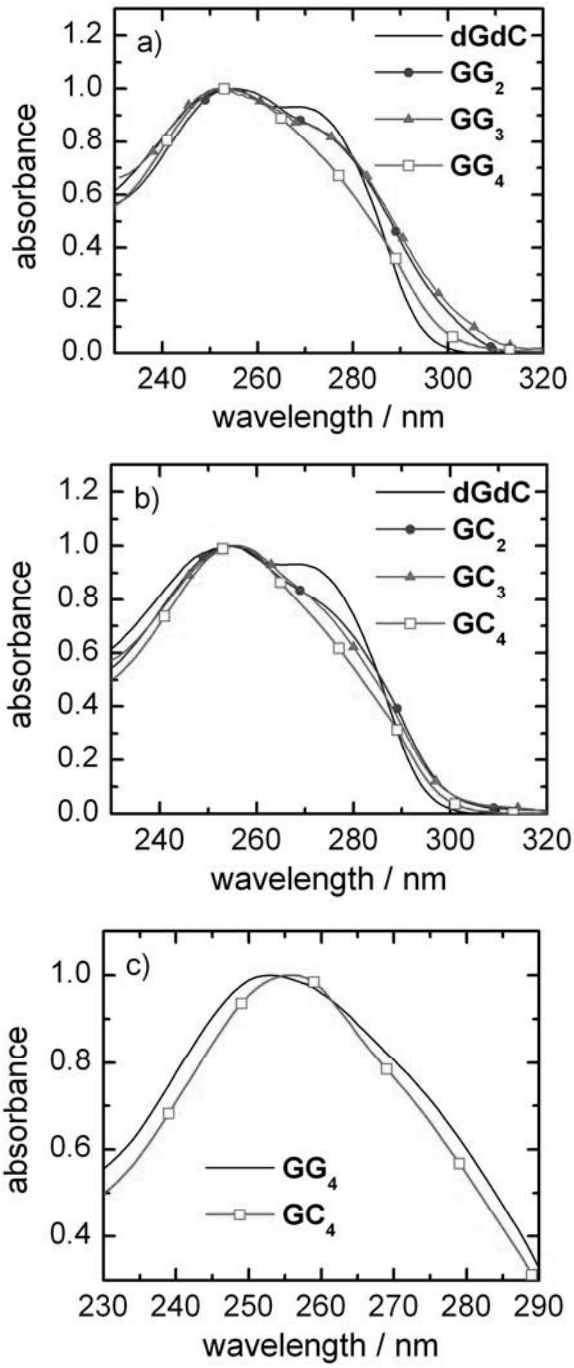

Figure 3.8 Normalized absorption spectra of a) nonalternating duplexes, b) alternating duplexes and c) comparison of the normalized spectrum of GG4 to GC4. All spectra are normalized at the absorption maximum ~255 nm.

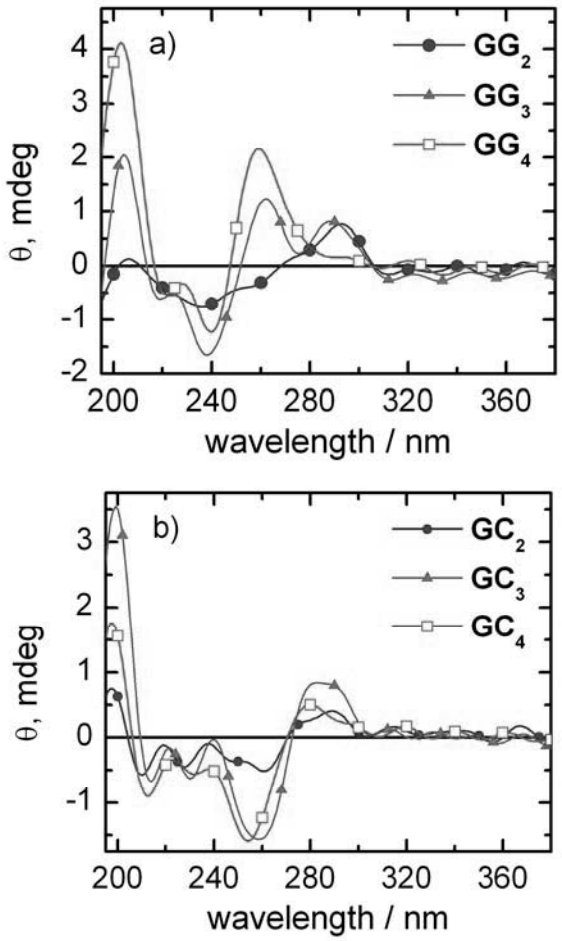

Figure 3.9 Circular dichroism spectra of a) nonalternating duplexes and b) alternating duplexes

The UV/Vis absorption and CD spectra presented above suggest that there are strong electronic interactions between bases in the investigated systems. To explore them further we measured the emission spectra and determined the quantum yields of all nonalternating duplexes. The emission properties of alternating sequences have been

investigated in the past.[77,83] An aqueous solution of phenol was used as a reference in the QY determinations. The excitation wavelength was set to 275 nm.

To test the validity of our experiments we determined the QY of dGMP to be 1.2×10^{-4}, which agrees well with the literature values.[28] All nonalternating duplexes have emission spectra that differ from the spectrum of **dGdC** (broadening and bathochromic shift of the bands are observed, Figure 3.10) Their quantum yields are 4 to 8 times higher than the corresponding mononucleotides; $\mathbf{GG_4}$ – 5.3×10^{-4}, $\mathbf{GG_3}$ – 8.3×10^{-4} and $\mathbf{GG_2}$ – 3.7×10^{-4}. Furthermore, the duplexes themselves show different emission: $\mathbf{GG_4}$ and $\mathbf{GG_3}$ have band with maximum at 395 nm and $\mathbf{GG_2}$ at 430 nm. Based on the steady-state spectroscopy measurements it can be concluded that the duplex constituent bases lose their mononucleotide character when incorporated in the duplex structures. Moreover, due to the difference in the electronic interactions between AT and AA bases the UV absorption band of alternating sequences shifts with 5 nm from that of the nonalternating sequences.

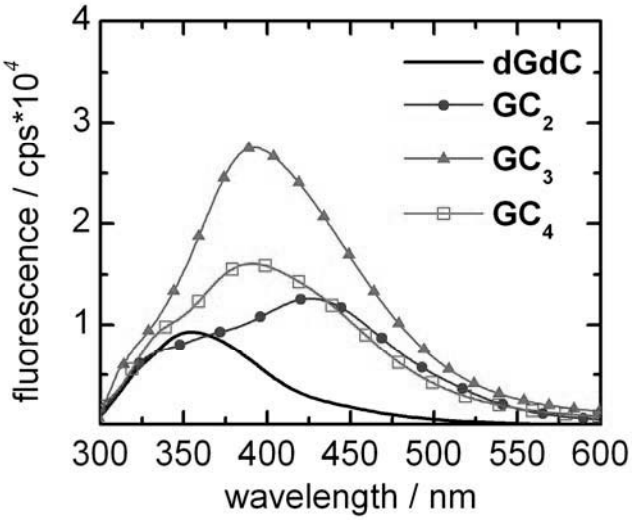

Figure 3.10 Fluorescence spectra of the nonalternating duplexes and **dGdC**. The excitation wavelength was 275 nm.

3.3.2 Time-resolved pump-probe measurements

For the femtosecond pump-probe measurements excitation pulses at 270 nm wavelength were used. All duplexes have similar spectral shape that consists of ESA signals composed of at least two different transitions. A representative plot of the pump-probe spectra of **GG_4** (0.25-50 ps) is shown on Figure 3.11a. The amplitude of the ESA increases gradually toward shorter wavelengths. This signal is due to absorption from the

hot ground state, which peaks deeper in the UV (~290 nm). On the other hand, the excited states of the duplexes absorb in the VIS region.[47]

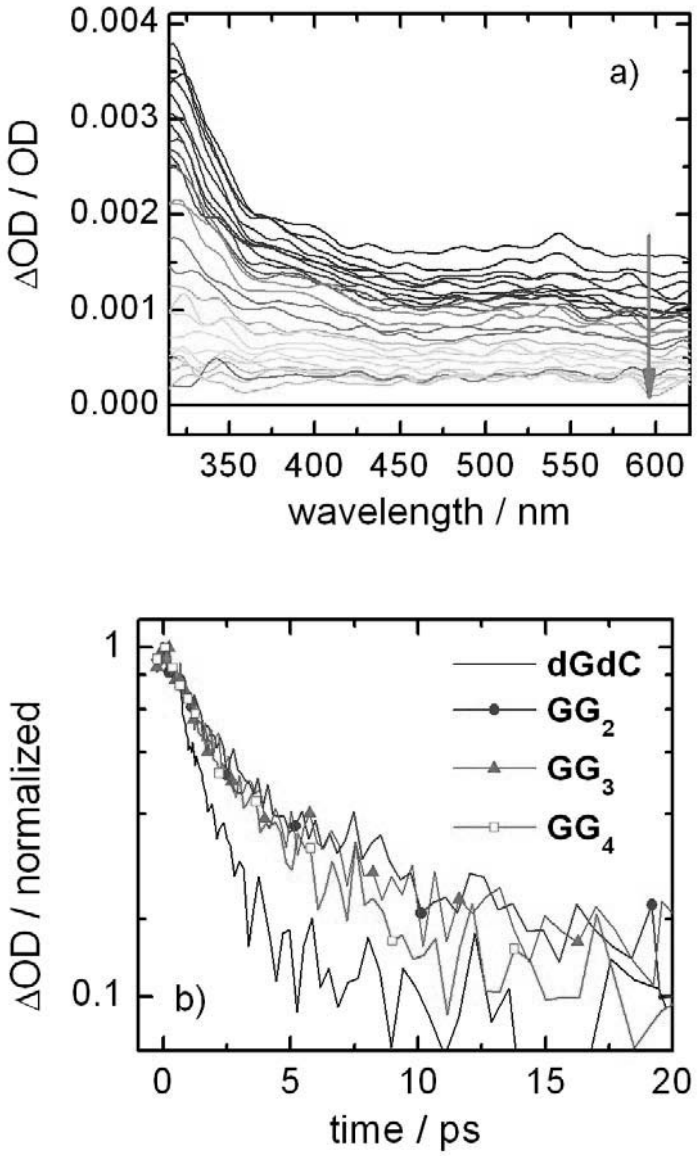

Figure 3.11 a) Representative pump-probe spectra of **GG_4** from 0.25 ps to 50 ps. Pump-pulse is 270 nm. The arrow indicates the temporal evolution of the pump-probe spectra; b) Single wavelength kinetics at 315 nm of the nonalternating duplexes and **dGdC**.

A plot of the temporal changes of the ESA at 315 nm reveals significant differences in the relaxation dynamics of duplexes and mononucleotides.[84] (Figure 3.11b) The duplexes have slower decays than the equimolar mixture. We needed two exponents to fit all kinetics; see Table 2 for results. The ESA of **dGdC** decays with τ_1 = 1.4 ps and τ_2 = 16 ps. The assignment of these time components is straightforward, because the transient signals of **dGdC** are a result of linear combination of the signals from dGMP and dCMP.[46] According to the widely accepted mechanism for excited state relaxation in the mononucleotides (presented in **Chapter 3.1.1)** we assign τ_1 to relaxation of the $^1\pi\pi^*$ states and the subsequent vibrational cooling of the hot ground state and τ_2 to relaxation of the dark $^1n\pi^*$ states of dCMP. However, the duplexes decay with $\tau_1 \sim 2.4$ ps and $\tau_2 \sim 25$ ps. The fast ps time constant does not change significantly with increasing duplex length and is assigned to the relaxation of bases with mononucleotide character.[84] Interestingly, the second time constant decreases with increasing length of the duplexes. Hence, the excited state of the longer $\mathbf{GG_4}$ decays faster than the excited state of the shorter $\mathbf{GG_2}$. This result is unexpected in light of previous time-resolved measurements including our length dependent measurements on dA-dT duplexes.[49] Recently, Crespo-Hernández et al. published femtosecond pump-probe measurements on similar hairpins $d(C_5A_5G_5)$ and $d(C_5T_5G_5)$.[84] In their experiments, only single kinetics at 250 nm and 570 nm were recorded. The temporal evolution of the ESA was globally fitted with two exponents to yield 1.1 ps and 41 ps at 570 nm and 3.0 ps and 41 ps at 250 nm. These results are consistent with our kinetic data. Note that the small difference in the long time

component could be due to the uncertainty of the structure of d($C_5A_5G_5$) and d($C_5T_5G_5$) duplexes and the presence of A and T tracks in their hairpins, which additionally complicates the transient absorption signals. A- and T-rich ds oligonucleotides have lifetimes longer than 100 ps – see **Chapter 3.2**.[47]

315 nm	c_1 [%]	τ_1 [ps]	c_2 [%]	τ_2 [ps]
GG_2	78 ±2	2.6 ±0.1	22 ±2	30 ±5
GG_3	77 ±2	2.4 ±0.1	23 ±2	28 ±6
GG_4	77 ±3	2.2 ±0.1	23 ±3	16 ±3
GC_2	84 ±2	2.3 ±0.1	16 ±2	24 ±6
GC_3	81 ±7	2.7 ±0.3	19 ±8	13 ±6
GC_4	32 ±3	0.9 ±0.2	68 ±4	6 ±0.3
dGdC	91 ±2	1.4 ±0.1	9 ±2	16 ±7

Table 2 Results from exponential fitting of the kinetics at 315 nm. The errors were estimated as described in **Chapter 2.1.5**.

Exponential fitting of the temporal evolution of the ESA in the case of the alternating duplexes (at 315 nm) was satisfactory when two exponents were used. The results in Table 2 show that longer duplexes decay faster than shorter ones. Also, the alternating duplexes exhibit shorter lifetimes than the corresponding nonalternating duplexes. The amplitudes of the time constants change with the length of the duplex. For example, for **GC_2** c_2 is ~16% and for GC_4 c_2 is ~68%. In comparison, c_2 of the nonalternating

duplexes is relatively constant revolving around 23%. Finally, it should be noticed that the results presented in this section show small, but significant differences between duplexes with different length that demand further analysis and discussion.

3.3.3 Discussion

The results from the time-resolved and steady-state spectroscopy measurements revealed significant length and sequence dependencies of the optical properties of the dG-dC duplexes. The excited state lifetimes in these duplexes are shorter for systems with a higher number of bases in the stacks. In agreement with our previous work, we conclude that the size-dependent properties are indicative of the presence of delocalized excitons.

The origin of the changes in the absorption spectrum between mono- and oligonucleotides has been a matter of intense debate over the years.[28,30,45,51,58] In some theoretical studies the change in the spectrum upon base stacking is attributed to Frenkel excitons.[23,61-63,68,85] Others propose that charge transfer states have strong influence on the optical properties of the oligonucleotides.[71-73] In addition to the length dependant absorption spectra presented here only two experimental studies have reported similar results.[49,78] Lewis et al. showed that the absorption maximum of short nonalternating A and T duplexes shifts weakly to higher energies with increasing length of the stacks.[78] In a follow-up theoretical work it was concluded that the electronic coupling between neighboring bases is very weak and that exciton delocalization along the base stack is not

responsible for the blue shifted absorbance.[86] This conclusion is in stark contrast with the interpretation of the results in reference 49, where exciton delocalization was used to explain the band shifts.[49]

In addition to the spectral shifts in the absorption, the fluorescence spectra of the nonalternating duplexes also depend sensitively on the length. (Figure 3.10) **GG_2** has a broad emission band with maximum at ~430 nm, which bears similarity with the emission of ss TG_4T oligonucleotides observed and interpreted by Markovitsi et al. as excimer emission.[87] The CD spectrum suggests that **GG_2** folds in right-handed-like helix that is different from the structure of **GG_4**. (Figure 3.9) Due to the small number of bases (n = 2) and the presence of the hydrophobic C_{12} linker we assume that base stacking in **GG_2** is not "perfect" and that its structure deviates from B-form. Note that such a perturbed structure should be more conducive for excimer formation (which requires nuclear rearrangement) and less supportive for exciton delocalization. The same will not be true for the longer **GG_3** and **GG_4**, because their absorption and CD spectra show stronger excitonic coupling. Also, it is known that longer oligonucleotides fold in more ordered and stiffer structures.[47,49] Accordingly, **GG_3** and **GG_4** emission spectra shift to 390 nm. Similar emission spectra were recorded for G-quadruplexes.[87] It was suggested that due to favorable stacking and the rigidity of the quadruplex structures, the exciton coupling between the bases is increased, which would lead to enhanced exciton emission. Similarly, we are tentatively assigning the emission from the **GG_3** and **GG_4** to exciton fluorescence. Nevertheless, a conclusion based only on emission and absorption spectra is not reasonable. To answer the question whether excitons or excimers are formed in the

nonalternating duplexes we need to include the results from the pump-probe measurements.

The pump-probe spectroscopy showed that longer duplexes relax faster than shorter ones. According to the mechanism for energy dissipation in DNA proposed by Kohler et al., the charge separation between two neighboring bases in a stack (this is the formation of an exciplex) happens almost instantaneously after photon absorption.[45,74] Due to the limited time resolution of the femtosecond pump-probe spectroscopy setups used in the studies on DNA photophysics, exciplex formation kinetics have never been resolved. Actually, only charge recombination (exciplex relaxation) is observed.[43,45] Takaya et al. found that the charge recombination rates display "inverted Marcus" behavior.[43] Therefore, when the driving force ΔG_{ET} for charge recombination increases, the recombination rates will decrease. For example, the GC dimer will relax faster than the AT dimer because of its smaller ΔG_{ET}.

Following this logic it is difficult for us to explain the results from our pump-probe measurements. Why does the lifetime (the rate of charge recombination) of the nonalternating duplexes depend on the number of bases in the base stack? If only exciplexes are formed in the nonalternating duplexes, then no matter what the size of the duplex is its lifetime (the rate of charge recombination) should be the same. Moreover, if emission originates only from exciplexes, then the exciplex state in **GG_4** must be higher in energy than that of **GG_2,** since the emission of **GG_4** is blue shifted from that of **GG_2**. Energetically higher exciplexes (in longer duplexes) in the Marcus inverted region should

recombine more slowly than the lower-lying exciplexes (in shorter duplexes). Yet, our results show the exact opposite behavior. Therefore, we conclude that the main species formed in dG-dC duplexes upon absorption of UV light are not exciplexes. Instead, we assign the observed properties to delocalized excitons. We recall previous experimental and theoretical studies by different groups in which the excited state relaxation in ss and ds oligonucleotides was explained by the formation of delocalized excitons.[47,58,63,68]

In addition, there have been proposals that in dG-dC rich ds DNA, when G and C base pairing is present, proton-coupled electron transfer is the main mechanism for excited state relaxation.[55,70,72,73] Nonetheless, recent experiments by Kohler's group showed that nonalternating dG-dC duplexes are not influenced by substitution of H_2O with D_2O. However, isotope effects should be observed if PCET is involved in the relaxation of the excited states. The reason for the lack of PCET in the nonalternating structures is that either excitons are delocalized along the base stack, or that in the C^+C^- and G^+G^- exciplexes charge separation is very weak and cannot enable proton transfer. In both cases, PCET should not influence the excited states decay of the nonalternating oligonucleotides.

3.3.4 Charge transfer excitons in alternating duplexes

In contrary to the nonalternating, the alternating duplexes have longer lifetimes when D_2O is used instead of H_2O for a solvent.[45,54,55] The observation of an isotope effect suggests that different mechanisms for excited state relaxation are in effect for alternating and nonalternating duplexes. It is likely that PCET plays an important role in the excited state relaxation of dG-dC duplexes.[54,55,69] In that case, it is not surprising that there are differences between the pump-probe and the absorption spectra (Figure 3.11 and Figure 3.8, correspondingly) of the alternating to that of the nonalternating sequences, such as shorter lifetimes of ESA and 5 nm shift of the UV absorption maximum. In fact, the alternating $d(AT)_3d(AT)_3$ duplex also shows a ~5 nm red shift of the absorption band compared to $(dA)_6(dT)_6$ and shorter lifetimes. Moreover, the absorption band of the alternating dG-dC duplexes shifts to the red with increasing length. The opposite is seen for the nonalternating structures. This could be due to the different nature of the intra and interstrand interactions between G and C bases and the rise of different types of states such as charge transfer excitons (CT excitons).

In a picosecond transient IR study Doorley et al. found that the excited states of poly$(dGdC)_2$ decay with two time constant 7 ps and 30 ps.[54] Very similar results were published from femtosecond UV/Vis pump-probe spectroscopy experiments on $d(GC)_9d(GC)_9$. In both measurements D_2O was used as the solvent. Interestingly, in the IR study the transient absorption bands do not shift during the first ten ps as opposed to the transient bands of the mononucleotides. The authors proposed that after excitation,

the vibrational energy is rapidly distributed between the bases in the polymer because of exciton delocalization and/or very strong exciton-phonon couplings. Our results show that the lifetime of the excited states of alternating dG-dC duplexes is influenced by their length, (Table 2) which we already proposed to be due to the different extent of exciton delocalization. Based on the observations discussed above, we would like to propose that charge transfer excitons are involved in the excited state relaxation dynamics of alternating ds dG-dC oligonucleotides. This is not the first time CT excitons are mentioned in the context of DNA. Theoretical calculations by Conwell et al. actually suggest that CT excitons exist in ds AT oligonucleotides and that they are delocalized over several bases.[67] The difference between Frenkel and CT excitons is that the Frenkel excitons are neutral species, while the CT excitons posses a dipole moment. Therefore, the solvent around the bases will be polarized by the CT exciton and it will play an important role in the relaxation dynamics of the alternating dG-dC duplexes. Hence, a solvent isotope effect should be observed. Also, Conwell et al. elaborated that the CT excitons can have lower energies than the intrachain Frenkel excitons, because the electron and the hole are more separated (smaller Coulomb interactions) when residing on opposing strands. The polarization of the solvent can also decrease the energy of the CT exciton state. Both effects explain the changes in the absorption spectrum that are observed in our alternating duplexes.

The partial charge separation in the CT excitons can force proton transfer between bases and produce the isotope effects seen only for alternating GC duplexes. Very important is the fact that exciplexes are essentially self-trapped CT excitons and the only

significant difference between them is the extent of nuclear reorganization.[88] Thus, the excess energy is delocalized over two bases for exciplexes and over several bases for delocalized CT excitons. Finally, the notion that CT excitons are formed in our alternating dG-dC duplexes is entirely consistent with our findings and does not reject the present common understanding that a large number of exciplexes are formed in ds alternating GC oligonucleotides.

3.3.5 Pitfalls in the investigations of DNA duplexes.

In the investigations on DNA photophysics, research groups have used different experimental conditions, techniques and sample suppliers.[89] Typically, constantly varied from one laboratory to another are pH, buffer concentration and ionic strength of the solvents. In some instances pure water was used for quantum yield determinations, while time-resolved measurements are usually performed with Na-phosphate buffer at pH ~ 7.[28] This change of solvent, pH, ionic strength, etc. could potentially lead to different structures of the oligonucleotides.

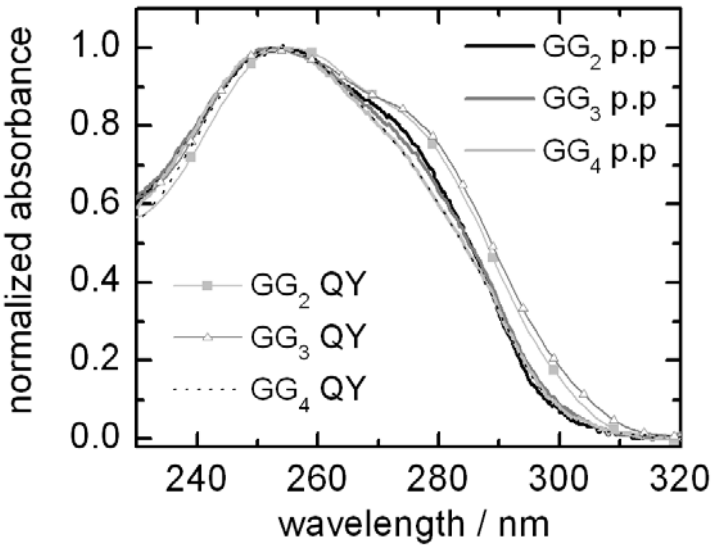

Figure 3.12 Absorption spectra of samples used for pump-probe spectroscopy (p.p) are compared to the spectra of samples used for QY determinations.

In the investigations of the dG-dC duplexes we used Li-phosphate buffer instead of the more common Na-phosphate. This change was provoked by the well known property of G-rich oligonucleotides to form G-quadruplexes and our prediction that the Li-phosphate buffer will suppress this formation while facilitating the formation of stable B-DNA duplexes. Consecutively, the results from the CD, absorption and pump-probe spectroscopy suggested that the duplexes fold in the typical B-DNA fashion. However, only for the determination of the QY Na-phosphate buffer was used. During the later data analysis, it was discovered that the absorption spectra of the same nonalternating duplexes dissolved in Li- or Na-phosphate buffer have small but significant differences. (Figure 3.12) This observation could be explained only with differences in the

oligonucleotide conformations, which of course underscores the findings presented in this section. Presently, more experiments are underway to test the validity of our results and to determine which buffer facilitates the formation of B-DNA-like structures. However, this outcome raises important issues that are typically underestimated in spectroscopic studies of complex biological systems, such as DNA. First, structural determinations must be thorough. Either NMR or X-ray diffraction should be applied for precise structural assignments. Second, a common protocol for spectroscopy measurements has to be established, so that different groups work under the same experimental conditions using the same pH, solvent, etc. Markovitsi's group have already discussed these issues and proposed a list of standard conditions that can be found in reference 89.

4 Thiazole orange dimers as base surrogates in DNA

4.1 Introduction

4.1.1 Molecular beacons

In DNA analytics, nucleic acid recognition probes are used for detection of specific oligonucleotide sequences within the genetic information. Molecular beacons, developed twenty years ago, are a type of recognition probes,[90,91] which are widely used for genetic screening,[92] development of biosensors[93] or microarrays.[94]

Molecular beacons are single-stranded oligonucleotides that fold in hairpin structures.[95] (Figure 4.1) Their termini have a complementary base sequence that hybridizes to form the hairpin, while the rest of the loop is designed to complement a target DNA. In addition, fluorophore and quencher dyes are covalently linked to the 5' and 3' termini. When the molecular beacon forms a hairpin, the two chromophores stay in close proximity and the fluorescence from the fluorophore is quenched by the quencher through energy transfer. In the presence of the target DNA the hairpin opens up and the loop hybridizes with the target. During this process, the quencher is forced to stay apart from the fluorophore and the result is increase in the fluorescence intensity.

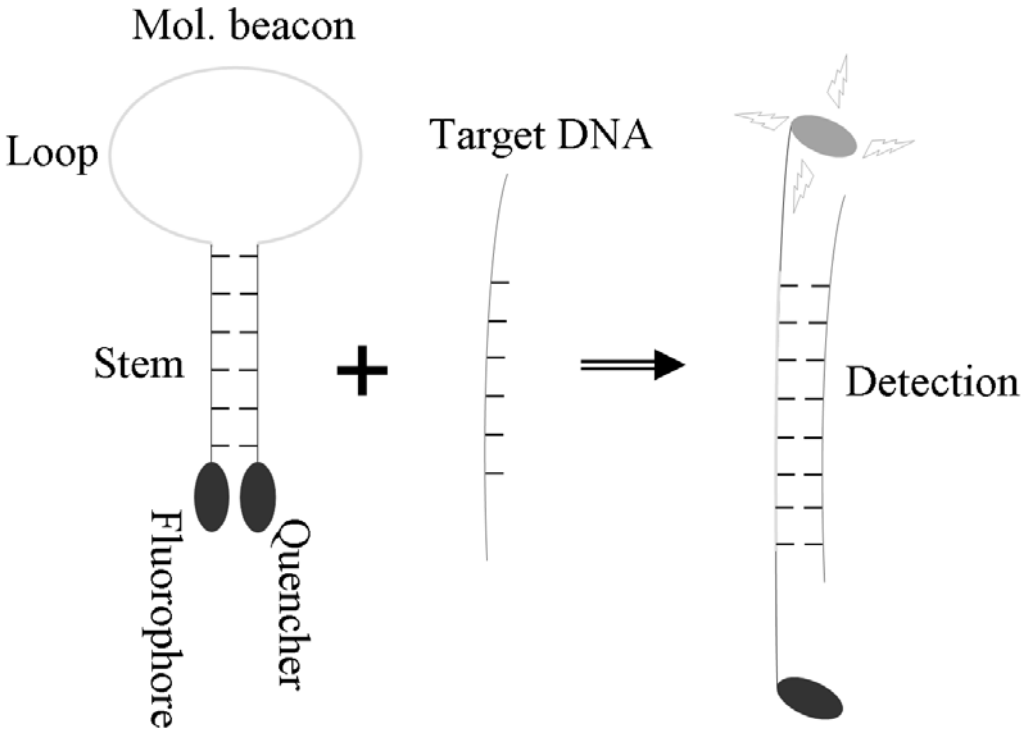

Figure 4.1 A model diagram of molecular beacon and its function.

Molecular beacons display the complementary sequential information through enhancement or decrease of the emission intensities. However, such intensity changes could potentially result from side effects. An inherent problem of the fluorescence read-out recognition is that the detection depends on the emission of a single chromophore, which limits the signal range and lowers the target detection limit. In biological systems undesired quenching is a significant problem. One way to overcome this obstacle is to design molecular beacons capable of *shifting* their emission maximum, instead of or in addition to changes in the emission intensity. Zhang et al. designed wavelength shifting

probes with donor and acceptor chromophores that are based on Förster resonance energy transfer (FRET).[96]

4.1.2 Excimer-type molecular beacons and thiazole orange

Excimer formation is an alternative to the FRET process. For this purpose two identical chromophores with strong excimer emission are linked to the termini. Pyrene has been widely used for such constructs, because of its strong excimer emission and well understood excited state properties.[1,7,97-102] Nevertheless, its absorption in the UV-A range at ~340 nm is a major disadvantage for the detection in biological systems. In order to limit the background fluorescence and enhance the photostability of the probes, excitation wavelengths higher than 450 nm are desirable.

Thiazol orange (TO) has suitable properties to become a promising alternative to pyrene-excimer systems. TO has an oxidation potential ($TO^{+}/TO^{\bullet 2+}$) of 1.4 V vs. NHE and an energy of the lowest excited state of E_{00}=2.4 eV.[103] Hence, TO cannot photoxidize the DNA bases, which is in contrast to pyrene and perylene bisimides (PDI).[104] Furthermore, TO is extensively used as a staining agent[105] or for the detection of single-base variations.[106,107] Recently, Wagenknecht's group reported the synthesis of base surrogated interstrand TO dimers.[2,108] Their emission maximum shifts from the monomer green (520 nm) to orange (580 nm) accompanied with an increase in the emission intensity. The color change can be used as fluorescence readout for multiple applications:

DNA[2] and RNA[108] recognition as well as for excimer-like molecular beacons[2]. Moreover, the fact that TO dimers are applicable in any sequential context provides a great advantage over other fluorophores, especially the PDI dye. [109,110]

4.2 Results and discussion

This work gives a full account of the optical spectroscopic properties of dimeric TO base surrogates in different base-sequence environments. Preliminary steady state spectroscopy results and the synthesis of the oligonucleotides were previously published by our collaborators in reference 2. I utilized time-resolved pump-probe and fluorescence excitation spectroscopy to elucidate the optical properties of the TO dimers.

4.2.1 TO-modified oligonucleotides: synthesis and structures

The synthesis of the oligonucleotides was performed at University of Regensburg by Wagenknecht's group. The protocols for the DNA synthesis are described in references 111, 112. Shortly, thiazole orange was incorporated in a given DNA sequence by substituting the 2'-deoxyribofuranoside with (*S*)-1-aminopropane-2,3-diol as the acyclic linker between the phosphodiesters. This acyclic linker facilitates the synthesis, because it avoids the acid/base labile glycosidic bond that would result between TO as a positively charged heterocycle and the 2'-deoxyribofuranoside. The (*S*)-configuration of

the propandiole linker resembles the stereochemistry at C-3' of the 2'-deoxyribofuranoside, although we found that the stereochemistry of the linker has minor influence on the intercalation properties of the nile blue chromophore.[113] Structurally similar glycol linkers were previously used by others in order to prepare, e.g. glycol nucleic acids,[96,114] and twisted intercalating nucleic acids.[115,116] This type of linking has been used extensively for the attachment of nile blue, ethidium, indole, perylene bisimide, and phenothiazine.[113,117-123] There are two positions at which TO can be attached to (*S*)-1-aminopropane-2,3-diol at the quinoline nitrogen or the thiazole nitrogen. This study concentrates on the second attachment, because the shift of the fluorescence maximum that is important for the work of the molecular beacons was observed only from the thiazole nitrogen attachment.[2]

The spectroscopic properties of the TO dimer were studied in the context of different DNA sequence environments. (Figure 4.2) TO-modified oligonucleotides were identified by ESI mass spectrometry and quantified by their absorbance at 260 nm using an extinction coefficient of 9.400 $M^{-1}cm^{-1}$ for the TO dye.[124] Duplexes were formed by heating of the modified oligonucleotides to 90°C (15 min) in the presence of 1.2 eq. of the corresponding complementary unmodified or modified oligonucleotide strand. **DNA1** represents a reference duplex that has only a single TO surrogate. **DNA2-DNA5** contain the interstrand TO dimer in a similar base pair environment (A-T/T-A), but with varying DNA bases in the counter strand opposite to the TO base surrogate. In a second set of double strands, the adjacent base pairs were also varied: in contrast to **DNA2**, duplex **DNA6** contains the TO dimer in a G-C/C-G environment. In **DNA7** and **DNA8**, the

flanking base pair on one side was swapped. Finally, **DNA9** contains an intrastrand TO dimer; in **DNA10** TO and TO' (TO linked to the quinoline nitrogen) are located in direct contact on the same strand.

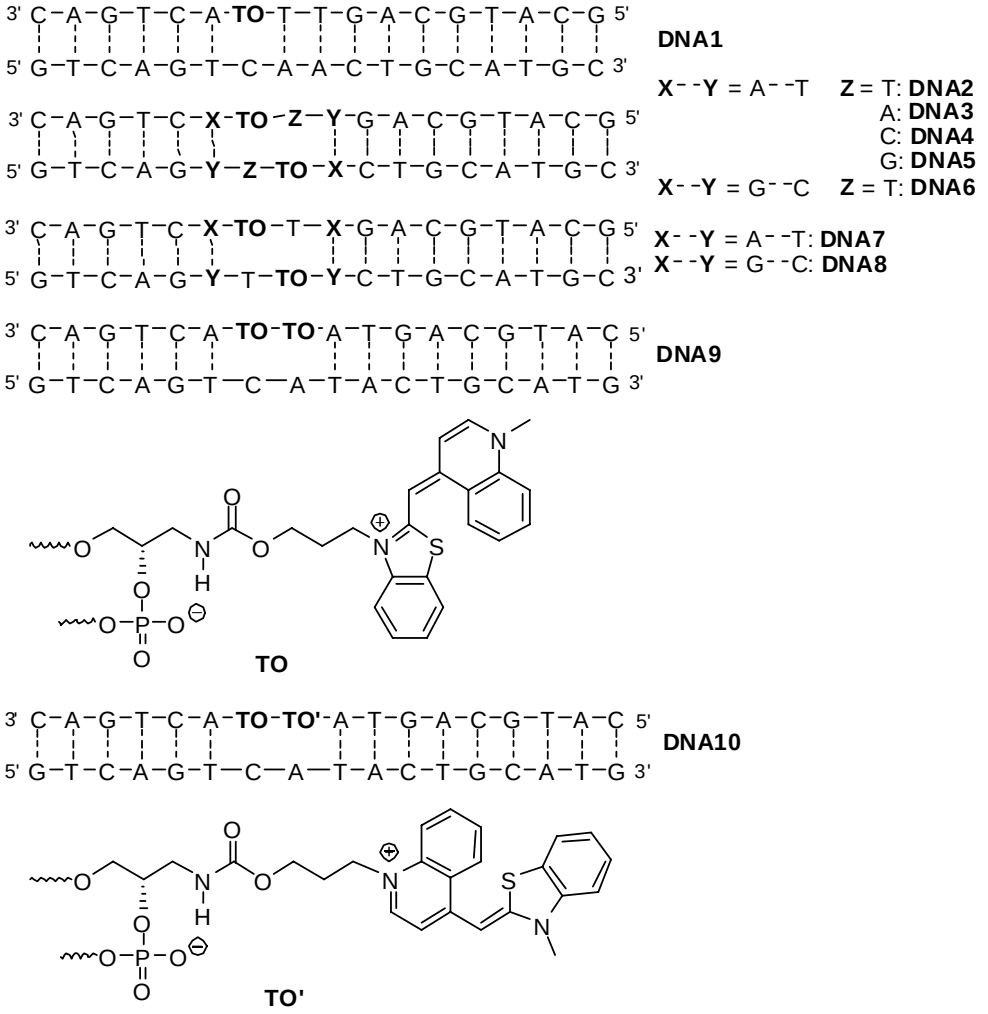

Figure 4.2 Sequences of **DNA1-DNA10.**

4.2.2 Optical properties of TO dimers in different DNA conjugates

The steady state absorption spectra (Figure 4.3) of all duplexes bearing the interstrand TO base surrogate dimer, **DNA2-DNA8**, and the intrastrand TO dimers, **DNA9** and **DNA10**, exhibit significant differences compared to the singly labeled reference **DNA1**. Consistent with the characteristic vibronic transitions of single TO chromophores, the absorption of **DNA1** exhibits two major absorption bands at 485 nm and 510 nm. The absorption of the single TO base surrogate in other DNA base environments possesses a similar structure.[111] The two major absorption bands of the TO dimers in **DNA2-DNA8** as well as in **DNA9**/**DNA10** lack the characteristic vibronic structure of the TO monomers and are hypsochromically shifted. Moreover, there are differences in the relative intensities of the absorption bands compared to the single TO in **DNA1**. The main absorption peak of the TO dimers in **DNA2-DNA8** is located between 486 and 490 nm. The ratios of the extinction coefficients at 490 and 510 nm change from 0.6 for **DNA1** to 1.3-1.5 for all other duplexes, except **DNA5** (1.0). The absorption maxima of the intrastrand TO dimers in **DNA9** and **DNA10** are shifted even more hypsochromically to 475 nm. Similar absorption changes have been observed in non-covalently formed aggregates of cyanine dyes[125,126], in dimeric forms of cyanines (e.g. TOTO) that bind non-covalently to DNA[105,127,128] and in doubly cyanine-labeled DNA bases.[129-131] Accordingly, we interpret our observations for **DNA2-DNA10** as the result of strong electrostatic interactions in the electronic ground state that occur between the TO dyes.

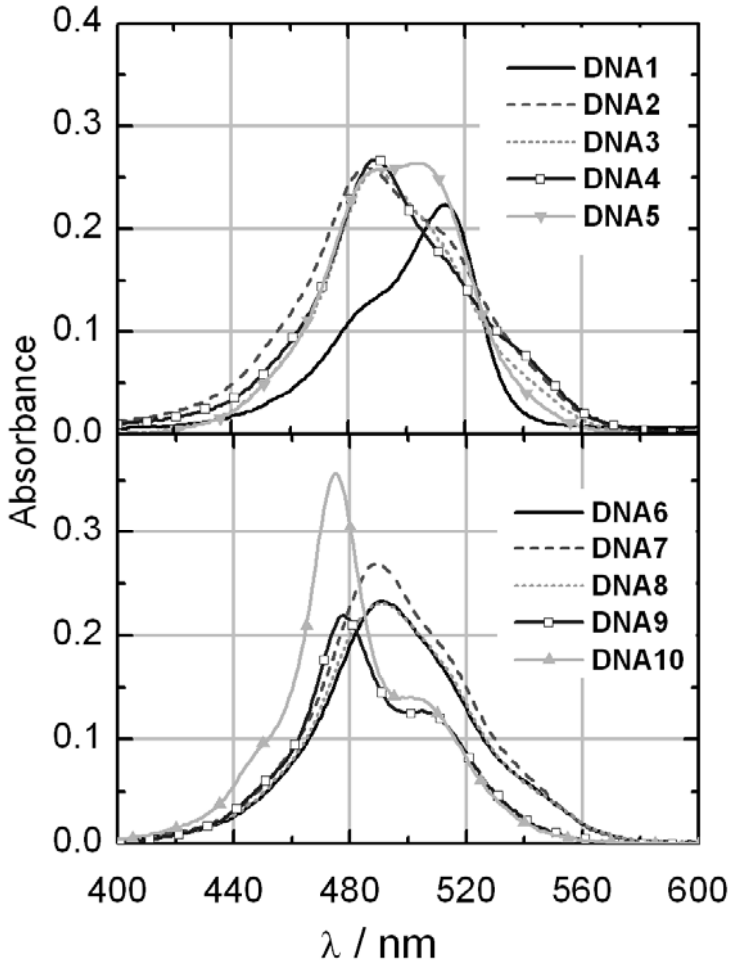

Figure 4.3 UV/Vis absorption spectra of **DNA1-DNA5** (top) and **DNA6-DNA10** (bottom). 2.5 μM DNA, 10 mM NaP_i, pH 7, 250 mM NaCl, 20 °C.

The thermal stability of the DNA duplex and the influence of the synthetic modifications are routinely characterized by the melting temperature (T_m). For the DNA duplexes with the interstrand TO dimer base surrogates (**DNA2-DNA8**) the T_m values

give additional information about the ground state interactions between the TO chromophores. All melting curves were measured by the Wagenknecht's group and the results are presented in Table 3. The reference system **DNA1** has a T_m of 65.5 °C which is only 2.0 °C lower than the completely unmodified duplex that includes guanine instead of the TO modification.[2,111] The observed destabilization is remarkably small. In comparison, the incorporation of indole as a base surrogate into oligonucleotides via a similar acyclic linker system results in a substantial destabilization of the DNA duplexes (approx. -12 °C).[123] Such a strong destabilization is typical for single glycol modifications.[78] Obviously, the ground state interactions of TO with the adjacent bases regain the thermal stability of the duplexes that was lost from the substitution of the sugar backbone with the glycol linker. Compared to **DNA1**, the melting temperatures of all duplexes carrying the interstrand TO dimer (**DNA2**-**DNA8**) are increased, ranging from 66.3 to 69.4 °C in the A-T environments, and 72.4-72.7 °C in the C-G environments. However, there seems to be no simple correlation between the increase of thermal stability in the duplex and the extinction coefficients ratio at 490/510 nm. This correlation should be expected, if upon oligonucleotides hybridization, all TO monomers form interstrand TO dimers. In the case of such two-state process, the extinction coefficients ratio would correlate with the thermal stability of the duplexes. The thermal dehybridization of the interstrand TO dimers in **DNA2**-**DNA8** is observable not only at the standard wavelength of 260 nm (where the DNA bases absorb!) but also at 507 nm which is the typical absorption of the single TO base surrogate in DNA. It is remarkable that the dehybridization of the TO dimer is observable at the typical absorbance

wavelength of TO and that it occurs at very similar temperatures as the cooperative dehybridization of the whole duplex (measured at 260 nm). This result clearly indicates that the intermolecular interactions between the TO chromophores are coupled to the structural framework of the duplex architecture. If the duplex framework breaks down, the TO interactions are interrupted, too. Note, that this is not the case for the intrastrand TO dimers in **DNA9** and **DNA10**, because the ground state interaction between the TO dyes is still observed even at room temperature for the single stranded oligonucleotides.[2] In **DNA9** and **DNA10**, the intrastrand TO dimers destabilize the duplexes.

Duplex	T_m 260 nm	T_m 507 nm	Φ_F	$\Delta A_{490\ nm}/\Delta A_{511}$
DNA1[2]	65.5[a]	-	0.22	0.6
DNA2[2]	69.4	70.5	0.08	1.3
DNA3	67.3	66.4	0.16	1.4
DNA4	69.8	69.0	0.20	1.5
DNA5	66.3	65.0	0.17	2.4
DNA6	72.7	71.0	0.15	1.4
DNA7	67.8	67.2	0.20	1.4
DNA8	72.4	69.6	0.14	1.3
DNA9	60.5	-	0.04	1.2
DNA10	59.5	-	0.03	1.3

Table 3 Melting temperatures (at 260 nm and 507 nm), quantum yields and the ratio of the extinction coefficients at 490 and 511 nm of **DNA1**-**DNA10**. [a]The corresponding unmodified DNA duplex that contained a G instead of TO shows T_m=67.5 °C.[2]

In order to explore the ground state interactions between the dimeric TO base surrogates in the DNA duplexes, we measured CD spectra of all modified duplexes, not only in the DNA-typical absorption range between 220 and 300 nm (which only reports

on the B-type DNA conformation) but also in the TO-typical absorption range between 420 nm and 580 nm (Figure 4.4). As expected, the reference duplex **DNA1** does not show a significant induced CD signal in the latter wavelength range. With the duplexes **DNA2-DNA8**, however, a strong CD signal could be observed which is attributed to exciton coupling between the two TO. The intensity of the signal varies significantly with the different DNA base contents surrounding the TO dimer: The CD signal intensity depends more strongly on the type of base that is located directly opposite to TO in the counter strand (**DNA2-DNA5**) than on the type of adjacent base pairs (**DNA2** in comparison with **DNA6-DNA8**). In an A-T environment the strongest CD signal has been observed for **DNA4** bearing a C opposite to each TO base surrogate.

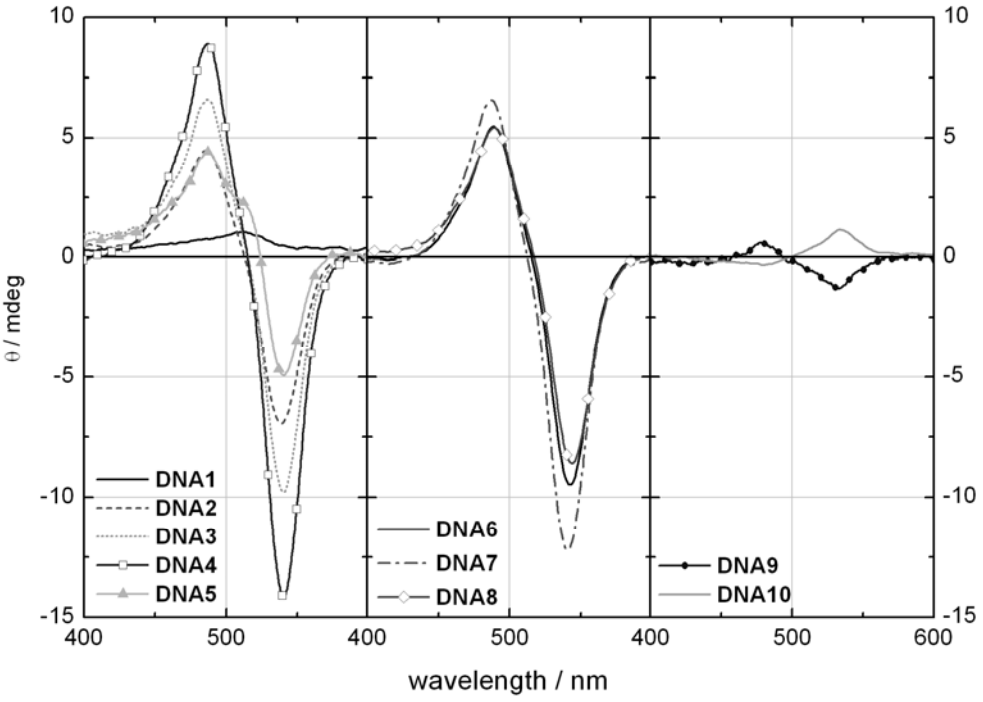

Figure 4.4 CD spectra of **DNA1-DNA5** (left), **DNA6-DNA8** (middle) and **DNA9-DNA10** (right).

The CD spectra of **DNA9** and **DNA10** each display a split Cotton effect. However, the lineshapes are nearly inverted for the two systems; **DNA9** shows a negative first and a positive second Cotton effect whereas **DNA10** shows a positive first and a negative second Cotton effect, indicating opposite chiralities of the two structures. The exciton chirality that governs the sign and amplitude of split Cotton effects is given by $\mathbf{R}_{ij} \cdot(\boldsymbol{\mu}_{i0a} \times \boldsymbol{\mu}_{j0a})V_{ij}$ where $\mathbf{R}_{ij}$ is the distance vector between the centers of the TO chromophores, $\boldsymbol{\mu}_{i0a}$ and $\boldsymbol{\mu}_{j0a}$ are the electronic transition dipole moments of i and j for the excitations 0→a on i and j, respectively. V_{ij} is the electronic interaction energy between the two TO chromophores.[132] If one assumes dipole-dipole coupling the rotary strength ($R_{\pm}$) is approximately proportional to *sin* 2α, where α is the angle between the two local transition dipole moments $\boldsymbol{\mu}_{i0a}$ and $\boldsymbol{\mu}_{j0a}$.[133] Consequently, an inversion of the Cotton effect requires a *difference* in the chromophore orientation of ~90°. A maximum Cotton effect is obtained for ~45° (positive chirality, **DNA10**) and ~135° (negative chirality, **DNA9**). Moreover, the small amplitudes of the CD spectra (in both **DNA9** and **DNA10**) suggest that these angles do not reflect the exact orientations of the chromophores. However, independent of the absolute orientation, the observed inversion of the Cotton effects represents strong evidence for an angular difference of 90° between **DNA9** and **DNA10**. The much larger CD intensities for the interstrand TO dimers in **DNA2**-**DNA8** may suggest that the two interacting TO chromophores bear angles between their transition dipole moments that are closer to 135° (negative chirality) than the corresponding ones in **DNA9**.

With respect to potential applications of the TO dimer in chemical bioanalysis and live cell imaging,[108,111] the most remarkable results were obtained by steady state fluorescence spectroscopy using the TO-typical absorption wavelength of 490 nm for excitation. Not surprisingly, the fluorescence spectrum of the single labeled reference **DNA1** shows the characteristic green TO emission at ~530 nm (Figure 4.5) including the characteristic vibronic fine structure. In contrast, the fluorescence of all duplexes bearing the interstrand TO dimer (**DNA2**-**DNA8**) is shifted to a broad structureless band with a maximum at around 580 nm (orange). We have shown recently, that concomitantly with the cooperative thermal dehybridization of the whole duplex, the orange fluorescence of the TO dimer in the DNA double strand shifts back to the TO-typical green color in the single strands. Similar to the absorption properties, the intact helical duplex is required as a structural framework for the bathochromic fluorescence shift. In contrast to **DNA2**-**DNA8**, the fluorescence of the intrastrand TO dimers in **DNA9** and **DNA10** is not shifted but quenched significantly. The latter result is expected when cyanine dyes are excitonically coupled with each other in aggregates.[125-131,134,135]

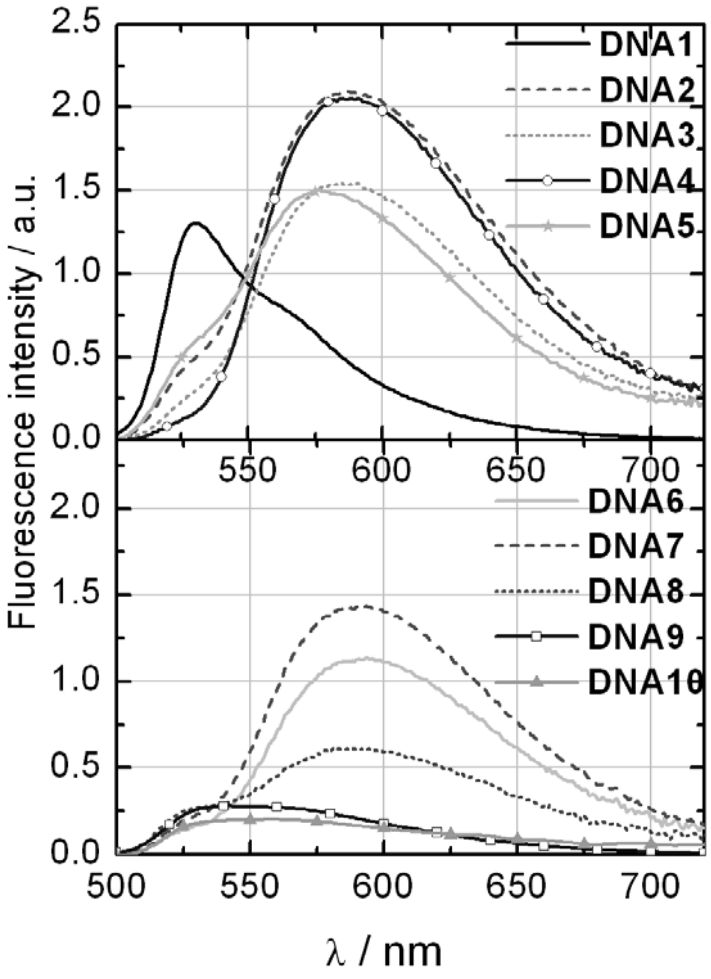

Figure 4.5 Fluorescence spectra of **DNA1**-**DNA5** (top) and **DNA6**-**DNA10** (bottom). λ_{exc} = 490 nm.

4.2.3 Pump-probe spectroscopy analysis: excimer and exciton formation

In a previous report, Wagenknecht et al. attributed the fluorescence changes in **DNA2** to excimer-type emission from the TO chromophores.[2] This interpretation was based mainly on three experimental observations: (i) bathochromic shift, (ii) loss of vibronic structure, and (iii) increased lifetime of the excited state (τ = 1.55 ns for **DNA1** vs. 2.83 ns for **DNA2**). In order to verify (or falsify) the excimer formation we performed time-resolved pump-probe spectroscopy.

It is known that excitation of "free" in aqueous solution TO leads to very fast internal conversion from the S_1 to the S_0 state, which is accompanied by twisting of the methine bridge connecting the quinoline and thiazole rings. As a result aqueous solutions of TO have very low fluorescence quantum yields (2×10^{-4}).[136] In **DNA1**, TO is located in the DNA minor groove and the twisting of the methine bridge is suppressed. Therefore, the non-radiative IC does not take place and longer lived emission and a higher quantum yield (0.22) are observed. The dimers **DNA2** and **DNA9** have smaller quantum yields than **DNA1** (0.08 for **DNA2** and 0.04 for **DNA9**) that are still enhanced compared to the free TO in aqueous solutions.[136] Similar behavior has been previously reported for cyanine dyes, in which the enhancement of the fluorescence intensity was attributed to the formation of H-aggregates.[127,137,138]

For the femtosecond pump-probe experiments, the NOPA was tuned to 515 nm in order to excite the S_1 state of TO. The temporal evolution of the pump-probe spectra of

DNA1 (TO monomer) is presented in Figure 4.6a. As mentioned in **Chapter2**, there are three contributions to the pump-probe signal: (i) Excited state absorption (around ~370 nm), (ii) ground state bleaching (~510 nm), and (iii) stimulated emission (~550 nm). The major differences of the pump-probe spectra of **DNA2** (Figure 4.6b) to that of **DNA1** are that (i) the ground state bleaching occurs hypsochromically shifted at ~490 nm (from 510 nm) and (ii) the stimulated emission is a bathochromically shifted broad signal at ~600 nm (from ~550 nm), the wavelength range of the TO dimer emission. It is important to note that the ground state bleaching at ~490 nm appears simultaneously with the pump pulse (515 nm), which indicates that an exciton state of the TO ground state complex is vertically excited in **DNA2**.

The pump-probe spectra of **DNA9** represent a mixture of the pump-probe spectra of **DNA1** and **DNA2**. (Figure 4.6b) The ground state bleaching occurs at 475 nm, the wavelength of the intrastrand TO exciton, and at 510 nm, the wavelength of the uncoupled TO chromophore. This result shows that in **DNA9** only part of the TO chromophores are coupled in the intrastrand fashion. Moreover, the bleaching band of **DNA9** is more hypsochromically shifted than the bleaching band of **DNA2**, which indicates stronger exciton coupling in **DNA9**. If one assumes only dipole-dipole interactions, the exciton coupling can be described by the equation: $\mathbf{V}_{ij} \sim (\boldsymbol{\mu}_{i0a} \cdot \boldsymbol{\mu}_{j0a})\mathbf{R}_{ij}^{-3} - 3(\boldsymbol{\mu}_{i0a} \cdot \mathbf{R}_{ij})(\boldsymbol{\mu}_{j0a} \cdot \mathbf{R}_{ij})\ \mathbf{R}_{ij}^{-5}$. In the case of H-aggregates the angle between $\mathbf{R}_{ij}$ and $\boldsymbol{\mu}_{i0a}$ and/or $\boldsymbol{\mu}_{j0a}$ is close to 90°. Therefore, the alignment of the transition dipole moments of the two TO chromophores will govern the coupling strength, and the enhancement of the

exciton coupling in **DNA9** indicates a more coplanar orientation of the TO chromophores.

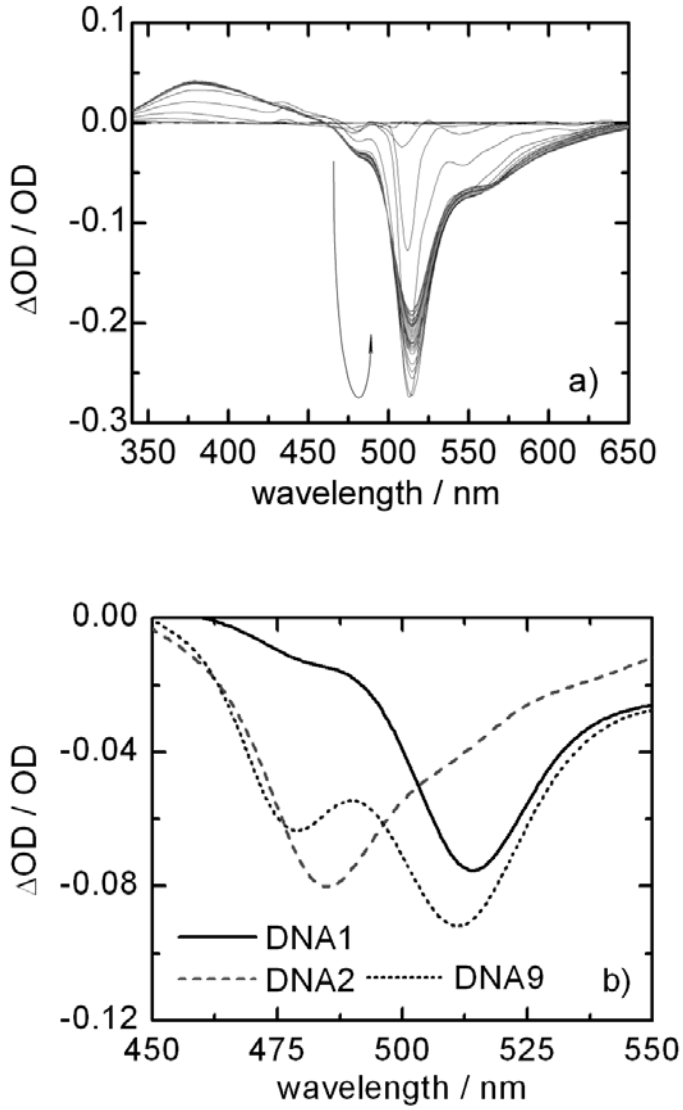

Figure 4.6 a) Temporal evolution of the pump-probe spectra of **DNA1** in the time range -0.1 to 10.0 ps. The excitation wavelength is 515 nm. The arrow indicates the evolution of the spectra; b) Comparison of the pump-probe spectra of **DNA1**, **DNA2** and **DNA9,** 10 ps after excitation.

To analyze the temporal evolution of the pump-probe spectra we performed single value decomposition (SVD) and a subsequent global fit analysis. The fits were carried out with the commercial software Surface Xplorer Pro (Ultrafast Systems, LLC). The results from the global fitting of **DNA1**, **DNA2** and **DNA9** are presented in Figure 4.7. The spectral evolution of **DNA1** is described by three lifetime components: 0.1 ps, 16.0 ps and 1.2 ns. (Figure 4.7a) This result shows the existence of multiple conformations in the sample. The dominating ns component corresponds to emitting TO monomers that are confined in the DNA minor grove and do not undergo IC. There is also a small amount of TO monomers with different conformation that are again confined by DNA and have 16 ps lifetime. On the other hand, the ultrafast component corresponds to poorly confined – likely in the DNA groove – TO monomers that undergo fast IC to the ground state. The global fitting of **DNA2** (Figure 4.7b) shows that, similar to **DNA1**, multiple conformations contribute to its pump-probe spectra. The major difference between **DNA2** and **DNA1** is in the presence of blue-shifted bleaching band with maximum at ~490 nm that corresponds to excitation of an exciton state formed upon aggregation of two TO dyes in their ground state. The exciton lifetime estimated by the global fitting is 2.5 ns. It should be noted that the TO dimers are separate species and they do not convert to TO monomers. We made this conclusion based on the fact that the lifetime of the TO dimers is longer than the lifetime of the TO monomers in **DNA1**. Although, TO dimers are the predominant species in **DNA2**, there is a small amount of TO chromophores that do not aggregate and behave like TO monomers. They are described in the global fits by the 470

ps lifetime component with maximum at ~515 nm. This lifetime is shorter than the lifetime of the TO monomers in **DNA1**, which is most likely due to the presence of a quencher (a second TO chromophore) in **DNA2**. In addition, the 470 ps lifetime component has contribution from stimulated emission that resembles well the steady state fluorescence of **DNA2**. These observations are a strong indication for excimer formation and confirm our previous conclusion that the red-shifted emission from **DNA2** is due to excimer formation. Because the pump-probe spectra are dominated by stimulated emission and bleaching of the exciton state, we cannot extract a rise time for the excimer formation. Also, the fact that the time component of the stimulated emission is identical to the monomer lifetime suggests that there is a fast thermodynamic equilibrium between these two states.[7]

Since all principle components present in **DNA2** and **DNA1** are observed in **DNA9**, the results from SVD and global fitting of **DNA9** (Figure 4.7c) confirmed our previous conclusion that the pump-probe spectra of **DNA9** consist of TO monomers and TO dimers. Therefore, the 13 and 490 ps components are assigned to two different conformations of TO monomers that do not undergo fast IC. Some of these monomers form excimers that give the weak red-shifted fluorescence from **DNA9**. The small number of TO monomers not buried in the DNA minor grove relaxes very quickly to the ground state by IC. This phenomenon causes the observation of the ultrafast component. Lastly, the ns component corresponds to the exciton state in **DNA9** that is found to relax slightly faster than the exciton state in **DNA2**.

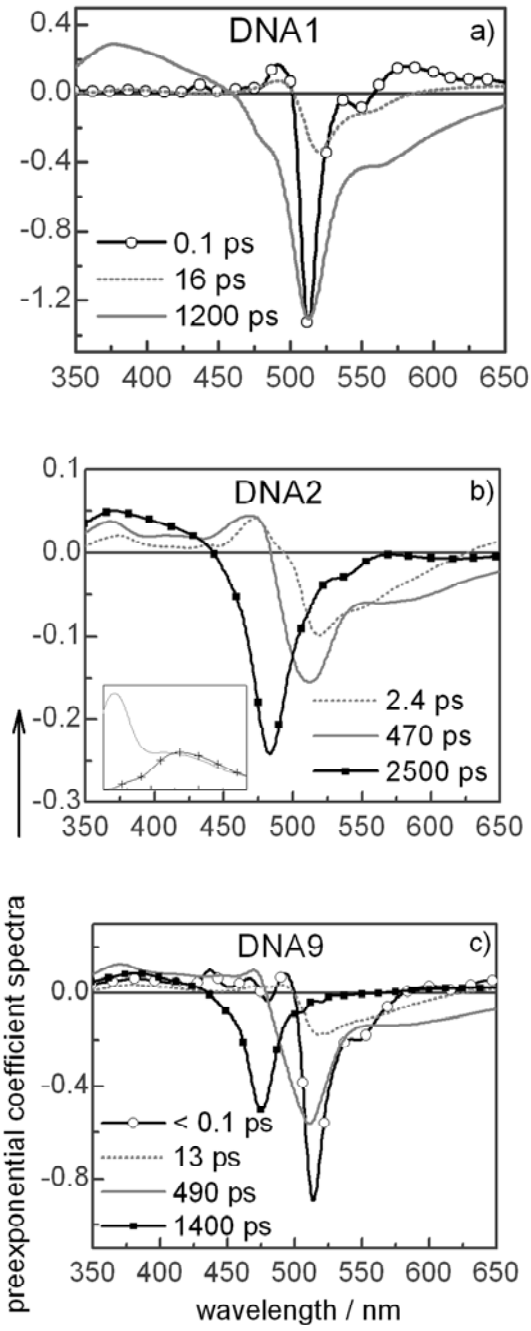

Figure 4.7 Preexponential coefficient spectra obtained from global fitting of a) **DNA1**, b) **DNA2** and c) **DNA9**. The inset in b) compares the band-shape of the 470 ps component (solid gray line) with the steady-state fluorescence (black line with crosses) of **DNA2**.

4.2.4 Fluorescence excitation spectra analysis: excimer vs. exciton formation

This section presents the results from fluorescence excitation spectroscopy experiments. They were used as a starting point for an alternative analysis (to the one in **Section 4.2.3**) of the optical properties of the TO dimers. According to this analysis the red-shifted fluorescence spectrum of the TO dimers (**DNA2-DNA8**) was assigned to exciton and not excimer emission. However, after careful examination of the pump-probe and fluorescence excitation spectra, we were urged to re-examine this data interpretation and finally draw the conclusions described in the preceding **Section 4.2.3**.

The excitation spectra of **DNA2** were recorded for three emission wavelengths – 535, 580 and 670 nm. (Figure 4.8) Probing at 535 nm (the emission maximum of **DNA1**) resulted in an excitation spectrum corresponding to the UV/Vis absorption of **DNA1**, while probing at 580 and 670 nm yielded a spectrum that corresponds to the absorption of **DNA2**. The 535 nm excitation spectrum is explained with the existence of **DNA1**-like chromophores in the samples. Their concentration is not high, because the emission band at 535 nm, typical for **DNA1,** is seen as a small shoulder imposed on the bigger 580 nm emission. More importantly, the correspondence of the 580 and 670 nm excitation spectra to the absorption of **DNA2** shows convincingly that the dominant broad emission band (at 580 nm) originates from ground state complexes that form exciton states, but not from

excimers. If the broad and red-shifted emission were to originate from excimers, then the fluorescence excitation spectrum would have to correspond to the absorption of the TO monomer (**DNA1**). However, as seen from the results for **DNA2**, this is not the case.

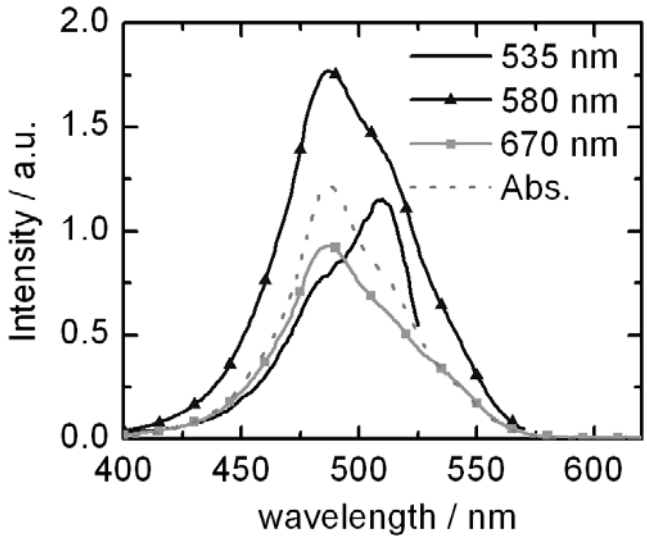

Figure 4.8 Excitation spectra of **DNA2** recorded at three emission wavelengths are compared to the absorption spectrum of **DNA2** (dashed line).

The assignment of the **DNA2** fluorescence spectrum to exciton transitions was confirmed by the observation that the ground state bleaching in the pump-probe spectra at ~490 nm appears simultaneously with the pump pulse (515 nm). This indicates that a TO ground state complex is excited in **DNA2** thereby ruling out the possibility for (dynamic) excimer formation in the excited state. It is worth discussing the relation between quantum yields and lifetimes of the bleaching and stimulated emission bands. The

quantum yields of the three systems decrease in the order **DNA1** (0.22), **DNA2** (0.08) and **DNA9** (0.04), which coincides with corresponding decrease in the fluorescence lifetimes deduced from the decay of their stimulated emission bands. On the contrary, the bleaching shows that the excited state population of **DNA2** and **DNA9** recovers back to the ground state two times slower than what is observed through the stimulated emission. **DNA1** has almost identical decay times of bleaching and stimulated emission proving that no other channel for energy dissipation is available in the reference **DNA1**. The ground state recovery of **DNA2** and **DNA9** happens with three time constants (Figure 4.7). We assign the fastest to **DNA1**-like chromophores that are present in the solutions. Because there are more noninteracting **DNA1**-like chromophores in **DNA9** than **DNA2** (see fluorescence spectra), the amplitude of the ps component is larger in **DNA9** than in **DNA2**. The ~500 ps component in the dimers (**DNA2** and **DNA9**) is due to hypsochromic shifting of the bleaching band, which can be attributed to structural reorganization.[10] The longest time component (1.4 and 2.5 ns) is directly related to the lifetime of the exciton state.

4.3 Conclusion

Using the base surrogate approach in combination with (S)-2-amino-1,3-propanediol as a substitute for the 2'-deoxyribofuranoside TO can be incorporated in monomeric and dimeric form into double-stranded DNA. The *intrastrand* TO dimer shows excitonic interactions that are observable by UV/Vis absorption and CD spectroscopy, and

quenching of the green fluorescence due to aggregation. The *interstrand* TO dimer shows a characteristic red-shifted orange emission. The interstrand TO dimer is applicable in any sequential context which is a great advantage over perylene bismide dimers which require guanine free base environments to gain their full potential as fluorescence label. The optical properties of the TO dimers were investigated by time-resolved pump-probe, fluorescence excitation, UV/Vis absorption, fluorescence and circular dichroism spectroscopy. The optical changes of TO inside the helical framework of double-stranded DNA can be explained by excimer and ground state complex formation. Accordingly, the unique red-shifted fluorescence of the interstrand TO dimer is the result of excitation of TO monomers and consecutive formation of emitting excimers.

5 Femtosecond dynamics in CdTe and CdSe nanocrystals for photovoltaic applications

5.1 Optical phonon dynamics in quantum-confined CdTe nanocrystals

5.1.1 Introduction

Upon absorption of a photon from a semiconductor material a coulombically bound electron-hole pair, exciton, is generated. The spatial separation of the electron and the hole is an inherent property of the specific material, and the radius of this hydrogen-like particle is the exciton Bohr radius. Semiconductor nanocrystals (NCs) show distinctly different optical and electronic properties than their corresponding bulk materials, because their diameters are comparable to the exciton Bohr radius.[139] The resulting quantum confinement effect makes them potential candidates for solar energy conversion,[140] lasing,[141] and biological labeling[142] applications. Of major importance in these applications is the particles' response to photon absorption events. Quantum confinement effects have a strong influence on exciton relaxation, which can lead to numerous nonradiative pathways for carrier cooling such as an Auger mechanism,[143] relaxation to surface trapped states,[143] and nonadiabatic surface crossings.[144,145] However, the effect of quantum confinement on optical phonon modes and their coupling to exciton states are still under debate.[146]

Optical phonons affect the nonlinear optical properties of semiconductors by broadening the discrete electronic transitions in quantum dots and by influencing their oscillator strengths.[147] Furthermore, optical phonons are involved in radiationless exciton relaxation processes. Hence, an estimation of the exciton-phonon coupling is crucial for the description of the excited-state dynamics in NCs. In II-VI semiconductor crystals, the displacement of the charged nuclei (which extends over many unit cells) creates an electric field that is coupled to the excited electron and hole through a Coulomb interaction, thus changing the exciton polarizability with time.

Here, I present a femtosecond time-resolved study of the size dependence of the optical phonon properties in CdTe NCs using our broadband pump-probe technique.[7] To study the quantum confinement effect on the longitudinal optical (LO) phonons, different sizes of CdTe NCs capped with 3-mercaptopropionic acid (MPA) were synthesized.

5.1.2 Synthesis of CdTe nanocrystals

A detailed protocol used for the synthesis of the CdTe nanocrystals can be found in a reference 148. Briefly, sodium hydrogen telluride (NaHTe) is prepared by reacting tellurium powder with sodium borohydride ($NaBH_4$) in H_2O under N_2 atmosphere. Approximately 30 mg of Te is put in a flask and mixed with 1 ml aqueous $NaBH_4$ solution (~60mg of $NaBH_4$). The reaction mixture is heated to 70° and stirred until no powder is seen in the flask. An aqueous solution of NaHTe is clear and transparent.

During the reaction, the resulting H_2 should be carefully released. The fresh NaHTe precursor is injected into a flask with an aqueous solution of $CdCl_2$ and MPA (the stabilizing ligand) with pH ~ 8. The reaction is stirred and heated to ~80°C. Also, it is subjected to a reflux. The concentrations of Cd^{2+}, MPA and HTe^- are 2.5 mM, 6.25 mM and 1.25 mM respectively. Soon after the injection of NaHTe the color of the solution turns to yellow, thus indicating that CdTe crystals are formed. Upon continuous heating, the crystals grow and the color of the solution changes. Aliquots are taken to ensure that CdTe nanocrystals with different sizes are produced. Typically, after 1000 minutes no change in color is observed and the heating is ceased.

The absorption spectra of nanocrystals with different diameters are shown in Figure 5.1. The crystallinity of the nanocrystals is confirmed with transmission electron microscopy (TEM). The NC diameters were determined by the positions of the $1S\text{-}1S_{3/2}$ absorption band.[149] For the size dependent pump-probe spectroscopy measurements nanocrystals with sizes between 2.5 and 3.5 nm were used.

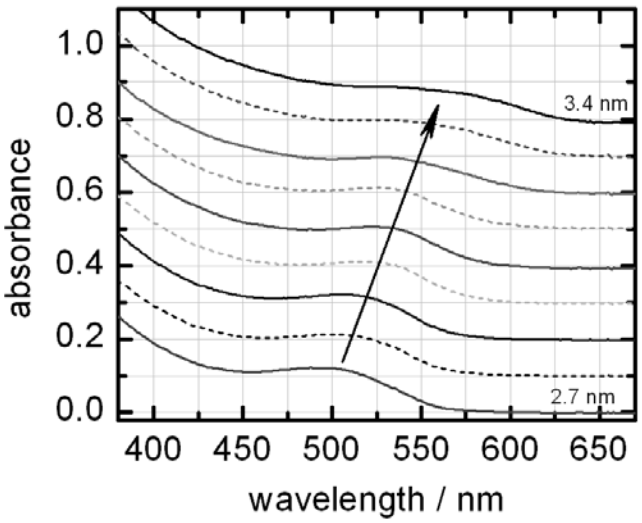

Figure 5.1 Representative absorption spectra of CdTe NCs (MPA ligand) with different sizes received from a single pot synthesis. The diameter of the dots increases from 2.7 nm to 3.4 nm. The absorption spectra of the NCs are offset for better presentation.

5.1.3 Quantum beats in the femtosecond pump-probe spectra

The wavelength of the excitation pulses was tuned to the red edge of the second lowest excitonic peak (1S-2$S_{3/2}$). To avoid multiexciton generation and the concomitant complications in the observed exciton relaxation dynamics, the pump pulse fluence was set to create less than 0.3 exciton per particle.[143] This value was calculated by $N_{ex} = \sigma j$, where N_{ex} is the average number of excitons per particle, j is the fluence of the excitation pulse, and σ is the absorption cross-section at the excitation wavelength which can be calculated from the extinction coefficient. The extinction coefficients were determined from the CdTe 1S-1$S_{3/2}$ absorption peak.[150] The pump-probe spectra in the visible region

of type II-VI NCs are dominated by state-filling signals from the excitonic states, and the temporal recovery of the bleaching bands provides direct information of the exciton relaxation dynamics.[151]

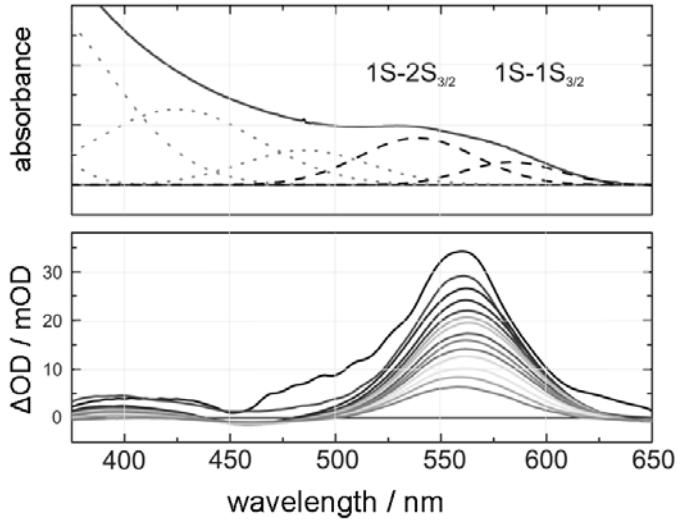

Figure 5.2 Representative steady-state absorption (upper graph) and pump-probe spectra (bottom graph) from 0.1 ps (black) to 2 ns (gray) of aqueous CdTe quantum dots with 3.3 nm diameter. The steady state absorption spectrum was fitted with a sum of Gaussian functions (dotted and dashed lines) to identify the two lowest energy excitonic states (dashed lines) $1S\text{-}1S_{3/2}$, $1S\text{-}2S_{3/2}$.

Figure 5.2 presents the temporal evolution of pump-probe spectra of 3.3 nm CdTe quantum dots. Here, the lowest-energy bleaching band appears around 560 nm, and it has been assigned to the $1S\text{-}1S_{3/2}$ and $1S\text{-}2S_{3/2}$ transitions.[143] This band shows highly nonexponential recovery dynamics due to surface trapping of the carriers, ranging from subpicoseconds to nanoseconds, consistent with previously published data.[143,152] It is well

known that coherent vibrations can modulate the transient spectrum by either wavepacket motion in the population of the excited state or an impulsive resonant Raman process (displaced holes left in the ground state).[153] The resulting oscillations are superimposed on the excitonic transient signals.[153,154] To separate these two contributions, a standard procedure for analysis of quantum beats was used.[155] The transients were fitted with a multiexponential function, which was subsequently subtracted from the data to yield oscillating residuals with amplitudes of about 4% of the total bleaching signal. The Fourier transformation of the oscillating signal yielded only one major peak at 162 cm^{-1}, corresponding to the frequency of the LO phonons.[154,155] This value agrees reasonably well with the phonon frequency reported for bulk CdTe (169.5 cm^{-1}).[154] The same procedure was performed for all NC sizes and the frequency of the observed quantum beats does not significantly depend on the size of the NCs (in the range between 2.5 and 3.5 nm).

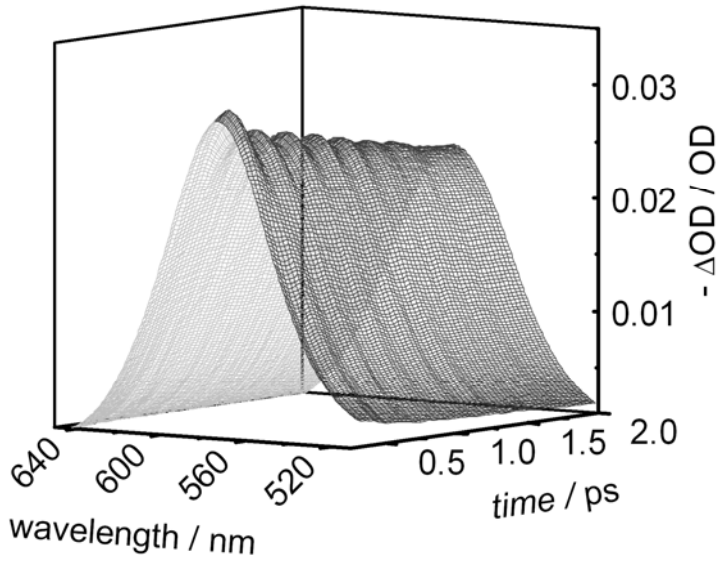

Figure 5.3 Pump-probe data for CdTe quantum dots with 3.3-nm diameter: (a) 3D plot of the lowest-energy transient bleaching band. The oscillations are present only at the blue side of the bleaching band corresponding to the frequency modulation of the 1S-$2S_{3/2}$ state. (b) Fourier transform of the oscillations at 540 nm (see text for details).

The pump-probe spectra of 3.3-nm NCs (Figure 5.3) have oscillations in two distinct spectral regions. These oscillations have the same frequencies but opposite phases, with a phase crossover at around 550 nm (Figure 5.4). It is worth noticing that there are no observable oscillations in the red shoulder of the spectra corresponding to the bleaching from the band edge exciton. To identify the origin of the oscillations, we fitted the steady-state absorption spectrum with Gaussian functions (Figure 5.2). The two lowest-energy Gaussians (marked with arrows) are assigned to the 1S-$1S_{3/2}$ and 1S-$2S_{3/2}$ exciton transitions. We compared the positions of the bands with the pump-probe spectra of the same samples and found that the oscillations span over the 1S-$2S_{3/2}$ band only and no

oscillations were detected at other probe wavelengths. Very similar results were obtained for the other particle diameters as well, but for simplicity, only the data for NCs with 3.3-nm diameters are shown.

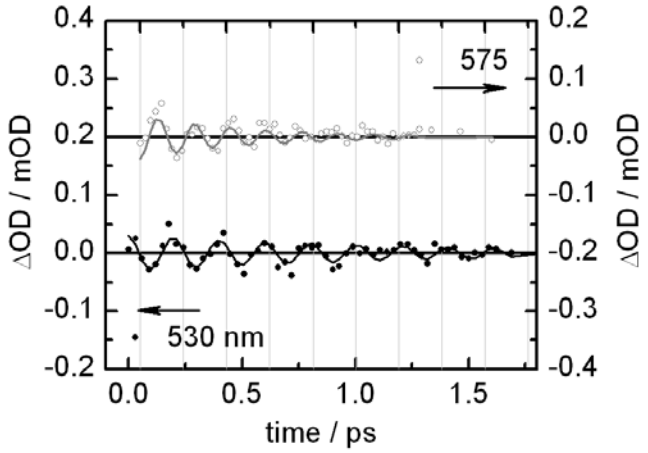

Figure 5.4 Oscillations at 530 nm (solid circles) and 575 nm (open circles). The estimated phase shift between the quantum beats is 180°. The solid lines represent least-squares fits with a damped sinusoidal function.

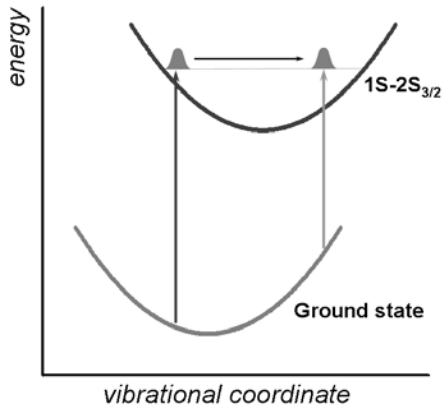

Figure 5.5 Illustration of the wavepacket motion in the excited state. As the wavepacket travels along the potential well, different parts of the white-light probe pulse are absorbed at different times and therefore give rise to the oscillations observed in the pump-probe spectra.

To explain these observations, we invoke a simple displaced harmonic-oscillator model illustrated in Figure 5.5. Here, a femtosecond pump pulse excites several phonon states coherently, thus creating a wavepacket in the exciton state. While traveling along the potential energy surface, the wavepacket broadens at the bottom of the potential and passes twice through its center. The result observed in the pump probe spectrum is "washed-out" oscillations with minimal amplitudes at the bottom of the well.[153] Consequently, to the red and blue sides of this region, the oscillations must have a 180° phase shift, which, in fact, was experimentally observed for all NC sizes (Figure 4). Based on these observations, we concluded that the oscillatory signals in the pump-probe transients of CdTe NCs are mainly due to excited-state wavepacket motion and there is little (if any) contribution from impulsive stimulated Raman scattering.[153]

5.1.4 Strength of the exciton-phonon coupling

Previously published values[146] for the exciton-phonon coupling strength were estimated from oscillations in the pump-probe signal (when the probe was tuned to the red-edge absorption of the steady-state absorption spectrum). According to some theoretical models,[146,156] the coupling strength is expected to decrease with $1/r^3$ (where r is the radius of the NC); however, our size-dependent experiments do not show a significant change in the exciton-phonon couplings. The strength of the exciton-phonon coupling was

estimated by the dimensionless Huang-Rhys parameter (S), that is, a measure of the vibrational relaxation energy in a two states electronic transition.[144] The Huang-Rhys parameter is related to the reorganization energy of the transition and was computed from the following set of equations[155]:

$$A_{osc} = \left[\frac{dOD}{d\omega}\right]\lambda$$

A_{osc} is the amplitude of the oscillations in OD units, OD is the optical density of the absorption spectrum at the excitation wavelength, λ is the reorganization energy.

$$S = \lambda/\hbar\omega$$

S was calculated to be 0.013±0.006 for all particle sizes. These results support earlier theoretical and experimental work by Schmitt-Rink et al.[139] and Klein et al.,[157] where the so-called Fröhlich coupling was found to be independent of the NC diameter once the diameter is smaller than the exciton Bohr radius. In that case, the electron and hole wave functions are confined into a smaller volume where the electric field caused by the phonons is less effective in polarizing the exciton, and thus the exciton-phonon coupling diminishes (it becomes exactly zero for a perfect spherical crystal).

5.1.5 Size-dependence of the optical phonons dephasing times

Another characteristic of the vibrational wavepacket motion that can provide important information not only for the phonon properties but also for the exciton relaxation dynamics is the dephasing times. Because the 1S-$1S_{3/2}$ and 1S-$2S_{3/2}$ bleaching bands partially overlap, the oscillations were extracted from the blue edge of the band where the contribution from the 1S-$1S_{3/2}$ level is negligibly small. The oscillations for all NC sizes were fitted with a damped sinusoid function, and the characteristic dephasing times are presented in Figure 5.6. The shown size dependence clearly indicates that the coherent wavepacket relaxes faster in smaller particles. Although an inhomogeneity of the samples could explain the faster times in smaller dots, we can exclude this possibility, because the frequencies and the phases of all measured samples are very similar (independent of the particle size). Finally, the loss of coherence could be simply attributed to a decay of the exciton population. Such a decay process could be induced by radiationless transitions of the electron or the hole to lower electronic states, including surface trapped states. Alternatively, the electron and the hole could recombine radiatively.[158] It is well-known that, because of differences in their effective masses, hole relaxations are generally faster than electron relaxations. Consequently, one could equate the observed dephasing time of the phonon motions to the time for hole relaxation to the lower hole state.

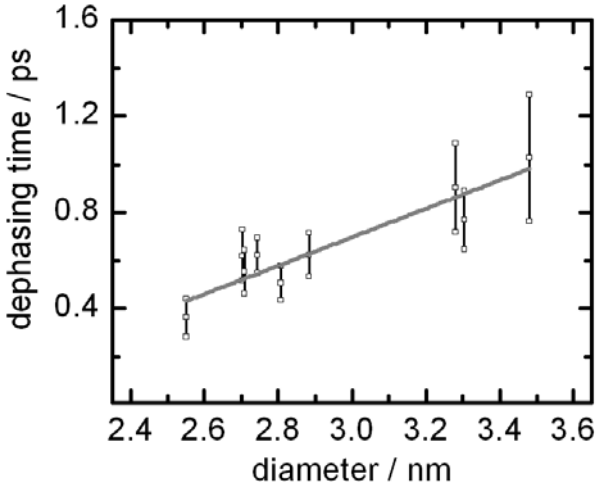

Figure 5.6 Dephasing times of the oscillations plotted vs. NC diameters. The gray solid line represents a linear fit of the points and it indicates the trend in the size-dependent dephasing times.

In the regime of quantum confinement the "valence band" consists of discrete states. According to studies on CdSe, these states are closely spaced, and hole relaxation can happen through single-phonon emission acts (similarly to the phenomenon in bulk crystals). The rate of such relaxation is 1.5 eV/ps.[159] Only near the band edge, where the levels are sparse, is the relaxation slower (0.26 eV/ps).[159] Until now, the question of whether this "near-band-edge" relaxation is size-dependent has remained unclear. In Xu et al.'s study, smaller particles were found to have longer relaxation times, suggesting phonon-mediated processes,[159] whereas in the state-resolved studies of Cooney et al.[160] and Hendry et al.,[161] the relaxation from $2S_{3/2}$ to $1S_{3/2}$ states was found to be size-independent. Here, it is important to note the differences between CdSe and CdTe NCs.

In CdTe, the valence band is less complicated than in CdSe.[162,163] The energy spacing between the $2S_{3/2}$ and $1S_{3/2}$ states is larger than 0.12 eV for the size range of interest. Therefore, at least six phonons are needed for hole relaxation from the $2S_{3/2}$ to the $1S_{3/2}$ state, and one would expect that smaller particles relax more slowly than larger ones. However, as mentioned above (and presented in Figure 5.6), the dephasing times exhibit the opposite trend. An explanation for the observed size dependence of the phonon dephasing times can be found in recent publications, in which surface ligands were shown to play a major role in hole and electron relaxation dynamics.[145,159,160,164,165] In the case of hole relaxation, the rates are determined by two simultaneous (competing) mechanisms: an intrinsic phonon-assisted mechanism and a nonadiabatic transition to a surface state.[145,160]

The rate constant for the suggested nonadiabatic mechanism is influenced by the coupling between the initial hole and the final surface ligand states. Because the hole wave function in smaller NCs can have an amplitude outside the crystal, and thus larger overlap with that of the ligands, the rates for hole relaxation should be higher than in larger particles. In CdSe, because of the dense spectrum of hole states, the phonon-assisted channel competes with the size-dependent nonadiabatic one. In CdTe, on the other hand, the nonadiabatic transition seems to dominate because the larger level spacing prevents phonon-assisted relaxation. Therefore, the exciton state lifetime, and thus the dephasing time of the phonon wavepacket, is limited by the rate of the nonadiabatic transition. It is worth noting that this scenario bears similarities to

vibrational wavepacket dynamics in molecules, e.g., the time scale for phonon dephasing matches the vibrational dephasing time in NaI.[166]

5.1.6 Conclusion

In conclusion, we have observed quantum beats in the pump-probe spectra of CdTe NCs. The oscillations exhibit a frequency of 162 cm^{-1} and were attributed to LO phonon modes. We found that the wavepacket motions are coupled to the excited 1S-$2S_{3/2}$ exciton state and not to the lowest exciton state. In addition, measurements of the NC-diameter dependence showed that the phonon coupling to a higher exciton state is NC-size-independent, whereas the phonon dephasing becomes faster with decreasing NC diameters. The loss of coherence in the phonon wavepacket is correlated with the 1S-$2S_{3/2}$ state depopulation to the lowest excitonic state, which is a hole-relaxation process. Because the energy splitting between these two exciton states is larger than the energy of the optical phonons, this relaxation is expected to be mediated by a multiphonon process. However, we found the dephasing times to be shorter for smaller particles and concluded that hole relaxation must occur through an alternative deactivation pathway, most likely a nonadiabatic surface crossing.

5.2 Electron transfer dynamics in CdSe/CdTe donor-acceptor nanorods

5.2.1 Introduction

The optical properties of semiconductor nanocrystals depend on the crystals' size, shape and surface passivation.[163,167-169,143] In the recent years significant advancement in the control over these parameters have been achieved.[167,170-172] That and the easiness with which the nanocrystals can be implemented in various matrices, such as glass, polymers[173] and photonic crystals,[174] have made them promising candidates for nanophotonics and photovoltaic applications.

Over the past twenty years, reports of devices based on semiconductor nanoparticles and organic/inorganic hybrids[3,175,176] have emerged as scientists have continued to search for new materials to replace silicon-based technologies for solar energy conversion. For the construction of efficient solar cells most of the solar energy spectrum has to be absorbed and successful electron and hole separation achieved. Second generation heteromaterial-nanostructures with two or more components within a single NC are potentially well-suited for photovoltaic applications as charge donor and acceptor band structures can easily be tuned by varying particle geometries.[177]

In order to achieve efficient charge separation, charge transfer (CT) needs to compete with the ultrafast recombination dynamics of the carriers. Charge carrier dynamics in NCs have been studied extensively using ultrafast pump-probe spectroscopies.[159,178-185] Following optical excitation, carrier cooling occurs through multiple processes ranging

from sub-ps timescales to times longer than nanoseconds.[182] Saykally et al. have studied CdSe/CdTe nanotetrapods using femtosecond spectroscopy and have observed carrier cooling dynamics for interband, band-edge and intraband transitions. However, these authors were not able to identify dynamics that could be attributed to CT.[179] Studying a type-I CdS/HgS/CdS quantum dot-quantum well structure, El-Sayed and co-workers have observed electron and hole transfer from CdS to HgS occurring with ~1.5 and 0.4 ps time constants, respectively.[180] Similarly, using a tunable pump pulse and broadband (350-750 nm) white-light probe pulse, we have studied the carrier dynamics in CdSe/CdTe hNRs with well-defined band structures and have determined the rate of electron transfer from CdTe-donor to CdSe-acceptor particles.

While type-II core/shell NPs have been shown to exhibit photoinduced CT,[171,172,185] these materials are presumably not suitable for photovoltaic applications as one of the carriers is always confined to the particle core. Heteromaterial nanorods can be regarded as a logical extension of electron donor-acceptor substituted molecules. Scholes and co-workers recently reported the synthesis of type-II CdSe/CdTe hNRs using classical colloidal chemistry and identified characteristic optical absorption and emission bands for the CT state.[4,169] By describing the photoluminescence decay dynamics with a stochastic kinetic model, they showed that trap-states play an important role in carrier recombination and concluded that electron transfer from the conduction band of CdTe to that of CdSe occurs on the 200 ps time scale.[186] Here, I present experimental data that indicate that the electron transfer occurs on the time scale of several hundred femtoseconds.

5.2.2 Characterization of the CdSe/CdTe heterostructured nanorods

CdSe/CdTe hNRs were synthesized in our lab adopting the procedure from ref. 4. In a single-pot synthesis, first, CdSe seed particles were grown and then Te-precursor is injected to the CdSe solution to grow CdTe crystal on the seed particle. The materials reported here are on average 3.5 nm in diameter and 10-15 nm in length with CdSe seeds of the same diameter and 6-8 nm in length as characterized by TEM (Figure 5.7) and exhibit three important absorption bands. The steady state absorption and emission spectra of a representative batch of hNR in toluene are shown in Figure 5.8. The first two bands (a and b) correspond to the lowest energy 1S transitions of CdSe and CdTe (here referred to as $CdSe_{1S}$, 570 nm and $CdTe_{1S}$, 620 nm, respectively). The third feature (c) is a broad peak at >670 nm corresponding to the CT band where the electron and hole are spatially separated. This band is not present in mixed solutions of CdTe and CdSe NRs. Comparison with the absorption spectrum of the seed material identifies the CdSe 1S transition in the hNR spectrum and suggests that the CdSe NRs do not grow during the CdTe deposition stage.

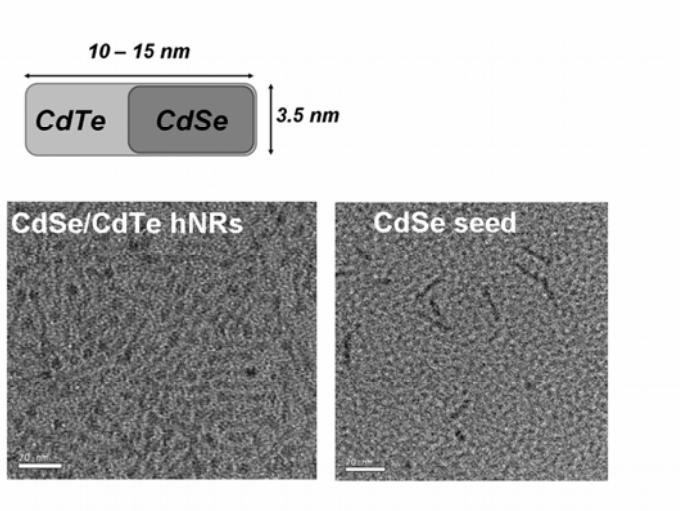

Figure 5.7 Representative TEM micrographs of CdSe and CdSe/CdTe nanocrystals and a simplified diagram of the structure of the CdSe/CdTe hNRs.

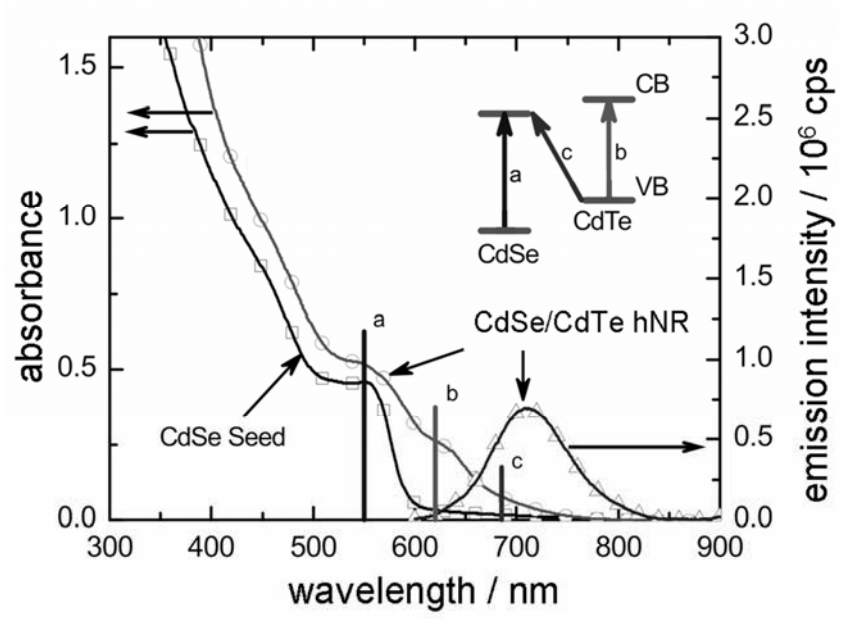

Figure 5.8 Steady-state absorption and emission spectra of CdSe/CdTe hNR. The inset energy level diagram identifies the three absorption bands of interest corresponding to the lowest energy CdSe, CdTe and CT optical transitions (a-c respectively).

5.2.3 Femtosecond dynamics

Light excitation at 620 nm leads to the formation of two distinctly different excited states, i.e., $CdTe_{1S}$-CdSe (where one electron has been promoted from the valence band of CdTe to the conduction band of CdTe) and $CdTe^{+}$-$CdSe^{-}$ (where one electron has been promoted from the valence band of CdTe to the conduction band of CdSe). Figure 5.9 illustrates these states and identifies three optical transitions that are observable as spectral bleaching (after photoexcitation) due to the difference in electron occupation numbers in the respective conduction bands.[151] These three state-filling signals are the CdTe/CdSe CT transition (~680 nm), and the lowest energy transitions (1S) of CdTe (620 nm) and CdSe (550 nm). Hence, by monitoring the temporal evolution of the three bleaching signals one can probe the time-dependent populations of the (optically prepared) $CdTe_{1S}$-CdSe and $CdTe^{+}$-$CdSe^{-}$ states. To simplify the observed dynamics and to extract the contributions from electron transfer, a pump wavelength slightly to the red of the absorption maximum of CdSe has been chosen to effectively eliminate the population of the CdTe-$CdSe_{1S}$ state and thus to ensure that dynamic population of the CT state may solely originate from the $CdTe_{1S}$-CdSe precursor state.

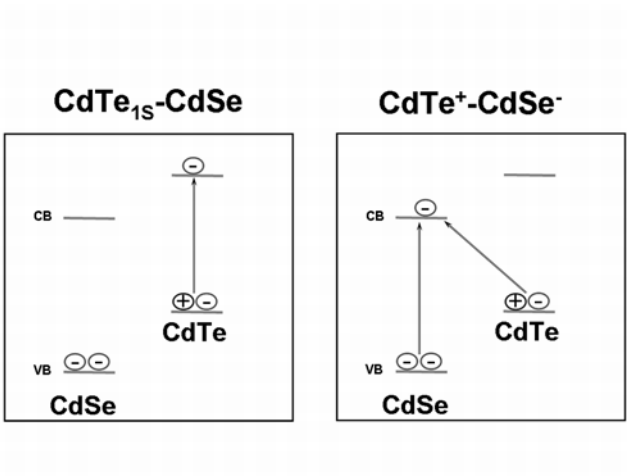

Figure 5.9 Energy level diagrams of the two excited states that are populated by the pump pulse. The arrows illustrate the possible state-filling signals that can be observed as bleaching bands in the femtosecond broadband pump-probe spectra.

In the present experiment, the pump pulse was tuned to 620 nm, i.e., just to the red-side of the 1S transition of CdTe. In order to minimize the effects of multiexciton generation on cooling dynamics and to avoid Auger-type processes, a low-intensity pump pulse was used such that the average number of excitons per particle was less than 0.05. The extinction coefficient was determined based on the $CdTe_{1S}$ absorbance energy.[150] Figure 5.10a displays the temporal evolution of the hNR pump-probe spectra which consists of three separate bleaching bands with maxima at 570, 620, and ~680 nm. As pointed out above, these bands are the state-filling signals that represent the populations of the $CdTe_{1S}$-CdSe and $CdTe^{+}$-$CdSe^{-}$ states. As a control, we examined a mixture of CdTe and CdSe nanorods with similar dimensions (d) 3.5 nm, l) 5-10 nm) in a 1:1 mol

ratio which yielded spectra dominated by bleaching of the $CdTe_{1S}$ transition, however, without the CT band or the state-filling from $CdSe_{1S}$ (Figure 5.10b).

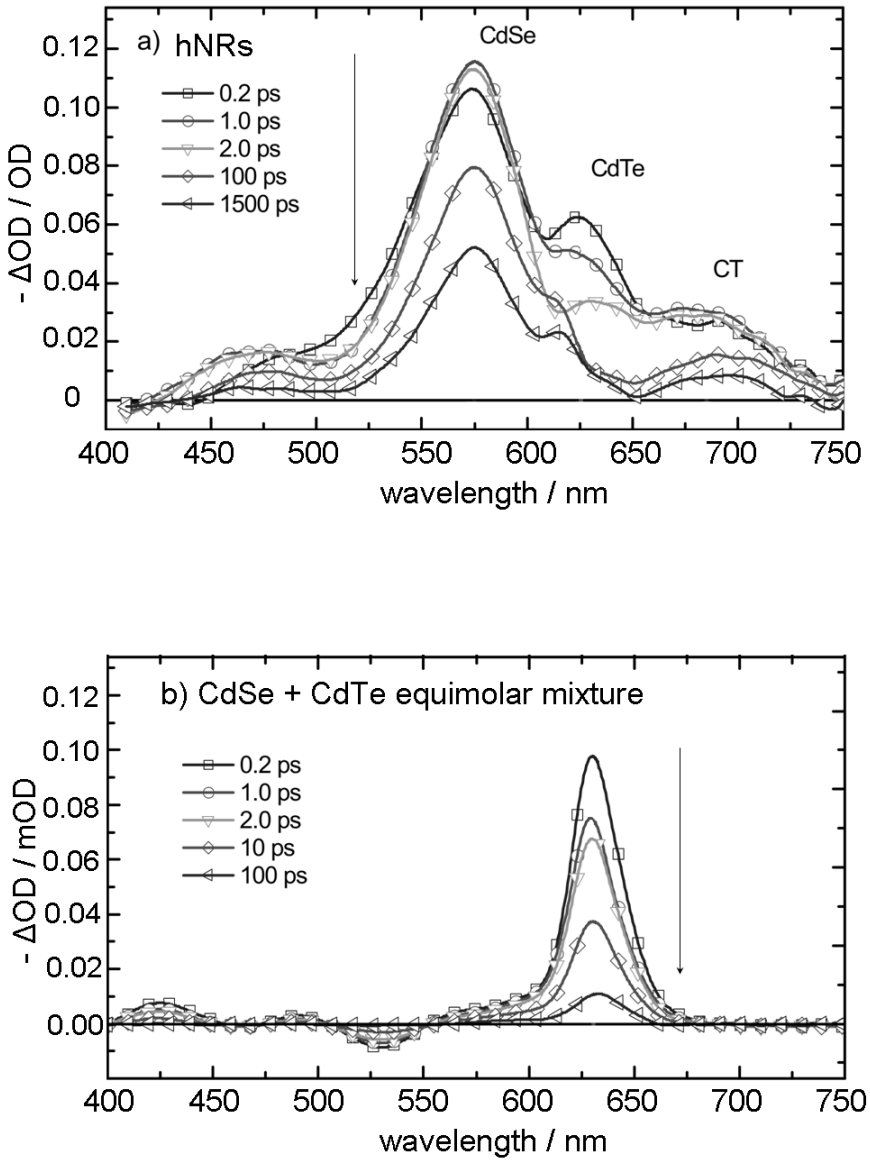

Figure 5.10 Pump-probe spectra (λ_{exc} = 620 nm) of (a) CdSe/CdTe hNR and (b) mixed CdSe and CdTe nanorods at selected time points following photoexcitation of CdTe.

Excitation (620 nm) of CdTe in hNRs leads to a strong state-filling band from electron injection into the 1S(e) level of CdSe (570 and 680 nm). In mixed colloids of similar sized CdSe and CdTe, no state-filling from CdSe is observed.

5.2.4 Electron transfer rates

Plotting the normalized change in absorption at the maxima of the $CdSe_{1S}$, $CdTe_{1S}$, and CT bands as a function of time reveals an ultrafast decay of the $CdTe_{1S}$-CdSe state population (as identified by the $CdTe_{1S}$ band), accompanied by a corresponding increase of the $CdSe_{1S}$ and CT state-filling bands (which are assigned to the $CdTe^{+}$-$CdSe^{-}$ state population, Figure 5.11a). It is noteworthy that the $CdSe_{1S}$ and CT bleaching bands exhibit nearly identical buildup dynamics during the first 2 ps after excitation. Following a sub-100 fs buildup, a second rise with a time constant of ~500 fs is observed. Similarly, a fit of the $CdTe_{1S}$-CdSe population decay at 620 nm in Figure 5.11a reveals a time constant of ~600 fs, a value that is within the error bar of the CT rise-time. The similarity in the rise times of the charge separated $CdTe^{+}$-$CdSe^{-}$ state on the one hand and the decay time of the electron donor $CdTe_{1S}$-CdSe state on the other is consistent with the injection of an electron from the CdTe conduction band into the conduction band of CdSe. The 500 fs buildup only accounts for about 20% of the total signal amplitude indicating that most of the electron population in the CdSe conduction band level arrives on the time scale of the pump pulse. This quasi-instantaneous buildup can occur by either excitation of a

CdSe valence band electron or via the direct optical electron transfer of an electron from the valence band of CdTe to the conduction band of CdSe without forming the $CdTe_{1S}$-CdSe intermediate state. Since our pump wavelength (620 nm) does not overlap with the $CdSe_{1S}$ transition, one must conclude that direct optical CT takes place upon photoexcitation. Note that following the formation of the CT state, hole-transfer to the CdSe valence band would yield a $CdSe_{1S}$ state, but this transition is endothermic in a type-II structure and thus energetically less favorable. While electron-hole-coupled Auger-like relaxation dynamics might be able to stimulate such a transfer, the low pump energy and intensity used should exclude such complications due to multiexciton generation suggesting again that the signal originates from an electron injection event. Entirely consistent with our conclusion (that optical CT takes place) is the presence of a (weak) CT absorption band in the steady-state UV/Vis spectrum (see Figure 5.8) as well as the state-filling bleaching band. Furthermore, since the dynamics of the CT and $CdSe_{1S}$ bands are coupled, the optical transition at >680 nm must involve at least one electron or hole from the CdSe crystal and cannot be associated with an optically allowed transition to a shallow trap-state within the CdTe bandgap. If the broad red-shifted emission observed stemmed from a trap-state, then it would involve states confined within the CdTe band structure and not contribute to the CdSe signal.

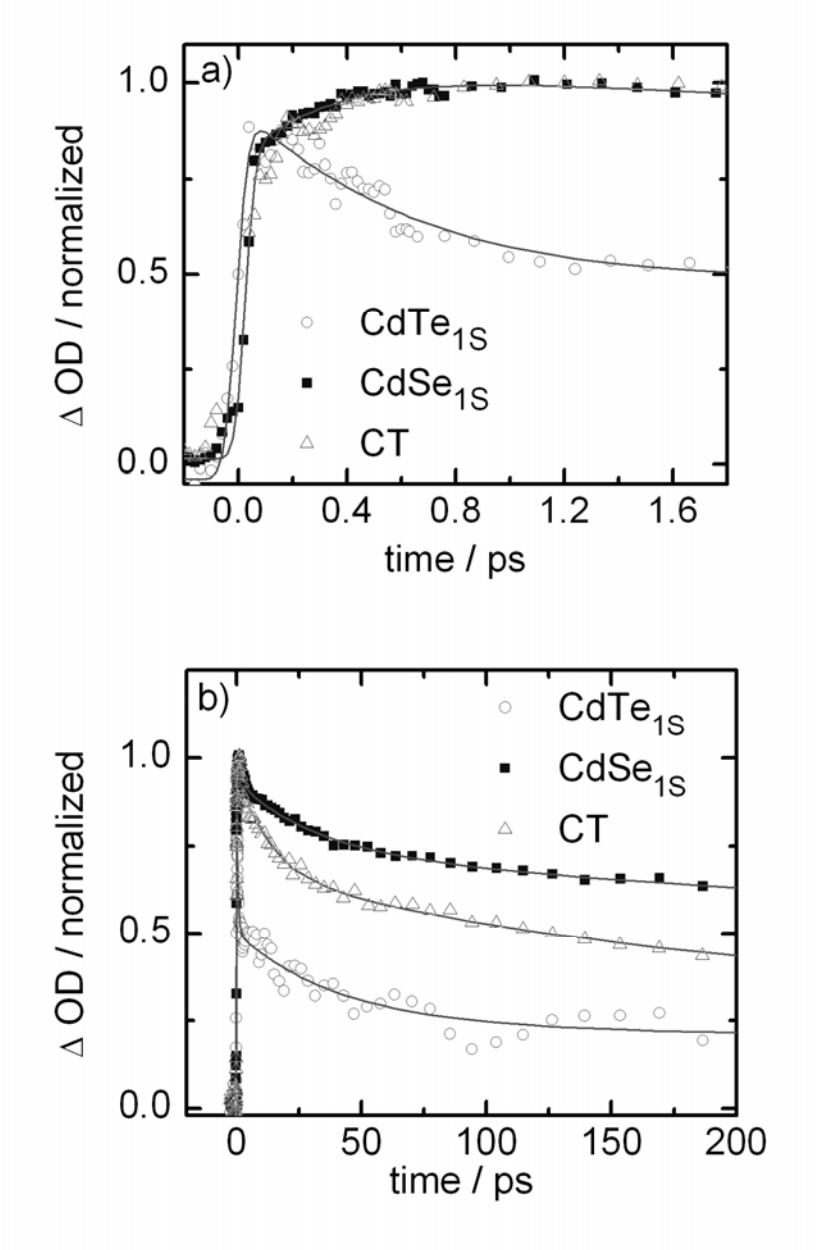

Figure 5.11 Single wavelength kinetics of CdSe, CdTe and CT state-filling signals during the first 1.7 ps (a) and 200 ps (b) following photoexcitation. Differences in decay kinetics on the 10-200 ps time scales originate from partial spectral overlap of the CdTe and CT spectral bands.

Following similar buildup dynamics, the $CdSe_{1S}$ band exhibits a 280 ps decay while the CT band decays with a 200 ps time constant (see Figure 5.11b). We note that if the dynamics of the CT band were monitored between 690 and 700 nm (instead of 685 nm) this discrepancy in the time constants was less pronounced. On the other hand, monitoring the absorption dynamics at wavelengths shorter than 685 nm resulted in a larger discrepancy in the two time constants. On the basis of this observation, we tentatively attribute the difference in dynamics to spectral inhomogeneities in the state-filling bleaching signal due to spectral overlap with the $CdTe_{1S}$ band. Thus, at wavelengths closer to the $CdTe_{1S}$ band, the spectrum is more affected by the decay of the $CdTe_{1S}$ population. Furthermore, as detailed previously,[186] the various dynamical processes involved in carrier relaxation are sufficiently complicated that some deviations from our simple model are not surprising. With an injection time of 500 fs, the interfacial electron transfer event in CdSe/CdTe hNR occurs 3 orders of magnitude faster than previously assumed[186] and on a time scale that is competitive to the ultrafast relaxation dynamics observed in quantum dots.[182] The observed time scale is similar to that of electron-transfer in model dye-sensitized semiconductor systems,[5] hole-transfer across the CdS/HgS interface, and about three times faster than electron transfer at the CdS/HgS interface.[180] The similarity with the observed kinetics in the CdS/HgS system can be explained qualitatively by considering the energy overlap of the respective conduction and valence bands as done in ref. 180. At the CdS/HgS interface, both valence band states are composed of atomic orbitals from S^{2-} giving them more closely matching carrier

effective masses[187] and, correspondingly, favorable condition for resonant CT. In the type-II CdSe/CdTe hNR band structure, both conduction band levels are composed of orbital contributions from Cd^{2+}. By an extension of this analysis, we would expect the hole-transfer process from $CdSe_{1S}$ to CdTe to be slightly slower as a result of less favorable overlap between valence bands states of Te^{2-} and Se^{2-}. This transfer event, however, cannot be isolated from state-filling bleaching signals alone as the hole-transfer dynamics, activated by pumping at or above the CdSe bandgap energy, would be mixed in with the electron transfer mechanism and a number of other cooling processes occurring on a similar time scale.

5.2.5 Conclusion

In conclusion, the electron transfer dynamics in type-II CdSe/CdTe hNRs was examined using ultrafast broadband pump-probe spectroscopy to simultaneously monitor and correlate the state-filling dynamics of the $CdSe_{1S}$, $CdTe_{1S}$, and CT bands on the sub-picoseconds to nanoseconds time scale. By selective photoexcitation of CdTe, we found that photoinduced electron transfer from CdTe to CdSe occurs with a time constant of 500 fs. This ultrafast electron transfer, comparable to the hole transfer in CdS/HgS, is the result of favorable resonance conditions of the corresponding conduction band states.

6 Optical and electronic properties of pyrene-functionalized Single-Walled Carbon Nanotubes

6.1 Introduction

Single-Walled Carbon Nanotubes are one-dimensional nanomaterials with unique mechanical and electronic properties that are attractive for the development of photovoltaic and optoelectronic applications.[188,189] SWNT could be thought as a rolled-up cylindrical graphene sheets with hollow centers that are either metallic or semiconducting. Due to their extended π-electronic structure SWNT readily adsorb various materials on their surface through van der Waals forces and π-π interactions.[190,191] Furthermore, they are good electron acceptors and have excellent electron transport properties that can be effectively used for the construction of large supramolecular complexes for successful charge separation and electron transport.[192,193]

SWNT are difficult to process. They are not soluble in solvents and form bundles from different SWNT sizes. One way to achieve stable nanotube dispersions is through covalent functionalization of the walls of the nanotubes.[191,194] However, such chemical treatment changes the hybridization of the carbon atoms in the nanotubes and disrupts the SWNT electronic structure. Another approach for fabrication of SWNT dispersions is a noncovalent functionalization by polymer or surfactant wrapping.[191,195-198] This approach allows different molecular designs to be achieved without compromising the SWNT structure and properties.

Electron-donating organic chromophores can be noncovalently attached to the sidewalls of SWNT to produce donor-acceptor constructs for photovoltaic applications.[191,194,196] Pyrene derivatives have been used for the dispersion of SWNT as well as for the attachment of various electron donors to SWNT. Examples for such electron donor systems are metalloporphyrins and even inorganic quantum dots.[191,196,199] In addition to the photovoltaic applications, pyrene derivatized SWNT have been applied in biomolecule immobilization for new type biosensors.[197]

An extensive number of spectroscopic studies have focused on investigating the basic optical (and electronic) properties of SWNT and the charge transfer processes in the supramolecular donor-acceptor constructs.[191,196,199-202] Nevertheless, the understanding of the optical and electronic properties of the precursor pyrene-SWNT complex is poor.[199,203,204] Here, we present our spectroscopic investigations on the photophysical properties of SWNT-Pyr complex.

6.2 Results

SWNT purchased from Unidym Inc. were used without further purification. SWNT with 0.8-1.2 nm diameter and 0.2-1000 nm length were synthesized by HiPCO technology. To investigate the optical properties of pyrene and SWNT the following procedure for SWNT dispersion was used.[205] Pyrenebutyric acid (Pyr) was dissolved in 0.1 M sodium tetraborate aqueous buffer with pH = 8.2 to generate 10 mM solutions.

One milligram of raw SWNT was added to 3 ml of the Pyr solution and the mixture was sonicated in a bath sonicator for 30 min. The resulting dispersion was centrifuged (4000 rpm) for four hours to separate the non-tubular hydrocarbons, amorphous carbon and catalyst iron nanoparticles from the heavier nanotubes. After decanting the supernatant, the precipitate consisting of non-dispersed SWNT and SWNT-Pyr was washed (3 times) and re-dispersed in water by short (<1 min) sonication. The final SWNT-Pyr sample was received by decanting the solution over the solid-nondispersed SWNT. A principle structure of SWNT-Pyr is presented on Figure 6.1.

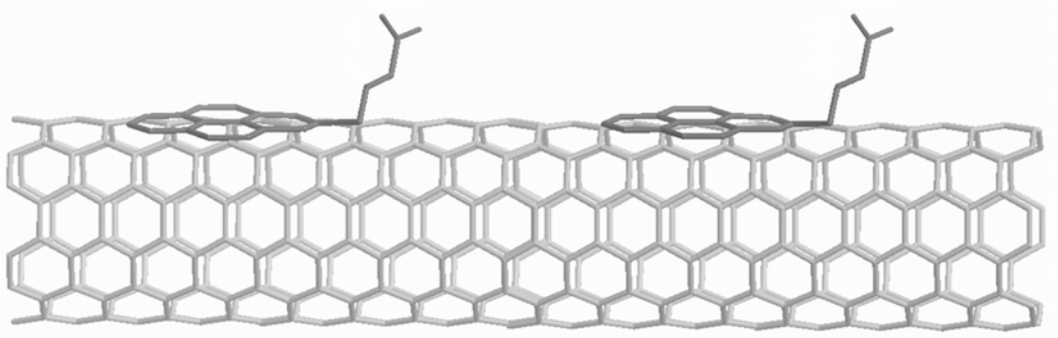

Figure 6.1 Principle structure of the complex formed from SWNT and Pyr.

The absorption spectrum of the SWNT-Pyr is shown on Figure 6.2 together with the spectra of aqueous solutions of pyrenebutyric acid and SWNT dispersed with sodium deoxycholate (SWNT-DOC). Note that semiconductor SWNT absorb light further into the NIR spectral region (~1500 nm) and the transitions in the UV-spectral region correspond to metallic nanotubes. The fluorescence of SWNT-Pyr corresponds to the

fluorescence of the pyrenebutyric acid and is only weakly quenched by SWNT. Based on these observations, we assume that the observed pyrene fluorescence and absorption signals are due to the existence of nonattached Pyr molecules.

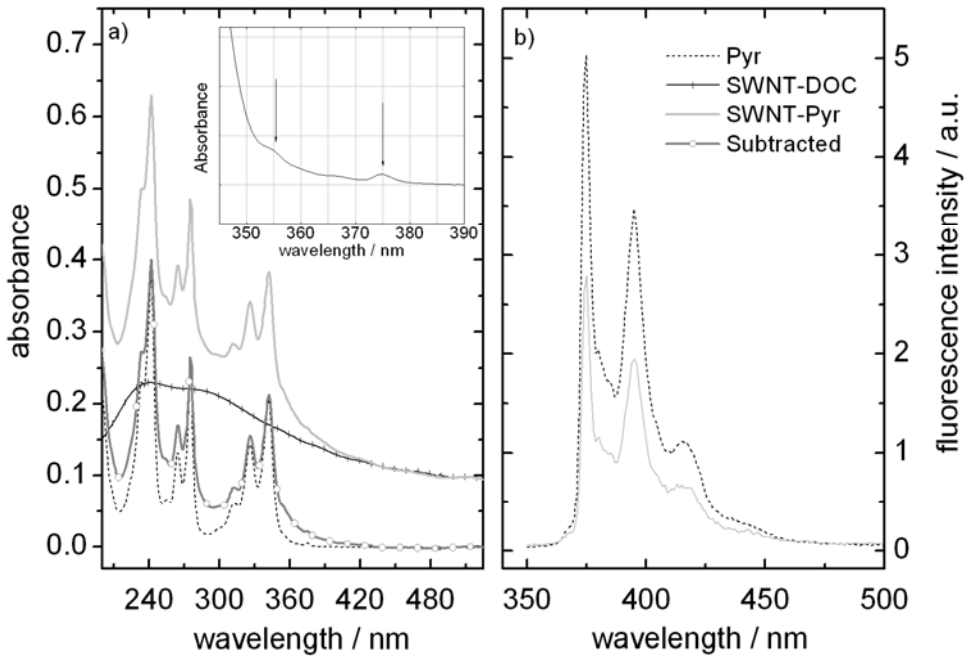

Figure 6.2 a) Absorption spectra of Pyr, SWNT-DOC, SWNT-Pyr and SWNT-DOC subtracted from SWNT-Pyr spectra; b) Fluorescence spectra of Pyr and SWNT-Pyr acquired with 342 nm excitation wavelengths. The fluorescence spectrum is corrected for the difference in the absorbed photons from SWNT in the SWNT-Pyr sample.

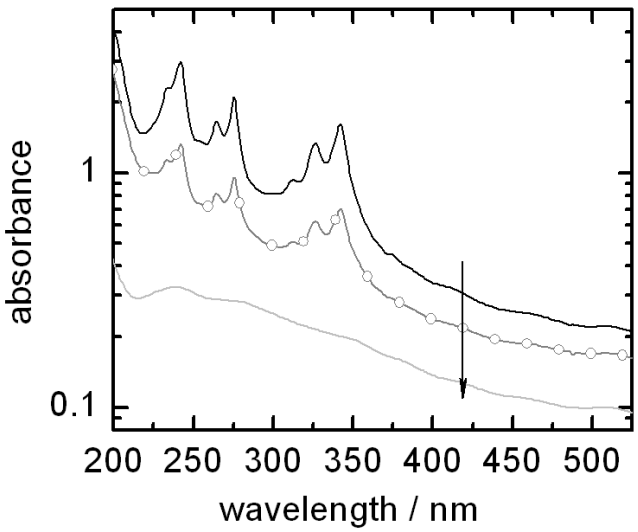

Figure 6.3 Changes in the absorption spectrum of the SWNT dispersions with an increasing number of chloroform extractions.

In order to remove the excess Pyr and to test our assumption we used multiple chloroform extraction steps. Figure 6.3 exhibits how the absorption of Pyr in the SWNT-Pyr samples decreases with increasing number of extraction steps, until Pyr is not observable in the spectrum. It should be noted that due to strong electronic interactions between SWNT and pyrene (vide infra) the latter can have broad absorption bands, which will be buried in the multitude of SWNT absorption bands and thus pyrene signals could be difficult to resolve. In fact, Pyr must be still present in the samples, otherwise the SWNT dispersions would not be stable (SWNT would precipitate quickly). Therefore, it can be concluded that SWNT-Pyr dispersions were free of nonattached Pyr.

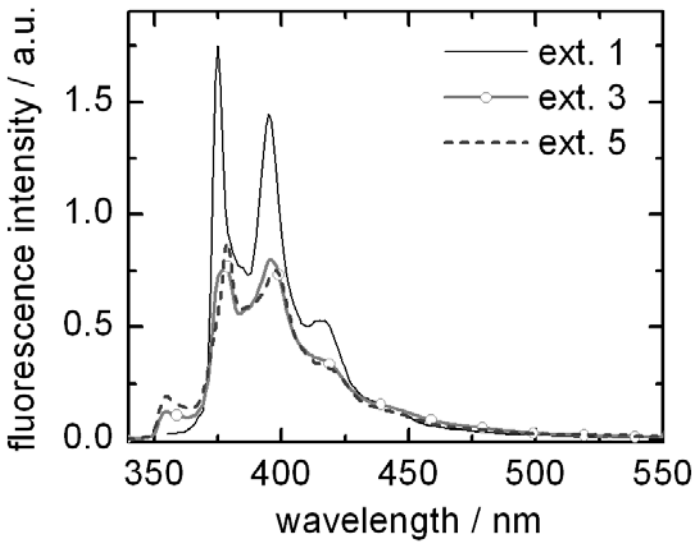

Figure 6.4 Changes in the fluorescence spectrum of the SWNT dispersions with an increasing number of chloroform extractions.

Similarly to the absorption changes, we followed the changes in the fluorescence properties of the SWNT-Pyr with each extraction step. Initially, the SWNT-Pyr fluorescence resembled the fluorescence of pure Pyr, but after each extraction step noticeable changes in the fluorescence were observed: a peak at 355 nm appeared. (Figure 6.4) These observations indicate that the Pyr aromatic ring interacts strongly with the delocalized π-electron system of the nanotubes. To gather more information about the origin of the fluorescence spectrum of Pyr in the SWNT-Pyr complex we performed multiple 2D-fluorescence scans varying the excitation wavelengths from 250 to 450 nm with 2 nm steps. The results are presented on Figure 6.5. Scans of the pyrenebutyric acid and SWNT dispersed with DOC are also included for reference. The comparison between

all spectra shows substantial differences between SWNT-Pyr fluorescence and that of its constituents. The band at 355 nm appears only at excitation wavelengths between 250 and 310 nm. Additionally, 320-350 nm excitations give broader and red-shifted fluorescence to that of nonattached Pyr. The weak intensity broad band at ~475 nm corresponds to emission from SWNT and it has been previously attributed to radiative transitions from defect sites at the ends and the sidewalls of the nanotubes. The number of defects increases with longer sonication times.[206]

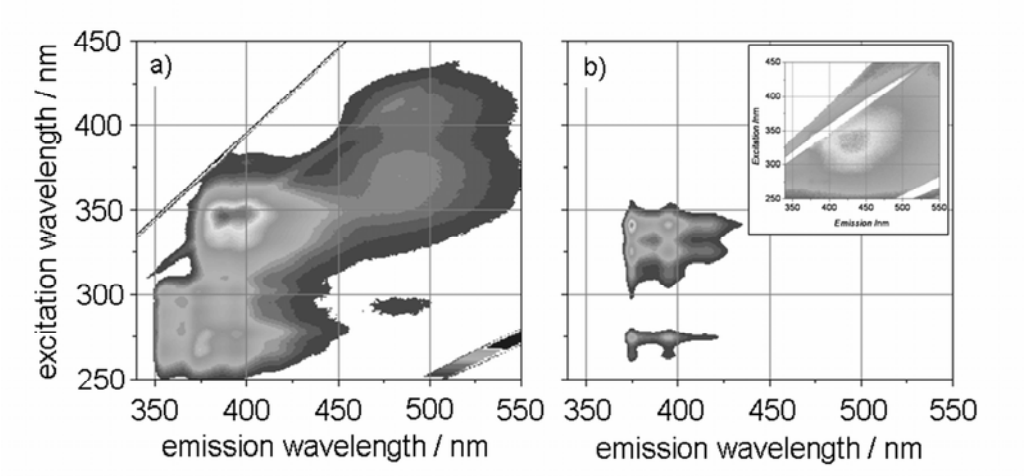

Figure 6.5 2D emission scans of a) SWNT-Pyr and b) Pyr solution. The inset in b) shows the emission spectrum of SWNT dispersed with DOC.

In addition to the observed changes in the fluorescence spectrum the fluorescence lifetime of SWNT-PYR (probed at 400 nm) was found to be substantially shortened compared to the lifetime of Pyr. (Figure 6.6 and Table 4) The fluorescence decays were recorded by TCSPC.[207] The signals are processed by a single photon counting PCI module (SPC-630, Becker-Hickl). Diluted Pyr solutions decay biexponentially with one

major 90 ns component. On the other hand, about 90% of the fluorescence intensity of SWNT-Pyr decays for 20 ns.

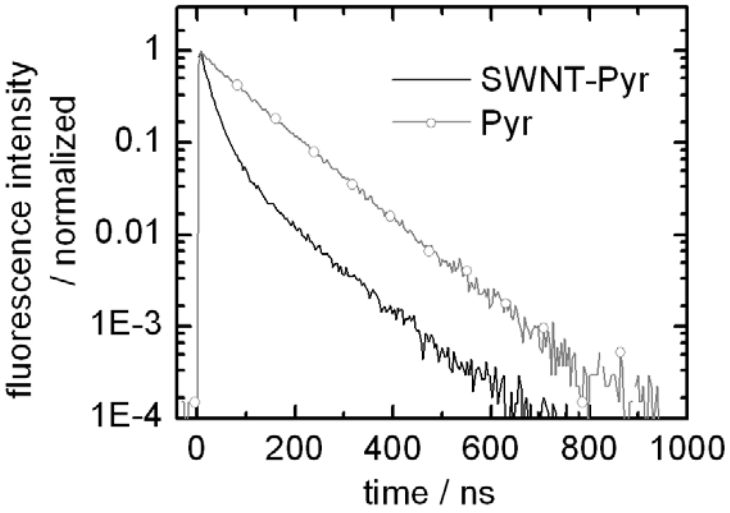

Figure 6.6 Decays of the fluorescence at 400 nm were recorded by TCSPC. Femtosecond (100 fs) pump-pulses with λ = 340 nm were used for an excitation.

Probe / 400 nm	c_1 [%]	τ_1 [ns]	c_2 [%]	τ_2 [ns]	c_2 [%]	τ_3 [ns]
SWNT-PYR	13	3 ±1	74	20 ±1	13	82 ±3
Pyr	100	92 ±1	–	–	–	–
Probe/350 nm						
SWNT-PYR	74	27 ±1	13	91 ±59	–	–

Table 4 Fluorescence lifetimes received from exponential fitting of the emission decays received by TCSPC.

6.3 Discussion and conclusion

Pyrenebutyric acid has absorption and fluorescence spectrum that are very similar to that of pyrene. The optical and electronic properties of pyrene are well understood.[7] Accordingly, the lowest energy band (342 nm) in the UV/Vis absorption spectrum of pyrenebutyric acid is assigned to the vibronic S_0 to S_2 transitions of the pyrene aromatic ring. S_2 is the second (lowest in energy) singlet excited state which is polarized along the molecule's long axis and S_0 is the ground state. The lowest in energy S_0 to S_1 transition is polarized on the short axis of the molecule and is forbidden in pyrene. S_1 can be populated from S_2 by ultrafast IC process that occurs for ~75 fs.[7] The inset of Figure 6.2a shows that pyrenebutyric acid (Pyr) has two very weak bands at ~355 and ~375 nm. Their intensities are ~40 times smaller than the intensity at 342 nm (S_0-S_2 transition). In addition, the first vibronic band in the fluorescence spectrum of Pyr coincides in energy with the band at 375 nm. We assign the 355 and 375 nm peaks to the vibronic S_0-S_1 transitions carrying very low oscillator strength.

In the fluorescence spectrum of SWNT-Pyr, besides the small bathochromic shifts and broadening of the bands (Figure 6.5), we observed the appearance of a new band at 355 nm that can only be excited with 250-310 nm light. The origin of this band is not clear. Its energy coincides with the energy of the absorption band at 355 nm. Previously, Guldi et al. showed that electron transfer does not take place between pyrene and SWNT,[191] which rules out the possibility for the formation of charge transfer states. Also,

concentration dependent experiments showed that Pyr does not aggregate at high concentrations and its absorption and fluorescence spectra do not change upon concentration variations. Therefore, the 355 nm band exists only due to the interactions between SWNT and Pyr.

The ratio in fluorescence intensities of the first (0-0) and the second (0-1) vibronic bands (at 375 and 395 nm, respectively) changes upon Pyr adsorption on the walls of the nanotubes: the intensity of the 0-1 band increases with respect to that of the 0-0 band. Similar fluorescence properties have been previously observed for aggregated organic chromophores, polymers and crystals, and have been assigned to the formation of H-aggregates.[208] In H-aggregates, the transition dipole moments of the stacked molecules are parallel to each other which cause blue shift in the aggregate absorption compared to the monomer molecules, as well as decrease in the oscillator strength of the 0-0 vibronic transition with respect to the 0-1 transition. Accordingly, the excitation spectra of Pyr (Figure 6.5) shows that the SWNT-Pyr fluorescence bands at 375-425 nm originate from emission from a single electronic state (with maximum at ~350 nm) that is red-shifted from the S_0-S_2 transition (342 nm) but blue shifted from the S_0-S_1 transition (375 nm). Based on this analysis, we propose that SWNT-Pyr can be viewed as an H-aggregated supramolecular complex.

Figure 6.6 shows that the fluorescence of SWNT-Pyr decays faster than that of Pyr. Similar shortening of the lifetimes of Pyr was previously observed in optical spectroscopy studies on covalently-linked to the sidewalls of SWNT pyrene

derivatives.[203,204] Sun et al. attributed the observed shorter lifetimes by them to excitation energy transfer from Pyr to SWNT. However, these authors did not observe any changes in the fluorescence spectrum of Pyr, except abundant pyrene excimer emission that additionally complicated their data analysis. On the other hand, our results do not indicate excimer formation, but indicate strong electronic interactions between SWNT and Pyr. The reason for the observed differences is that Sun et al.[203,204] tethered pyrene to the nanotubes with long alkane chains, which allowed the pyrene molecules to freely float in the solutions and to form excimers after light excitation. However, in our experiments the pyrene aromatic ring is directly adsorbs on the walls of the nanotubes and the rearrangement of Pyr to form excimer will cause the precipitation of SWNT.

In conclusion, the results from our initial investigations on organic-donor and SWNT-acceptor constructs were presented. For the first time a noncovalently bound SWNT-pyrene complex has been isolated. Absorption, fluorescence and fluorescence lifetime measurements revealed that the pyrene aromatic ring interacts strongly with SWNT. Hence, aromatic molecules lose their electronic signature when non-covalently attached to carbon nanotubes. Additional investigations with time-resolved techniques in the IR region, where the semiconducting nanotubes absorb light, are needed in order to investigate the changes in the properties (if any) of SWNT in the SWNT-Pyr complex.

7 Future directions

Chapter 3 of this dissertation presented our investigations on the excited state properties of short ds oligonucleotides. Duplexes with different base content and sequence were synthesized. Our results showed that excitons and exciton delocalization are decisive for the relaxation mechanisms in DNA. In the next three paragraphs I propose several directions for future research that can add to our conclusions and contribute to the advancement of the field of DNA photophysics.

Exciton delocalization in the duplexes investigated here increases with their length, but a more precise estimate of the maximum extent of the exciton delocalization is still not available. Longer duplexes with the same sequence and structures need be investigated in order to find the number of bases participating in the exciton state. A logical extension of this research will be the stepwise introduction of G and C bases in ss and ds dA-dT oligonucleotides until more realistic natural sequences are investigated.

In **Chapter 3.3.5** I discussed the need of establishing common experimental conditions that can be followed by all research groups working in this field. In this way experiments performed with different experimental techniques and setups could be directly related to each other. Typically different groups apply only a single experimental technique in their investigations. The utilization of more than one time-resolved technique in our laboratory could broaden our knowledge of the properties of DNA. For example, ultrafast UV/IR experiments could allow us to distinguish between delocalized

exciton states and exciplexes. Also, more knowledge of the excited state relaxation in general and specifically for our short duplexes can be gathered from combined femtosecond fluorescence up-conversion and transient absorption experiments. In the fluorescence experiments we can follow the relaxation of DNA bright states, while with the transient absorption DNA dark states are also detected.

Exciton delocalization is influenced by static and dynamic structural defects and vibrations. Except the static defects, all others are substantially decreased at very low temperatures. On the other hand, when exciplexes are formed structural fluctuations should not play such an important role in the relaxation dynamics.[21,24] Hence, TA measurements in reflection mode, fluorescence up-conversion and TCSPC can be combined to study the temperature dependence of the excited states in DNA.

From our investigations of the exciton-phonon interactions in CdTe NCs we learned that quantum confinement does not change the coupling between excitons and optical phonons in this material and size range. However, we revealed that the holes at the band-edge of CdTe NCs relax by two competing mechanisms: an intrinsic phonon-assisted mechanism and a nonadiabatic transition to a surface state. Future exploration of these two fundamental relaxation mechanisms can be accomplished by altering the surface properties of the NCs. This can be achieved by using different surface passivation ligands or by growing a thin layer of another crystal on the surface of the particle. In this way the surface states in the NCs can be altered, thus, potentially leading to domination of one of the two relaxation mechanisms.

Chapter 5.2 presented our study on the electron transfer in single-sized CdSe/CdTe hNRs. A synthesis of different aspect ratios of CdTe versus CdSe heterorods will allow us to understand the electron transfer properties of these materials. Previously published results proposed that the electron transfer in CdSe/CdTe hNCs happens in the inverted Marcus region. Efforts should be focused on the production of different diameters and lengths of CdSe and CdTe NCs, with which ΔG will be varied and the rate of electron transfer as well. An obstacle to our investigations with CdSe/CdTe hNCs has been the synthesis of homogeneous samples without the presence of nanobarbells and tetrapods. In the latter structures, the CdSe seed is surrounded by more than one CdTe particle, which obstructs the investigations of electron transfer in nanorods. Additionally, for the construction of photovoltaic devices, the electron residing on the seed needs be successfully utilized, which will be better accomplished by using nanorods structures. Therefore, improving the synthetic procedures will be desirable.

Another aspect of the electron transfer investigations is that hNCs with bigger sizes have their lowest exciton absorption bands in the near IR region. Therefore, extending our capabilities for probing and detection in the IR is a continuation of the proposed size-dependent studies. Due to the overlap of the $CdSe_{1S}$, $CdTe_{1S}$ and CT bleaching bands, the detection and separation of the useful signals is usually complicated. Ultrafast IR pulses can probe nanocrystals' intraband transitions – for example, $CdTe_{1S}$ to $CdTe_{1P}$ – which could potentially give more precise information about the electron transfer dynamics in these materials.

8 References

1. Fujimoto, K.; Shimizu, H.; Inouye, M., Unambiguous Detection of Target DNAs by Excimer-Monomer Switching Molecular Beacons. *Journal of Organic Chemistry* **2004**, 69, 3271–3275.
2. Berndl, S.; Wagenknecht, H.-A., Fluorescent Color Readout of DNA Hybridization with Thiazole Orange as an Artificial DNA Base. *Angewandte Chemie-International Edition* **2009**, 48, 2418-2421.
3. Gur, I.; Fromer, N. A.; Geier, M. L.; Alivisatos, A. P., Air-stable all-inorganic nanocrystal solar cells processed from solution. *Science* **2005**, 310, 462-465.
4. Kumar, S.; Jones, M.; Lo, S. S.; Scholes, G. D., Nanorod heterostructures showing photoinduced charge separation. *Small* **2007**, 3, 1633-1639.
5. Anderson, N. A.; Lian, T. Q., Ultrafast electron transfer at the molecule-semiconductor nanoparticle interface. *Annual Review of Physical Chemistry* **2005**, 56, 491-519.
6. Buchvarov, I.; Trifonov, A.; Fiebig, T., Toward an understanding of white-light generation in cubic media - polarization properties across the entire spectral range. *Optics Letters* **2007**, 32, (11), 1539-1541.
7. Raytchev, M.; Pandurski, E.; Buchvarov, I.; Modrakowski, C.; Fiebig, T., Bichromophoric interactions and time-dependent excited state mixing in pyrene derivatives. A femtosecond broad-band pump-probe study. *Journal of Physical Chemistry A* **2003**, 107, (23), 4592-4600.
8. Tzankov, P.; Buchvarov, I.; Fiebig, T., Broadband optical parametric amplification in the near UV-VIS. *Optics Communications* **2002**, 203, (1-2), 107-113.
9. Tzankov, P.; Fiebig, T.; Buchvarov, I., Tunable femtosecond pulses in the near-ultraviolet from ultrabroadband parametric amplification. *Applied Physics Letters* **2003**, 82, (4), 517-519.
10. Trifonov, A.; Raytchev, M.; Buchvarov, I.; Rist, M.; Barbaric, J.; Wagenknecht, H. A.; Fiebig, T., Ultrafast energy transfer and structural dynamics in DNA. *Journal of Physical Chemistry B* **2005**, 109, (41), 19490-19495.
11. Fork, R. L.; Martinez, O. E.; Gordon, J. P., Negative Dispersion Using Pairs of Prisms. *Optics Letters* **1984**, 9, (5), 150-152.
12. Maciejewski, A.; Naskrecki, R.; Lorenc, M.; Ziolek, M.; Karolczak, J.; Kubicki, J.; Matysiak, M.; Szymanski, M., Transient absorption experimental set-up with femtosecond time resolution. Femto- and picosecond study of DCM molecule in cyclohexane and methanol solution. *Journal of Molecular Structure* **2000**, 555, 1-13.
13. Ekvall, K.; van der Meulen, P.; Dhollande, C.; Berg, L. E.; Pommeret, S.; Naskrecki, R.; Mialocq, J. C., Cross phase modulation artifact in liquid phase transient absorption spectroscopy. *Journal of Applied Physics* **2000**, 87, (5), 2340-2352.

14. Lorenc, M.; Ziolek, M.; Naskrecki, R.; Karolczak, J.; Kubicki, J.; Maciejewski, A., Artifacts in femtosecond transient absorption spectroscopy. *Applied Physics B-Lasers and Optics* **2002**, 74, (1), 19-27.
15. Tokunaga, E.; Terasaki, A.; Kobayashi, T., Induced Phase Modulation of Chirped Continuum Pulses Studied with a Femtosecond Frequency-Domain Interferometer. *Optics Letters* **1993**, 18, (5), 370-372.
16. Kovalenko, S. A.; Dobryakov, A. L.; Ruthmann, J.; Ernsting, N. P., Femtosecond spectroscopy of condensed phases with chirped supercontinuum probing. *Physical Review A* **1999**, 59, (3), 2369.
17. Raytchev, M.; Mayer, E.; Amann, N.; Wagenknecht, H. A.; Fiebig, T., Ultrafast proton-coupled electron-transfer dynamics in pyrene-modified pyrimidine nucleosides: Model studies towards an understanding of reductive electron transport in DNA. *Chemphyschem* **2004**, 5, (5), 706-712.
18. Pfeifer, G. P.; You, Y. H.; Besaratinia, A., Mutations induced by ultraviolet light. *Mutation Research-Fundamental and Molecular Mechanisms of Mutagenesis* **2005**, 571, (1-2), 19-31.
19. Melnikova, V. O.; Ananthaswamy, H. N., Cellular and molecular events leading to the development of skin cancer. *Mutation Research-Fundamental and Molecular Mechanisms of Mutagenesis* **2005**, 571, (1-2), 91-106.
20. Dumaz, N.; vanKranen, H. J.; deVries, A.; Berg, R. J. W.; Wester, P. W.; vanKreijl, C. F.; Sarasin, A.; DayaGrosjean, L.; deGruijl, F. R., The role of UV-B light in skin carcinogenesis through the analysis of p53 mutations in squamous cell carcinomas of hairless mice. *Carcinogenesis* **1997**, 18, (5), 897-904.
21. Middleton, C. T.; de La Harpe, K.; Su, C.; Law, Y. K.; Crespo-Hernandez, C. E.; Kohler, B., DNA Excited-State Dynamics: From Single Bases to the Double Helix. *Annual Review of Physical Chemistry* **2009**, 60, 217-239.
22. Fiebig, T., Exciting DNA. *Journal of Physical Chemistry B* **2009**, 113, (27), 9348-9349.
23. Markovitsi, D.; Gustavsson, T.; Banyasz, A., Absorption of UV radiation by DNA: Spatial and temporal features. *Mutation Research-Reviews in Mutation Research* **2010**, 704, (1-3), 21-28.
24. Crespo-Hernandez, C. E.; Cohen, B.; Hare, P. M.; Kohler, B., Ultrafast excited-state dynamics in nucleic acids. *Chemical Reviews* **2004**, 104, (4), 1977-2019.
25. Eisinger, J.; Shulman, R. G., Excited Electronic States of DNA. *Science* **1968**, 161, (3848), 1311-1319.
26. Eisinger, J.; Gueron, M.; Shulman, R. G.; Yamane, T., Excimer Fluorescence of Dinucleotides Polynucleotides and DNA. *Proceedings of the National Academy of Sciences of the United States of America* **1966**, 55, (5), 1015-1019.
27. Gustavsson, T.; Improta, R.; Markovitsi, D., DNA/RNA: Building Blocks of Life Under UV Irradiation. *Journal of Physical Chemistry Letters* **2010**, 1, (13), 2025-2030.
28. Onidas, D.; Markovitsi, D.; Marguet, S.; Sharonov, A.; Gustavsson, T., Fluorescence properties of DNA nucleosides and nucleotides: A refined steady-state and femtosecond investigation. *Journal of Physical Chemistry B* **2002**, 106, (43), 11367-11374.

29. Peon, J.; Zewail, A. H., DNA/RNA nucleotides and nucleosides: direct measurement of excited-state lifetimes by femtosecond fluorescence up-conversion. *Chemical Physics Letters* **2001**, 348, (3-4), 255-262.
30. Pecourt, J. M. L.; Peon, J.; Kohler, B., DNA excited-state dynamics: Ultrafast internal conversion and vibrational cooling in a series of nucleosides. *Journal of the American Chemical Society* **2001**, 123, (42), 10370-10378.
31. Santoro, F.; Barone, V.; Gustavsson, T.; Improta, R., Solvent effect on the singlet excited-state lifetimes of nucleic acid bases: A computational study of 5-fluorouracil and uracil in acetonitrile and water. *Journal of the American Chemical Society* **2006**, 128, (50), 16312-16322.
32. Hare, P. M.; Crespo-Hernandez, C. E.; Kohler, B., Solvent-dependent photophysics of 1-cyclohexyluracil: Ultrafast branching in the initial bright state leads nonradiatively to the electronic ground state and a long-lived $^{1}n\pi$ state. *Journal of Physical Chemistry B* **2006**, 110, (37), 18641-18650.
33. Callis, P. R., Electronic States and Luminescence of Nucleic-Acid Systems. *Annual Review of Physical Chemistry* **1983**, 34, 329-357.
34. Hudock, H. R.; Martinez, T. J., Excited-State Dynamics of Cytosine Reveal Multiple Intrinsic Subpicosecond Pathways. *Chemphyschem* **2008**, 9, (17), 2486-2490.
35. Kosma, K.; Schroter, C.; Samoylova, E.; Hertel, I. V.; Schultz, T., Excited-State Dynamics of Cytosine Tautomers. *Journal of the American Chemical Society* **2009**, 131, (46), 16939-16943.
36. Asturiol, D.; Lasorne, B.; Robb, M. A.; Blancafort, L., Photophysics of the pi,pi* and n,pi* States of Thymine: MS-CASPT2 Minimum-Energy Paths and CASSCF on-the-Fly Dynamics. *Journal of Physical Chemistry A* **2009**, 113, (38), 10211-10218.
37. Matsika, S., Radiationless decay of excited states of uracil through conical intersections. *Journal of Physical Chemistry A* **2004**, 108, (37), 7584-7590.
38. Serrano-Perez, J. J.; Gonzalez-Luque, R.; Merchan, M.; Serrano-Andres, L., On the intrinsic population of the lowest triplet state of thymine. *Journal of Physical Chemistry B* **2007**, 111, (41), 11880-11883.
39. Hare, P. M.; Middleton, C. T.; Mertel, K. I.; Herbert, J. M.; Kohler, B., Time-resolved infrared spectroscopy of the lowest triplet state of thymine and thymidine. *Chemical Physics* **2008**, 347, (1-3), 383-392.
40. Kwok, W. M.; Ma, C.; Phillips, D. L., A doorway state leads to photostability or triplet photodamage in thymine DNA. *Journal of the American Chemical Society* **2008**, 130, (15), 5131-5139.
41. Nachtigallova, D.; Zeleny, T.; Ruckenbauer, M.; Muller, T.; Barbatti, M.; Hobza, P.; Lischka, H., Does Stacking Restrain the Photodynamics of Individual Nucleobases? *Journal of the American Chemical Society* **2010**, 32, (24), 8261-8263.
42. Johnson, W. C.; Tinoco, I., Circular dichroism of polynucleotides: A simple theory. *Biopolymers* **1969**, 7, 727–749.
43. Takaya, T.; Su, C.; de La Harpe, K.; Crespo-Hernandez, C. E.; Kohler, B., UV excitation of single DNA and RNA strands produces high yields of exciplex states between two stacked bases. *Proceedings of the National Academy of Sciences of the United States of America* **2008**, 105, (30), 10285-10290.

44. Crespo-Hernandez, C. E.; Kohler, B., Influence of secondary structure on electronic energy relaxation in adenine homopolymers. *Journal of Physical Chemistry B* **2004**, 108, (30), 11182-11188.
45. Crespo-Hernandez, C. E.; Cohen, B.; Kohler, B., Base stacking controls excited-state dynamics in A-T DNA. *Nature* **2005**, 436, (7054), 1141-1144.
46. Kwok, W. M.; Ma, C. S.; Phillips, D. L., "Bright" and "Dark" Excited States of an Alternating AT Oligomer Characterized by Femtosecond Broadband Spectroscopy. *Journal of Physical Chemistry B* **2009**, 113, (33), 11527-11534.
47. Buchvarov, I.; Wang, Q.; Raytchev, M.; Trifonov, A.; Fiebig, T., Electronic energy delocalization and dissipation in single- and double-stranded DNA. *Proceedings of the National Academy of Sciences of the United States of America* **2007**, 104, (12), 4794-4797.
48. de La Harpe, K.; Crespo-Hernandez, C. E.; Kohler, B., The Excited-State Lifetimes in a G center dot C DNA Duplex are Nearly Independent of Helix Conformation and Base-Pairing Motif. *Chemphyschem* **2009**, 10, (9-10), 1421-1425.
49. Onidas, D.; Gustavsson, T.; Lazzarotto, E.; Markovitsi, D., Fluorescence of the DNA double helix $(dA)_{20}{\cdot}(dT)_{20}$ studied by femtosecond Spectroscopy - Effect of the duplex size on the properties of the excited states. *Journal of Physical Chemistry B* **2007**, 111, (32), 9644-9650.
50. Plessow, R.; Brockhinke, A.; Eimer, W.; Kohse-Hoinghaus, K., Intrinsic time- and wavelength-resolved fluorescence of oligonucleotides: A systematic investigation using a novel picosecond laser approach. *Journal of Physical Chemistry B* **2000**, 104, (15), 3695-3704.
51. Kuimova, M. K.; Dyer, J.; George, M. W.; Grills, D. C.; Kelly, J. M.; Matousek, P.; Parker, A. W.; Sun, X. Z.; Towrie, M.; Whelan, A. M., Monitoring the effect of ultrafast deactivation of the electronic excited states of DNA bases and polynucleotides following 267 nm laser excitation using picosecond time-resolved infrared spectroscopy. *Chemical Communications* **2005**, (9), 1182-1184.
52. Conti, I.; Altoe, P.; Stenta, M.; Garavelli, M.; Orlandi, G., Adenine deactivation in DNA resolved at the CASPT2//CASSCF/AMBER level. *Physical Chemistry Chemical Physics* **2010**, 12, (19), 5016-5023.
53. Markovitsi, D.; Gustavsson, T.; Talbot, F., Excited states and energy transfer among DNA bases in double helices. *Photochemical & Photobiological Sciences* **2007**, 6, (7), 717-724.
54. Doorley, G. W.; McGovern, D. A.; George, M. W.; Towrie, M.; Parker, A. W.; Kelly, J. M.; Quinn, S. J., Picosecond Transient Infrared Study of the Ultrafast Deactivation Processes of Electronically Excited B-DNA and Z-DNA Forms of $[poly(dG\text{-}dC)]_2$. *Angewandte Chemie-International Edition* **2009**, 48, (1), 123-127.
55. de La Harpe, K.; Crespo-Hernandez, C. E.; Kohler, B., Deuterium Isotope Effect on Excited-State Dynamics in an Alternating GC Oligonucleotide. *Journal of the American Chemical Society* **2009**, 131, (48), 17557-17559.
56. Kwok, W. M.; Ma, C. S.; Phillips, D. L., Femtosecond time- and wavelength-resolved fluorescence and absorption spectroscopic study of the excited states of

adenosine and an adenine oligomer. *Journal of the American Chemical Society* **2006**, 128, (36), 11894-11905.
57. Markovitsi, D.; Talbot, F.; Gustavsson, T.; Onidas, D.; Lazzarotto, E.; Marguet, S., Molecular spectroscopy: Complexity of excited-state dynamics in DNA. *Nature* **2006,** 441, (7094), E7-E7.
58. Markovitsi, D.; Onidas, D.; Gustavsson, T.; Talbot, F.; Lazzarotto, E., Collective behavior of Franck-Condon excited states and energy transfer in DNA double helices. *Journal of the American Chemical Society* **2005,** 127, (49), 17130-17131.
59. Onidas, D.; Gustavsson, T.; Lazzarotto, E.; Markovitsi, D., Fluorescence of the DNA double helices $(dAdT)_n{\cdot}(dAdT)_n$ studied by femtosecond spectroscopy. *Physical Chemistry Chemical Physics* **2007,** 9, (37), 5143-5148.
60. Markovitsi, D.; Sharonov, A.; Onidas, D.; Gustavsson, T., The effect of molecular organisation in DNA oligomers studied by femtosecond fluorescence spectroscopy. *Chemphyschem* **2003,** 4, (3), 303-305.
61. Emanuele, E.; Zakrzewska, K.; Markovitsi, D.; Lavery, R.; Millie, P., Exciton states of dynamic DNA double helices: Alternating dCdG sequences. *Journal of Physical Chemistry B* **2005,** 109, (33), 16109-16118.
62. Emanuele, E.; Markovitsi, D.; Millie, P.; Zakrzewska, K., UV spectra and excitation delocalization in DNA: Influence of the spectral width. *Chemphyschem* **2005,** 6, (7), 1387-1392.
63. Bouvier, B.; Gustavsson, T.; Markovitsi, D.; Millie, P., Dipolar coupling between electronic transitions of the DNA bases and its relevance to exciton states in double helices. *Chemical Physics* **2002,** 275, (1-3), 75-92.
64. Bouvier, B.; Dognon, J. P.; Lavery, R.; Markovitsi, D.; Millie, P.; Onidas, D.; Zakrzewska, K., Influence of conformational dynamics on the exciton states of DNA oligomers. *Journal of Physical Chemistry B* **2003,** 107, (48), 13512-13522.
65. Davydov, A. S., *Theory of Molecular Excitons*. **1962**.
66. Kasha, M.; Rawls, H. R.; El-Bayoumi, M. A., The exciton model in molecular spectroscopy. *Pure and Applied Chemistry* **1965,** 11, 371-392.
67. Conwell, E. M.; McLaughlin, P. M.; Bloch, S. M., Charge-transfer excitons in DNA. *Journal of Physical Chemistry B* **2008,** 112, (7), 2268-2272.
68. Tonzani, S.; Schatz, G. C., Electronic excitations and spectra in single-stranded DNA. *Journal of the American Chemical Society* **2008,** 130, (24), 7607-7612.
69. Schwalb, N. K.; Temps, F., Ultrafast electronic relaxation in guanosine is promoted by hydrogen bonding with cytidine. *Journal of the American Chemical Society* **2007,** 129, (30), 9272-9273.
70. Schwalb, N. K.; Michalak, T.; Temps, F., Ultrashort Fluorescence Lifetimes of Hydrogen-Bonded Base Pairs of Guanosine and Cytidine in Solution. *Journal of Physical Chemistry B* **2009,** 113, (51), 16365-16376.
71. Sobolewski, A. L.; Domcke, W.; Hattig, C., Tautomeric selectivity of the excited-state lifetime of guanine/cytosine base pairs: The role of electron-driven proton-transfer processes. *Proceedings of the National Academy of Sciences of the United States of America* **2005,** 102, (50), 17903-17906.

72. Sobolewski, A. L.; Domcke, W., Ab initio studies on the photophysics of the guanine-cytosine base pair. *Physical Chemistry Chemical Physics* **2004,** 6, (10), 2763-2771.
73. Starikov, E. B., Importance of charge transfer excitations in DNA electron spectrum: A ZINDO semiempirical quantum-chemical study. *Modern Physics Letters B* **2004,** 18, (16), 825-831.
74. Kohler, B., Nonradiative Decay Mechanisms in DNA Model Systems. *Journal of Physical Chemistry Letters* **2010,** 1, (13), 2047-2053.
75. Schwalb, N. K.; Temps, F., Base sequence and higher-order structure induce the complex excited-state dynamics in DNA. *Science* **2008,** 322, (5899), 243-245.
76. Holm, A. I. S.; Nielsen, L. M.; Kohler, B.; Hoffman, S. V.; Nielsen, S. B., Electronic coupling between cytosine bases in DNA single strands and i-motifs revealed from synchrotron radiation circular dichroism experiments. *Physical Chemistry Chemical Physics* **2010,** 12, (14), 3426-3430.
77. Vaya, I.; Miannay, F. A.; Gustavsson, T.; Markovitsi, D., High-Energy Long-Lived Excited States in DNA Double Strands. *Chemphyschem* 11, (5), 987-989.
78. Lewis, F. D.; Zhang, L. G.; Liu, X. Y.; Zuo, X. B.; Tiede, D. M.; Long, H.; Schatz, G. C., DNA as helical ruler: Exciton-coupled circular dichroism in DNA conjugates. *Journal of the American Chemical Society* **2005,** 127, (41), 14445-14453.
79. Improta, R.; Santoro, F.; Barone, V.; Lami, A., Vibronic Model for the Quantum Dynamical Study of the Competition between Bright and Charge-Transfer Excited States in Single-Strand Polynucleotides: The Adenine Dimer Case. *Journal of Physical Chemistry A* **2009,** 113, (52), 15346-15354.
80. Novoderezhkin, V.; Monshouwer, R.; van Grondelle, R., Disordered exciton model for the core light-harvesting antenna of Rhodopseudomonas viridis. *Biophysical Journal* **1999,** 77, (2), 666-681.
81. Lewis, F. D.; Wu, Y. S.; Liu, X. Y., Synthesis, structure, and photochemistry of exceptionally stable synthetic DNA hairpins with stilbene diether linkers. *Journal of the American Chemical Society* **2002,** 124, (41), 12165-12173.
82. Tuma, J.; Tonzani, S.; Schatz, G. C.; Karaba, A. H.; Lewis, F. D., Structure and electronic spectra of DNA mini-hairpins with G_n:C_n stems. *Journal of Physical Chemistry B* **2007,** 111, (45), 13101-13106.
83. Miannay, F. A.; Banyasz, A.; Gustavsson, T.; Markovitsi, D., Ultrafast excited-state deactivation and energy transfer in guanine-cytosine DNA double helices. *Journal of the American Chemical Society* **2007,** 129, 14574-14575.
84. Crespo-Hernandez, C. E.; de La Harpe, K.; Kohler, B., Ground-state recovery following UV excitation is much slower in G center dot C - DNA duplexes and hairpins than in mononucleotides. *Journal of the American Chemical Society* **2008,** 130, (33), 10844-10845.
85. Lange, A. W.; Herbert, J. M., Both Intra- and Interstrand Charge-Transfer Excited States in Aqueous B-DNA Are Present at Energies Comparable To, or Just Above, the $1^1\pi\pi^*$ Excitonic Bright States. *Journal of the American Chemical Society* **2009,** 131, (11), 3913-3922.

86. Burin, A. L.; Dickman, J. A.; Uskov, D. B.; Hebbard, C. F. F.; Schatz, G. C., Optical absorption spectra and monomer interaction in polymers: Investigation of exciton coupling in DNA hairpins. *Journal of Chemical Physics* **2008,** 129, (9), 091102.
87. Miannay, F. A.; Banyasz, A.; Gustavsson, T.; Markovitsi, D., Excited States and Energy Transfer in G-Quadruplexes. *Journal of Physical Chemistry C* **2009,** 113, (27), 11760-11765.
88. Zhu, X. Y.; Yang, Q.; Muntwiler, M., Charge-Transfer Excitons at Organic Semiconductor Surfaces and Interfaces. *Accounts of Chemical Research* **2009,** 42, (11), 1779-1787.
89. Markovitsi, D.; Onidas, D.; Talbot, F.; Marguet, S.; Gustavsson, T.; Lazzarotto, E., UVB/UVC induced processes in model DNA helices studied by time-resolved spectroscopy: Pitfalls and tricks. *Journal of Photochemistry and Photobiology A: Chemistry* **2006,** 183, 1–8.
90. Tyagi, S.; Kramer, F. R., Molecular beacons: Probes that fluoresce upon hybridization. *Nature Biotechnology* **1996,** 14, (3), 303-308.
91. Tan, W. H.; Wang, K. M.; Drake, T. J., Molecular beacons. *Current Opinion in Chemical Biology* **2004,** 8, (5), 547-553.
92. Piatek, A. S.; Tyagi, S.; Pol, A. C.; Telenti, A.; Miller, L. P.; Kramer, F. R.; Alland, D., Molecular beacon sequence analysis for detecting drug resistance in Mycobacterium tuberculosis. *Nature Biotechnology* **1998,** 16, (4), 359-363.
93. Ramakrishnan, A.; Sadana, A., A kinetic study of analyte-receptor binding and dissociation for biosensor applications: a fractal analysis for two different DNA systems. *Biosystems* **2002,** 66, (3), 165-177.
94. Wang, Y. J.; Wang, H.; Gao, L.; Liu, H. P.; Lu, Z. H.; He, N. Y., Polyacrylamide gel film immobilized molecular beacon array for single nucleotide mismatch detection. *Journal of Nanoscience and Nanotechnology* **2005,** 5, (4), 653-658.
95. Wang, K. M.; Tang, Z. W.; Yang, C. Y. J.; Kim, Y. M.; Fang, X. H.; Li, W.; Wu, Y. R.; Medley, C. D.; Cao, Z. H.; Li, J.; Colon, P.; Lin, H.; Tan, W. H., Molecular Engineering of DNA: Molecular Beacons. *Angewandte Chemie-International Edition* **2009,** 48, (5), 856-870.
96. Zhang, P.; Beck, T.; Tan, W. H., Design of a molecular beacon DNA probe with two fluorophores. *Angewandte Chemie-International Edition* **2001,** 40, (2), 402-405.
97. Conlon, P.; Yang, C. J.; Wu, Y.; Chen, Y.; Martinez, K.; Kim, Y.; Stevens, N.; Marti, A. A.; Jockusch, S.; Turro, N. J.; Tan, W., Pyrene Excimer Signaling Molecular Beacons for Probing Nucleic Acids. *Journal of the American Chemical Society* **2008,** 130, (1), 336-342.
98. Hu, L. H.; Zhao, Y.; Wang, F.; Chen, G. H.; Ma, C. S.; Kwok, W. M.; Phillips, D. L., Are adenine strands helical H-aggregates? *Journal of Physical Chemistry B* **2007,** 111, (40), 11812-11816.
99. Balakin, K. V.; Korshun, V. A.; Mikhalev, II; Maleev, G. V.; Malakhov, A. D.; Prokhorenko, I. A.; Berlin, Y. A., Conjugates of oligonucleotides with polyaromatic fluorophores as promising DNA probes. *Biosensors & Bioelectronics* **1998,** 13, (7-8), 771-778.

100. Kashida, H.; Asanuma, H.; Komiyama, M., Insertion of two pyrene moieties into oligodeoxyribonucleotides for the efficient detection of deletion polymorphisms. *Chemical Communications* **2006**, (26), 2768-2770.
101. Malinovskii, V. L.; Samain, F.; Haner, R., Helical arrangement of interstrand stacked pyrenes in a DNA framework. *Angewandte Chemie-International Edition* **2007,** 46, (24), 4464-4467.
102. Yamana, K.; Iwai, T.; Ohtani, Y.; Sato, S.; Nakamura, M.; Nakano, H., Bis-pyrene-labeled oligonucleotides: Sequence specificity of excimer and monomer fluorescence changes upon hybridization with DNA. *Bioconjugate Chemistry* **2002,** 13, (6), 1266-1273.
103. Hosoi, K.; Hirano, A.; Tani, T., Dynamics of photocreated positive holes in silver bromide microcrystals with adsorbed cyanine dyes. *Journal of Applied Physics* **2001,** 90, (12), 6197-6204.
104. Zeidan, T. A.; Carmieli, R.; Kelley, R. F.; Wilson, T. M.; Lewis, F. D.; Wasielewski, M. R., Charge-transfer and spin dynamics in DNA hairpin conjugates with perylenediimide as a base-pair surrogate. *Journal of the American Chemical Society* **2008,** 130, (42), 13945-13955.
105. Glazer, A. N.; Rye, H. S., Stable dye-DNA intercalation complexes as reagents for high-sensitivity fluorescence detection. *Nature* **1992,** 359, 859-861.
106. Svanvik, N.; Nygren, J.; Westman, G.; Kubista, M., Free-probe fluorescence of light-up probes. *Journal of the American Chemical Society* **2001,** 123, (5), 803-809.
107. Jarikote, D. V.; Krebs, N.; Tannert, S.; Roder, B.; Seitz, O., Exploring base-pair-specific optical properties of the DNA stain thiazole orange. *Chemistry-a European Journal* **2007,** 13, (1), 300-310.
108. Berndl, S.; Breunig, M.; Gopferich, A.; Wagenknecht, H. A., Imaging of RNA delivery to cells by thiazole orange as a fluorescent RNA base substitution. *Organic & Biomolecular Chemistry* **2010***,* 8, (5), 997-999.
109. Baumstark, D.; Wagenknecht, H.-A., Perylene Bisimide Dimers as Fluorescent Glue for DNA and for Base Mismatch Detection. *Angewandte Chemie-International Edition* **2008,** 47, 2652-2654.
110. Baumstark, D.; Wagenknecht, H.-A., Fluorescent Hydrophobic Zippers inside Duplex DNA: Interstrand Stacking of Perylene-3,4:9,10-tetracarboxylic Acid Bisimides as Artificial DNA Base Dyes. *Chemistry-a European Journal* **2008,** 14, 6640-6645.
111. Holzhauser, C.; Berndl, S.; Menacher, F.; Breunig, M.; Gopferich, A.; Wagenknecht, H. A., Synthesis and Optical Properties of Cyanine Dyes as Fluorescent DNA Base Substitutions for Live Cell Imaging. *European Journal of Organic Chemistry* **2010**, (7), 1239-1248.
112. Menacher, F.; Rubner, M.; Berndl, S.; Wagenknecht, H. A., Thiazole orange and Cy3: Improvement of fluorescent DNA probes with use of short range electron transfer. *Journal of Organic Chemistry* **2008,** 73, (11), 4263-4266.
113. Lachmann, D.; Berndl, S.; Wolfbeis, O. S.; Wagenknecht, H. A., Synthetic incorporation of Nile Blue into DNA using 2 '-deoxyriboside substitutes: Representative comparison of (R)- and (S)-aminopropanediol as an acyclic linker. *Beilstein Journal of Organic Chemistry* **2010***,* 6, (13), 1-7.

114. Schlegel, M. K.; Essen, L. O.; Meggers, E., Duplex structure of a minimal nucleic acid. *Journal of the American Chemical Society* **2008,** 130, (26), 8158-8159.
115. Filichev, V. V.; Astakhova, I. V.; Malakhov, A. D.; Korshun, V. A.; Pedersen, E. B., 1-, 2-, and 4-Ethynylpyrenes in the Structure of Twisted Intercalating Nucleic Acids: Structure, Thermal Stability, and Fluorescence Relationship. *Chemistry-a European Journal* **2008,** 14, (32), 9968-9980.
116. Geci, I.; Filichev, V. V.; Pedersen, E. B., Stabilization of parallel triplexes by twisted intercalating nucleic acids (TINAs) incorporating 1,2,3-triazole units and prepared by microwave-accelerated click chemistry. *Chemistry-a European Journal* **2007,** 13, (22), 6379-6386.
117. Amann, N.; Huber, R.; Wagenknecht, H. A., Phenanthridinium as an artificial base and charge donor in DNA. *Angewandte Chemie-International Edition* **2004,** 43, (14), 1845-1847.
118. Baumstark, D.; Wagenknecht, H. A., Perylene bisimide dimers as fluorescent "Glue" for DNA and for base-mismatch detection. *Angewandte Chemie-International Edition* **2008,** 47, (14), 2612-2614.
119. Huber, R.; Amann, N.; Wagenknecht, H. A., Synthesis of DNA with phenanthridinium as an artificial DNA base. *Journal of Organic Chemistry* **2004,** 69, (3), 744-751.
120. Valis, L.; Wagenknecht, H. A., Phenanthridinium as an artificial DNA base: Comparison of two alternative acyclic 2'-deoxyribose substitutes. *Synlett* **2007**, (13), 2111-2115.
121. Wagner, C.; Wagenknecht, H. A., Perylene-3,4 : 9,10-tetracarboxylic acid bisimide dye as an artificial DNA base surrogate. *Organic Letters* **2006,** 8, (19), 4191-4194.
122. Wanninger, C.; Wagenknecht, H. A., Indole as an artificial DNA base incorporated via an acyclic 2 '-deoxyriboside substitute. *Synlett* **2006**, (13), 2051-2054.
123. Wanninger-Weiss, C.; Wagenknecht, H. A., Synthesis of 5-(2-pyrenyl)-2 '-deoxyuridine as a DNA modification for electron-transfer studies: The critical role of the position of the chromophore attachment. *European Journal of Organic Chemistry* **2008**, (1), 64-69.
124. Jarikote, D. V.; Koehler, O.; Socher, E.; Seitz, O., Divergent and linear solid-phase synthesis of PNA containing thiazole orange as artificial base. *European Journal of Organic Chemistry* **2005**, (15), 3187-3195.
125. Harrison, W. J.; Mateer, D. L.; Tiddy, G. J. T., Liquid-crystalline J-aggregates formed by aqueous ionic cyanine dyes. *Journal of Physical Chemistry* **1996,** 100, 2310-2321.
126. Sagawa, T.; Tobata, H.; Ihara, H., Exciton interactions in cyanine dye-hyaluronic acid (HA) complex: reversible and biphasic molecular switching of chromophores induced by random coil-to-double-helix phase transition of HA. *Chemical Communications* **2004**, (2090-2091).
127. Furstenberg, A.; Julliard, M. D.; Deligeorgiev, T. G.; Gadjev, N. I.; Vasilev, A. A.; Vauthey, E., Ultrafast excited-state dynamics of DNA fluorescent intercalators: New insight into the fluorescence enhancement mechanism. *Journal of the American Chemical Society* **2006,** 128, (23), 7661-7669.

128. Simon, L. D.; Aramo, K. H.; Sell, J. K.; McGown, L. B., Oxazole yellow dye interactions with short DNA oligomers of homogeneous base composition and their hybrids. *Biospectroscopy* **1998,** 4, 17-25.
129. Kubota, T.; Ikeda, S.; Yanagisawa, H.; Yuki, M.; Okamoto, A., Hybridization-Sensitive Fluorescent Probe for Long-Term Monitoring of Intracellular RNA. *Bioconjugate Chemistry* **2009,** 20, 1256-1261.
130. Ikeda, S.; Kubota, T.; Yuki, M.; Okamoto, A., Exciton-Controlled Hybridization-Sensitive Fluorescent Probes: Multicolor Detection of Nucleic Acids. *Angewandte Chemie-International Edition* **2009,** 48, 6480-6484.
131. Ikeda, S.; Kubota, T.; Kino, K.; Okamoto, A., Sequence dependence of fluorescence emission and quenching of doubly thiazole orange labeled DNA: Effective design of a hybridization-sensitive probe. *Bioconjugate Chemistry* **2008,** 19, 1719-1725.
132. Harada, N.; Nakanishi, K., *Circular dichroic spectroscopy: exciton coupling in organic stereochemistry*. University Science Books Mill Valley, CA, **1983**.
133. Zheng, Y.; Long, H.; Schatz, G. C.; Lewis, F. D., Duplex and hairpin dimer structures for perylene diimide-oligonucleotide conjugates. *Chemical Communications* **2005**, (38), 4795-4797.
134. West, W.; Pearce, S., Dimeric state of cyanine dyes. *Journal of Physical Chemistry* **1965,** 69, 1894-1903.
135. Fürstenberg, A.; Deligeorgiev, T. G.; Gadjev, N. I.; Vasilev, A.; Vauthey, E., Structure-fluorescence contrast relationship in cyanine DNA intercalators: Toward rational dye design. *Chemistry-a European Journal* **2007,** 13, 8600-8609.
136. Nygren, J.; Svanvik, N.; Kubista, M., The interactions between the fluorescent dye thiazole orange and DNA. *Biopolymers* **1998,** 46, (1), 39-51.
137. Rosch, U.; Yao, S.; Wortmann, R.; Wurthner, F., Fluoresceut H-aggregates of merocyanine dyes. *Angewandte Chemie-International Edition* **2006,** 45, (42), 7026-7030.
138. Ogul'chansky, T. Y.; Yashchuk, V. M.; Losytskyy, M. Y.; Kocheshev, I. O.; Yarmoluk, S. M., Interaction of cyanine dyes with nucleic acids. XVII. Towards an aggregation of cyanine dyes in solutions as a factor facilitating nucleic acid detection. *Spectrochimica Acta Part a-Molecular and Biomolecular Spectroscopy* **2000,** 56, (4), 805-814.
139. Schmittrink, S. D. A. B. M., Theory of the Linear and Nonlinear Optical-Properties of Semiconductor Microcrystallites. *Physical Review B* **1987,** 35, (15), 8113-8125.
140. Nozik, A. J., Quantum dot solar cells. *Physica E-Low-Dimensional Systems & Nanostructures* **2002,** 14, (1-2), 115-120.
141. Klimov, V. I.; Mikhailovsky, A. A.; Xu, S.; Malko, A.; Hollingsworth, J. A.; Leatherdale, C. A.; Eisler, H. J.; Bawendi, M. G., Optical gain and stimulated emission in nanocrystal quantum dots. *Science* **2000,** 290, (5490), 314-317.
142. Chan, W. C. W.; Nie, S. M., Quantum dot bioconjugates for ultrasensitive nonisotopic detection. *Science* **1998,** 281, (5385), 2016-2018.
143. Klimov, V. I.; McBranch, D. W.; Leatherdale, C. A.; Bawendi, M. G., Electron and hole relaxation pathways in semiconductor quantum dots. *Physical Review B* **1999,** 60, (19), 13740-13749.

144. Schaller, R. D.; Pietryga, J. M.; Goupalov, S. V.; Petruska, M. A.; Ivanov, S. A.; Klimov, V. I., Breaking the phonon bottleneck in semiconductor nanocrystals via multiphonon emission induced by intrinsic nonadiabatic interactions. *Physical Review Letters* **2005,** 95, (19), 196401.
145. Cooney, R. R.; Sewall, S. L.; Anderson, K. E. H.; Dias, E. A.; Kambhampati, P., Breaking the phonon bottleneck for holes in semiconductor quantum dots. *Physical Review Letters* **2007,** 98, (17), 177403.
146. Sagar, D. M.; Cooney, R. R.; Sewall, S. L.; Dias, E. A.; Barsan, M. M.; Butler, I. S.; Kambhampati, P., Size dependent, state-resolved studies of exciton-phonon couplings in strongly confined semiconductor quantum dots. *Physical Review B* **2008,** 77, (23), 235321.
147. Salvador, M. R.; Graham, M. W.; Scholes, G. D., Exciton-phonon coupling and disorder in the excited states of CdSe colloidal quantum dots. *Journal of Chemical Physics* **2006,** 125, 184709.
148. Dooley, C. J. New nanomaterials for photovoltaic applications: a study on the chemistry and photophysics of II-VI semiconductor nanostructures. Boston College, Boston, **2009**.
149. Dagtepe, P.; Chikan, V.; Jasinski, J.; Leppert, V. J., Quantized growth of CdTe quantum dots; Observation of magic-sized CdTe quantum dots. *Journal of Physical Chemistry C* **2007,** 111, (41), 14977-14983.
150. Yu, W. W.; Qu, L. H.; Guo, W. Z.; Peng, X. G., Experimental determination of the extinction coefficient of CdTe, CdSe, and CdS nanocrystals. *Chemistry of Materials* **2003,** 15, (14), 2854-2860.
151. Klimov, V. I., Optical nonlinearities and ultrafast carrier dynamics in semiconductor nanocrystals. *Journal of Physical Chemistry B* **2000,** 104, (26), 6112-6123.
152. Sanz, M.; Coffea-Duarte, M. A.; Liz-Marzan, L. M.; Douhal, A., Femtosecond dynamics of CdTe quantum dots in water. *Journal of Photochemistry and Photobiology a-Chemistry* **2008,** 196, (1), 51-58.
153. Bardeen, C. J.; Wang, Q.; Shank, C. V., Femtosecond chirped pulse excitation of vibrational wave packets in LD690 and bacteriorhodopsin. *Journal of Physical Chemistry A* **1998,** 102, (17), 2759-2766.
154. Bragas, A. V.; Aku-Leh, C.; Costantino, S.; Ingale, A.; Zhao, J.; Merlin, R., Ultrafast optical generation of coherent phonons in $CdTe_{1-x}Se_x$ quantum dots. *Physical Review B* **2004,** 69, (20), 205306.
155. Sagar, D. M.; Cooney, R. R.; Sewall, S. L.; Kambhampati, P., State-resolved exciton-phonon couplings in CdSe semiconductor quantum dots. *Journal of Physical Chemistry C* **2008,** 112, (25), 9124-9127.
156. Nomura, S.; Kobayashi, T., Exciton LO-Phonon Couplings in Spherical Semiconductor Microcrystallites. *Physical Review B* **1992,** 45, (3), 1305-1316.
157. Klein, M. C.; Hache, F.; Ricard, D.; Flytzanis, C., Size dependence of electron-phonon coupling in semiconductor nanospheres: the case of CdSe. *Physical Review B* **1990,** 42, (17), 11123-11132.

158. Mittleman, D. M.; Schoenlein, R. W.; Shiang, J. J.; Colvin, V. L.; Alivisatos, A. P.; Shank, C. V., Quantum-Size Dependence of Femtosecond Electronic Dephasing and Vibrational Dynamics in Cdse Nanocrystals. *Physical Review B* **1994,** 49, (20), 14435-14447.
159. Xu, S.; Mikhailovsky, A. A.; Hollingsworth, J. A.; Klimov, V. I., Hole intraband relaxation in strongly confined quantum dots: Revisiting the "phonon bottleneck" problem. *Physical Review B* **2002,** 65, (4), 045319.
160. Cooney, R. R.; Sewall, S. L.; Dias, E. A.; Sagar, D. M.; Anderson, K. E. H.; Kambhampati, P., Unified picture of electron and hole relaxation pathways in semiconductor quantum dots. *Physical Review B* **2007,** 75, (24), 245311.
161. Hendry, E.; Koeberg, M.; Wang, F.; Zhang, H.; Donega, C. D.; Vanmaekelbergh, D.; Bonn, M., Direct observation of electron-to-hole energy transfer in CdSe quantum dots. *Physical Review Letters* **2006,** 96, (5), 057408.
162. Richard, T.; Lefebvre, P.; Mathien, H.; Allegre, J., Effects of finite spin-orbit splitting on optical properties of spherical semiconductor quantum dots. *Physical Review B* **1996,** 53, (11), 7287-7298.
163. Klimov, V. I., *Semiconductor and Metal Nanocrystals: Synthesis and Electronic and Optical Properties*. Marcel Dekker, Inc.: New York, 2003.
164. Pandey, A.; Guyot-Sionnest, P., Slow Electron Cooling in Colloidal Quantum Dots. *Science* **2008,** 322, (5903), 929-932.
165. Guyot-Sionnest, P.; Wehrenberg, B.; Yu, D., Intraband relaxation in CdSe nanocrystals and the strong influence of the surface ligands. *Journal of Chemical Physics* **2005,** 123, (7), 074709.
166. Rose, T. S.; Rosker, M. J.; Zewail, A. H., Femtosecond Real-Time Observation of Wave Packet Oscillations (Resonance) in Dissociation Reactions. *Journal of Chemical Physics* **1988,** 88, (10), 6672-6673.
167. Scholes, G. D., Controlling the Optical Properties of Inorganic Nanoparticles. *Advanced Functional Materials* **2008,** 18, 1157-1172.
168. Murray, C. B.; Norris, D. J.; Bawendi, M. G., Synthesis and Characterization of Nearly Monodisperse Cde (E = S, Se, Te) Semiconductor Nanocrystallites. *Journal of the American Chemical Society* **1993,** 115, (19), 8706-8715.
169. Scholes, G. D.; Jones, M.; Kumar, S., Energetics of photoinduced electron-transfer reactions decided by Quantum confinement. *Journal of Physical Chemistry C* **2007,** 111, (37), 13777-13785.
170. Zhong, H.; Scholes, G. D., Shape Tuning of Type II CdTe-CdSe Colloidal Nanocrystal Heterostructures through Seeded Growth. *Journal of the American Chemical Society* **2009,** 131, (9170-9171).
171. Halpert, J. E.; Porter, V. J.; Zimmer, J. P.; Bawendi, M. G., Synthesis of CdSe/CdTe nanobarbells. *Journal of the American Chemical Society* **2006,** 128, 12590-12591.
172. Kim, S.; Fisher, B.; Eisler, H. J.; Bawendi, M., Type-II quantum dots: CdTe/CdSe(core/shell) and CdSe/ZinTe(core/shell) heterostructures. *Journal of the American Chemical Society* **2003,** 125, (38), 11466-11467.

173. Ginger, D. S.; Greenham, N. C., Photoinduced electron transfer from conjugated polymers to CdSe nanocrystals. *Physical Review B* **1999,** 59, (16), 10622-10629.
174. Klimov, V. I.; Mikhailovsky, A. A.; Xu, S.; Malko, A.; Hollingsworth, J. A.; Leatherdale, C. A.; Eisler, H. J.; Bawendi, M. G., Optical gain and stimulated emission in nanocrystal quantum dots. *Science* **2000,** 290, (5490), 314-317.
175. Huynh, W. U.; Dittmer, J. J.; Alivisatos, A. P., Hybrid nanorod-polymer solar cells. *Science* **2002,** 295, (5564), 2425-2427.
176. Gunes, S.; Fritz, K. P.; Neugebauer, H.; Sariciftci, N. S.; Kumar, S.; Scholes, G. D., Hybrid solar cells using PbS nanoparticles. *Solar Energy Materials and Solar Cells* **2007,** 91, (5), 420-423.
177. Brus, L. E., A Simple-Model for the Ionization-Potential, Electron-Affinity, and Aqueous Redox Potentials of Small Semiconductor Crystallites. *Journal of Chemical Physics* **1983,** 79, (11), 5566-5571.
178. Chen, C. Y.; Cheng, C. T.; Yu, J. K.; Pu, S. C.; Cheng, Y. M.; Chou, P. T.; Chou, Y. H.; Chiu, H. T., Spectroscopy and femtosecond dynamics of type-II CdSe/ZnTe core-shell semiconductor synthesized via the CdO precursor. *Journal of Physical Chemistry B* **2004,** 108, (30), 10687-10691.
179. Peng, P.; Milliron, D. J.; Hughes, S. M.; Johnson, J. C.; Alivisatos, A. P.; Saykally, R. J., Femtosecond spectroscom of carrier relaxation dynamics in type IICdSe/CdTe tetrapod heteronanostructures. *Nano Letters* **2005,** 5, (9), 1809-1813.
180. Braun, M.; Link, S.; Burda, C.; El-Sayed, M., Determination of the localization times of electrons and holes in the HgS well in a CdS/HgS/CdS quantum dot-quantum well nanoparticle. *Physical Review B* **2002,** 66, (20), 205312.
181. Ellingson, R. J.; Beard, M. C.; Johnson, J. C.; Yu, P. R.; Micic, O. I.; Nozik, A. J.; Shabaev, A.; Efros, A. L., Highly efficient multiple exciton generation in colloidal PbSe and PbS quantum dots. *Nano Letters* **2005,** 5, (5), 865-871.
182. Klimov, V. I.; McBranch, D. W., Femtosecond 1P-to-1S electron relaxation in strongly confined semiconductor nanocrystals. *Physical Review Letters* **1998,** 80, (18), 4028-4031.
183. Yu, P. R.; Nedeljkovic, J. M.; Ahrenkiel, P. A.; Ellingson, R. J.; Nozik, A. J., Size dependent femtosecond electron cooling dynamics in CdSe quantum rods. *Nano Letters* **2004,** 4, 1089-1092.
184. Mohamed, M. B.; Burda, C.; El-Sayed, M. A., Shape dependent ultrafast relaxation dynamics of CdSe nanocrystals: Nanorods vs nanodots. *Nano Letters* **2001,** 1, (11), 589-593.
185. Chou, P. T.; Chen, C. Y.; Cheng, C. T.; Pu, S. C.; Wu, K. C.; Cheng, Y. M.; Lai, C. W.; Chou, Y. H.; Chiu, H. T., Spectroscopy and femtosecond dynamics of type-II CdTe/CdSe core-shell quantum dots. *Chemphyschem* **2006,** 7, (1), 222-228.
186. Jones, M.; Kumar, S.; Lo, S. S.; Scholes, G. D., Exciton trapping and recombination in type II CdSe/CdTe nanorod heterostructures. *Journal of Physical Chemistry C* **2008,** 112, (14), 5423-5431.
187. Jaskolski, W.; Bryant, G. W., Multiband theory of quantum-dot quantum wells: Dim excitons, bright excitons, and charge separation in heteronanostructures. *Physical Review B* **1998,** 57, (8), R4237-R4240.

188. Saito, S.; Dresselhaus, G.; Dresselhaus, M. S., *Physical Properties of Carbon Nanotubes*. London, **1998**.
189. Murakami, H.; Nakashima, N., Soluble carbon nanotubes and their applications. *J. Nanosci. Nanotechnol.* **2006**, (6), 16-27.
190. Chen, R. J.; Zhang, Y.; Wang, D.; Dai, H., Noncovalent Sidewall Functionalization of Single-Walled Carbon Nanotubes for Protein Immobilization. *Journal of the American Chemical Society* **2001,** 123, 3838-3839.
191. Guldi, D. M.; Rahman, G. M. A.; Zerbetto, F.; Prato, M., Carbon Nanotubes in Electron Donor-Acceptor Nanocomposites. *Accounts of Chemical Research* **2005,** 38, 871-878.
192. Sorescu, D. C.; Jordan, K. D.; Avouris, P., Theoretical study of oxygen adsorption on graphite and the (8,0) single-walled carbon nanotube. *Journal of Physical Chemistry B* **2001,** 105, 11227-11232.
193. Javey, A. G., J.; Wang, Q.; Lundstrom, M.; Dai, H. J., Ballistic carbon nanotube field-effect transistors. *Nature* **2003,** 424, 654-657.
194. Hirsch, A., Functionalization of Single-Walled Carbon Nanotubes. *Angewandte Chemie-International Edition* **2002,** 41, 1853-1859.
195. O'Connell, M. J.; Bachilo, S. M.; Huffman, C. B.; Moore, V. C.; Strano, M. S.; Haroz, E. H.; Rialon, K. L.; Boul, P. J.; Noon, W. H.; Kittrell, C.; Jianoeng, M.; Hauge, R. H.; Weisman, R. B.; Smalley, R. E., Band gap fluorescence from individual Singe-Walled Carbon Nanotubes. *Science* **2002,** 297, 593-596.
196. Guldi, D. M.; Rahman, G. M. A.; Sgobba, V.; Kotov, N. A.; Bonifazi, D.; Prato, M., CNT−CdTe Versatile Donor−Acceptor Nanohybrids. *Journal of the American Chemical Society* **2006,** 128, (7), 2315-2323.
197. Chen, R. J.; Zhang, Y.; Wang, D.; Dai, H., Noncovalent Sidewall Functionalization of Single-Walled Carbon Nanotubes for Protein Immobilization. *Journal of the American Chemical Society* **2001,** 123, 3838-3839.
198. Wenseleers, W.; Vlasov, I. I.; Goovaerts, E.; Obraztsova, E. D.; Lobach, A. S.; Bouwen, A., Efficient isolation and solubilization of pristine Single-Walled Nanotubes in bile salt micelles *Advanced Functional Materials* **2004,** 14, 1105-1112.
199. Ehli, C.; Rahman, G. M. A.; Jux, N.; Balbinot, D.; Guldi, D. M.; Paolucci, F.; Marcaccio, M.; Paolucci, D.; Melle-Franco, M.; Zerbetto, F.; Campidelli, S.; Prato, M., Interactions in Single Wall Carbon Nanotubes/Pyrene/Porphyrin Nanohybrids. *Journal of the American Chemical Society* **2006,** 128, (34), 11222-11231
200. Sgobba, V.; Guldi, D. M., Carbon nanotubes — electronic/electrochemical properties and application for nanoelectronics and photonics. *Chemical society reviews* **2009,** 28, 165-184.
201. Hu, L.; Zhao, Y.-L.; Ryu, K.; Zhou, C.; Stoddart, J. F.; G., G., Light-Induced Charge Transfer in Pyrene/CdSe-SWNT Hybrids. *Advanced Materials* **2008,** 20, 939-946.
202. Pagona, G.; Sandanayaka, A. S. D.; Maign, A.; Fan, J.; Papavassiliou, G. C.; Petsalakis, I. D.; Steele, B. R.; Yudasaka, M.; Iijima, S.; Tagmatarchis, N.; Ito, O., Photoinduced Electron Transfer on Aqueous Carbon Nanohorn–Pyrene–Tetrathiafulvalene Architectures. *Chemistry-a European Journal* **2007,** 13, 7600-7607.

203. Martin, R. B.; Qu, L.; Lin, Y.; Harruff, B. A.; Bunker, C. E.; Gord, J. R.; Allard, L. F.; Sun, Y.-P., Functionalized Carbon Nanotubes with Tethered Pyrenes: Synthesis and Photophysical Properties. *Journal of Physical Chemistry B* **2004,** 108, 11447-11453.
204. Li, H.; Kose, M. E.; Qua, L.; Lina, Y.; Martin, R. B.; Zhoua, B.; Harruff, B. A.; Allard, L. F.; Sun, Y.-P., Excited-state energy transfers in single-walled carbon nanotubes functionalized with tethered pyrenes. *Journal of Photochemistry and Photobiology A: Chemistry* **2007,** 105, 94-100.
205. Guldi, D. M.; Rahman, G. M. A.; Jux, N.; Balbinot, D.; Hartnagel, H.; Tagmatarchis, N.; Prato, M., Functional Single-Wall Carbon Nanotube NanohybridssAssociating SWNTs with Water-Soluble Enzyme Model Systems. *Journal of the American Chemical Society* **2005,** 127, 9830-9838.
206. Guldi, D. M.; Holzinger, M.; Hirsch, A.; Georgakilas, V.; Prato, M., First comparative emission assay of single-wall carbon nanotubes—solutions and dispersions. *Chemical Communications* **2003**, 1130-1131.
207. Trifonov, A. A., Advancing and developing experimental methodologies for studying ultrafast photoinduced processes in liquid solutions. Technical University Munich, Munich, **2005**.
208. Spano, F. C., The Spectral Signatures of Frenkel Polarons in H- and J-Aggregates. *Accounts of Chemical Research* **2010,** 43, (3), 429-439.

9 Appendix I – List of Publications

1. Dimitrov, S. D.; Dooley, C. J.; Trifonov, A.; Fiebig, T., Femtosecond Probing of Optical Phonon Dynamics in Quantum-Confined CdTe Nanocrystals. *Journal of Physical Chemistry C*, **2009**, *113*, (10), 4198-4201.

2. Dooley, C. J.; Dimitrov, S. D.; Fiebig, T., Ultrafast Electron Transfer Dynamics in CdSe/CdTe Donor-Acceptor Nanorods. *Journal of Physical Chemistry C*, **2008**, *112*, (32), 12074-12076.